Surface-Sensitive and Surface-Specific Ultrafast Two-Dimensional Vibrational Spectroscopy

Kraack, Jan Philip ; Hamm, Peter

Abstract: Ultrafast two-dimensional infrared spectroscopy (2D IR) has been advanced in recent years toward measuring signals from only a monolayer of sample molecules at solid–liquid and solid–gas interfaces. A series of experimental methods has been introduced, which in the chronological order of development are 2D sum-frequency-generation (2D SFG), transmission 2D IR, and reflection 2D IR, the latter in either internal, attenuated total reflection (ATR), or external reflection configuration. The different variants of 2D vibrational spectroscopy are based on either the even-order or the odd-order nonlinear susceptibility, and all allow resolving similar molecular temporal and spectral information. In this review, we introduce the basic principles of the different methods of 2D vibrational spectroscopy at surfaces along with a balanced overview on the technological aspects as well as benefits and shortcomings. We furthermore discuss the current scope of applications for 2D vibrational surface spectroscopy, which spans an impressively broad range of samples from biological molecules to heterogeneous catalysts. The emphasis is on the ultrafast structural dynamics of molecules at interfaces, environmental interactions, and intermolecular interactions. We furthermore consider important recent technological developments of 2D vibrational surface spectroscopy, which employ (i) surface enhancement, (ii) methods for studying electrochemical interfaces, and (iii) extensions for resolving nonequilibrium processes (transient 2D IR). A detailed outlook is finally given regarding important future applications and technological developments of 2D vibrational surface spectroscopy.

DOI: https://doi.org/10.1021/acs.chemrev.6b00437

Surface-Sensitive and Surface-Specific Ultrafast Two-Dimensional Vibrational Spectroscopy

Jan Philip Kraack[‡] *and Peter Hamm*[*]

Department of Chemistry, University of Zurich,

Winterthurerstrasse 190, CH-8057, Zurich, Switzerland

TOC Graphic

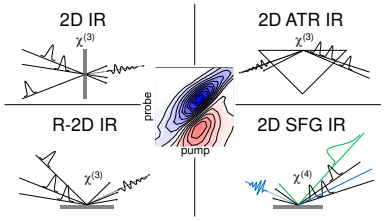

Keywords:

Surface-specific spectroscopy, surface-sensitive spectroscopy, 2D IR, 2D ATR IR, 2D SFG, Monolayers, Adsorbates, Sum-Frequency Generation, Attenuated Total Reflectance.

Abstract

Ultrafast two-dimensional infrared spectroscopy (2D IR) has been advanced in recent years towards measuring signals from only a monolayer of sample molecules at solid-liquid and solid-gas interfaces. A series of experimental methods has been introduced, which in the chronological order of development are: 2D sum-frequency-generation IR (2D SFG), transmission 2D IR, and reflection 2D IR, the latter in either internal, attenuated total reflection (ATR), or in external reflection configuration. The different variants of 2D vibrational spectroscopy are based on either the even- or the odd-order nonlinear susceptibility, and all allow resolving similar molecular temporal and spectral information. In this review, we introduce the basic principles of the different methods of 2D vibrational spectroscopy at surfaces along with a balanced overview on the technological aspects as well as benefits and shortcomings. We furthermore discuss the current scope of applications for 2D vibrational surface spectroscopy, which spans an impressively broad range of samples from biological molecules to heterogeneous catalysts. The emphasis is on the ultrafast structural dynamics of molecules at interfaces, environmental interactions, as well as intermolecular interactions. We furthermore consider important recent technological developments of 2D vibrational surface spectroscopy, which employ (i) surface-enhancement, (ii) methods for studying electrochemical interfaces, and (iii) extensions for resolving non-equilibrium processes (transient 2D IR). A detailed outlook is finally given regarding important future applications and technological developments of 2D vibrational surface spectroscopy.

Table of Contents

1. Introduction

1.1. The Importance of Solid-Liquid Interfaces

The properties of chemical bonds of molecules at solid-liquid/gas interfaces play a prominent role in chemistry, biology and physics. Although this importance is widely acknowledged[1–18], a detailed molecular understanding of dynamical properties at interfaces is still challenging to obtain experimentally. From a microscopic point of view, solid surfaces can adopt many different structures, such as nano-particulate patterns, porous textures, or extended crystalline areas. It is known that these interfacial structures can influence the conformations of molecules near interfaces and thus also determine their properties.[19–23] In this regard, many examples exist ranging from fundamental science to technical applications. Possibly the best-known process is related to molecular self-assembly of covalently bound adsorbates at surfaces[19,20,24–27] and nanostructures[28–32]. Self-assembly is strongly determined by intermolecular interactions between functional groups of adsorbate molecules, as well as the microscopic surface structure. The concept of self-assembly is equally important for the understanding of adsorption of biomolecules at surfaces and biological film growth[33–35], or surface molecular diffusion[25,36,37]. Moreover, great interest on solid-liquid/gas interfaces exists from the perspective of chemical synthesis or in the field of energy science, both of which have strong connections to heterogeneous (photo-) catalysis[38–45]. Here, pending goals are for instance to clarify the role of interactions between the surface and adsorbates[46–49], the impact of interfacial solvent flow[50,51], or vibrational energy flow at interfaces along with its relevance for chemical reactions[52–55]. Other aspects of surface science with high commercial and social relevance emerge from the fields of molecular electronics[56–59] or energy supply. The latter currently focusses predominately on the optimization of artificial solar light harvesting[60–63], design and performance of fuel cell assemblies[64–67], or the understanding of charge migration at electrode-electrolyte interfaces in, *e.g.* battery devices[68–70]. One of the

most challenging aspects common for all the above examples is to determine how molecules at an interface actually perform in order to make a physical or chemical process happen.

1.2. Vibrational Spectroscopy at Solid-Liquid/Gas Interfaces

Vibrational spectroscopy in its different forms is ideally suited to study structure, function and dynamics of molecules.[2,21,71–75] Out of the many existing methods for surface vibrational spectroscopy, this review focusses exclusively on techniques, which use electromagnetic radiation in the mid-infrared (IR) spectral range (3500–1000 cm^{-1}) for excitation of the sample. In a typical IR spectrum, the spectral position, bandwidth, band-shape and intensity of a transition responds sensitively to changes in molecular structure as well as the environment. For most of the examples discussed in this review, the molecules of interest are adsorbed on a surface by covalent substrate-sample interactions. Such adsorbate molecules generally contain specific functional groups, which are key-constituents for different processes, for instance as catalytically active sites or as sensitizer, *i.e.*, a part of a molecule, which can be externally activated by different methods to initiate a chemical process. When studying vibrational properties of adsorbates, one focusses on these functional groups.

Any surface vibrational spectroscopy must be sensitive enough to detect the response from a very small number of molecules, since one is often interested in a molecular layer that is in direct contact with the surface, *i.e.*, a monolayer (ML). Depending on the dimensions of the molecule of interest, the number of molecules in a ML is about 1 nmol cm^{-2} or less.[19] In addition, the extinction coefficients of functional groups in the IR spectral range are often quite small (< 1000 $M^{-1}cm^{-1}$). Both of the above points reduce the overall signal strengths, and are thus a technological challenge to surface-related vibrational spectroscopy. To make it even more challenging, any form of time-resolved, or transient vibrational spectroscopy, selects only a sub-set of molecules at the surface to generate a signal that is even weaker.

It is instructive to compare that number to a typical bulk solution sample in a time-resolved experiment: Assuming a 50 μm path length sample cell and a 1 mM concentration of the sample, the number of molecules in the solution phase is about a factor five larger than that in a typical ML. Hence, the number of molecules in a ML is small, but in fact within reach for "state-of-the-art" infrared laser experiments. That is, time-resolved vibrational spectroscopy at surfaces, and in particular multi-dimensional methods, have been demonstrated as very valuable spectroscopies for addressing a broad range of scientific questions.

1.3. The Importance of Ultrafast, Two-Dimensional Infrared Spectroscopy

Ultrafast, two-dimensional IR spectroscopy (2D IR) has been introduced a couple of years ago.[71,75–77] 2D IR spreads signals into two frequency dimensions, which allows one to measure different types of spectral correlations. Moreover, the time evolution of 2D IR signals can be followed with sub-picosecond temporal resolution. As such, 2D IR is ideally suited to resolve mechanisms of line-broadening of vibrational bands and to unravel the underlying timescales and origins of molecular dynamics.[71]

In addition, 2D IR is particularly powerful in determining interactions between functional groups or between molecules. In many cases, such interactions can be directly related to the formation and dissociation of chemical bonds. Several 2D IR studies in isotropic environments (*i.e.* in bulk solution) have demonstrated this, for instance the determination of intermolecular complex-formation[78], hydrogen-bond interactions[79–81], intramolecular isomerization reactions[82], or molecular structure elucidation, *e.g.* in peptides and proteins[83–88]. These capabilities of 2D IR have triggered interest to make this type of information also available to surface sciences in order to determine the impact of an interface on inter- and intramolecular molecular dynamics of adsorbates. For example, distinct properties of a surface can be controlled on demand, *e.g.* by modifications of the surface structure (crystal

facets, ad-atoms, or nanoparticles), or by variations of the surface-charge. Also, adsorbates can exist in different binding configurations, which can interconvert over time. Moreover, depending on the actual geometry, an adsorbate can interact with the substrate in different ways, *e.g.* chemically or electrostatically. Adsorbates can thus transfer energy from localized vibrations to phonons or to the electronic system of the substrate (substrate-adsorbate coupling).[89,90] The close packing of molecules in a ML can also facilitate intermolecular interactions and energy-transfer.[91,92] As a further impact of the surface, molecules are motionally much more confined and restricted as compared to isotropic environments. Finally, the surface serves as a reference plane for orientation, which determines the way in which the adsorbate is immobilized. As many of the above points are expected to be sensitive to intermolecular orientation, the adsorption process and the adsorbates structure on the surface can have strong influences on molecular dynamics. This can have important consequences also for the relevant molecular function.

1.4. Scope of this Review

There has been a considerable technological development during the last approximately ten years in the field of 2D vibrational spectroscopy at surfaces. Three dominant variants of 2D vibrational spectroscopy at solid-liquid/gas interfaces are currently expedited, *i.e.,* transmission, reflection and sum-frequency generation (SFG) versions. All three implementations have in common that they can measure 2D vibrational signals from a ML of molecules on a surface or less, *i.e.* they are all *surface-sensitive*. However, the methods exploit different nonlinear optical properties of the adsorbed samples. In particular, SFG selects only those molecules, which are influenced by the presence of an interface. This makes SFG vibrational spectroscopy strictly *surface-specific*. Despite the underlying fundamental differences in signal generation, most of the 2D spectra discussed here as

examples, which have been obtained with different methods, reveal very similar information. The similar information content calls for a combined overview of the different techniques, which we aim to provide in this review.

In section 2.1, we first give a brief overview on the theoretical background of 2D IR spectroscopy at surfaces, in particular with regard to the different orders of nonlinearity. Section 2.2 is dedicated to a balanced overview of the methods, including a discussion of certain experimental differences and their pros and cons. Section 3 then highlights a series of applications for the investigation of the ultrafast dynamics and molecular structures at solid-liquid interfaces. Here, the emphasis is on the applicability of the methods in terms of the range of functional groups, addressable timescales, applicable surface-coverages, structural constitutions of samples, or intermolecular interactions at surfaces. In addition, we present interesting extensions of the methods, which have been implemented to measure *e.g.* electrochemical processes or non-equilibrium dynamics in excited electronic states.

Surface 2D vibrational spectroscopy is a very recent, rapidly growing field of research, and we will discuss here more the potential of the developed experimental methods rather than a comprehensive understanding of new physico-chemical phenomena. Many new and ground-breaking experiments can be envisioned, which utilize the currently existing methods, or advance from them in future implementations. We therefore finally summarize the present results in section 4 and provide an outlook on important future advancements of 2D IR spectroscopy at surfaces. This includes a discussion of the wider scope of possible sample systems as well as experimental extensions.

Concerning a more precise definition of 2D vibrational spectroscopy, we note that there exists another form of two-dimensional IR spectroscopy,[93–96] *i.e.* 2D IR correlation spectroscopy. This method measures correlations in the change of the IR absorption in response to various external perturbations such as temperature, concentration, or mechanical stress. 2D IR

correlation spectroscopy reveals information that is very different from ultrafast 2D IR, and will not be considered here.

We also note that there exists a number of other time-resolved surface-related vibrational spectroscopies such as surface-enhanced Raman spectroscopy[97], surface-enhanced stimulated Raman spectroscopy[98], high-resolution electron energy loss spectroscopy[99], and more specialized approaches[2,21,72]. For none of these methods, an extension to 2D spectroscopy has been reported as of yet, and consequently they are not considered here either.

2. Two-Dimensional Vibrational Spectroscopy at Interfaces

2.1. Principles of Even and Odd-Order Nonlinear Spectroscopy

We start with a brief survey of the theoretical background of 2D IR spectroscopy of molecules at surfaces. Thorough reviews[100–102], books[71,103] and overviews[75] on the general theory of ultrafast nonlinear spectroscopy, including 2D IR spectroscopy, are available elsewhere. Here, we consider only aspects, which are necessary to highlight analogies and differences between odd- ($\chi^{(3)}$) and even-order ($\chi^{(4)}$) nonlinear techniques.

In general, the polarization ($P(\omega)$) of a sample induced by light of frequency ω is expanded in powers of the incident electric fields ($E_i(\omega)$). The contributions that are predominately relevant for this review article are those up to the 4th-order term (eqn. 1).[104]

$$P(\omega) = \epsilon_0 \left[\begin{array}{c} \chi^{(1)}(\omega)E_1(\omega) + \chi^{(2)}(\omega)E_1(\omega)E_2(\omega) + \chi^{(3)}(\omega)E_1(\omega)E_2(\omega)E_3(\omega) \\ +\chi^{(4)}(\omega)E_1(\omega)E_2(\omega)E_3(\omega)E_4(\omega) + \cdots \end{array} \right]$$

$$\equiv P^{(1)}(\omega) + P^{(2)}(\omega) + P^{(3)}(\omega) + P^{(4)}(\omega) + \cdots$$

(eqn. 1)

The lowest order of polarization is linearly proportional to the incident electric field strength with proportionality constant $\chi^{(1)}(\omega)$. This susceptibility is related to IR absorption

spectroscopy. Any molecule with a vibrational transition that is resonant with the frequency of the incident light will absorb, irrespective of whether it is adsorbed at a surface or dissolved in bulk solution. More generally speaking, only odd-order susceptibilities ($\chi^{(1)}(\omega)$, $\chi^{(3)}(\omega)$, ...) contribute to the signal in centro-symmetric media and under the assumption of the electric dipole approximation.[104] When the centro-symmetry of the sample is broken, for instance at an interface between two centro-symmetric media, a net orientation of molecules will be obtained. As a result, even orders of nonlinear susceptibilities ($\chi^{(2)}(\omega)$, $\chi^{(4)}(\omega)$, ...) become relevant as well.[105] As only molecules contribute to the even-order polarization for which the centro-symmetry is broken, only those result in the generation of a *strictly surface-specific* signal. In general, the susceptibilities are complex-valued with a real and imaginary component, each of which can have positive or negative values, depending on the specific molecular orientation.[104,106–110] It has become the objective of various types of multi-dimensional vibrational spectroscopy to selectively prepare the different orders of the non-linear polarization, and to exploit their properties in order to reveal maximum information from the sample and its dynamics.

2.1.1. Selection Rules for Molecules at Interfaces

IR vibrational activity implies that the dipole moment (μ) of a molecule changes with the vibrational coordinate (Q), *i.e.*, the transition dipole:[71]

$$\frac{\partial \mu}{\partial Q} \neq 0 \qquad \text{(eqn. 2)}$$

This also holds for any other high-order process of odd nonlinearity ($\geq \chi^{(3)}$), and therefore any method on the basis of these susceptibilities can measure IR-active vibrations. Maximum signal magnitudes are observed when the direction of the transition dipole is parallel to the polarization of the incident light.

Methods based on even-order nonlinear susceptibilities exhibit an additional requirement in terms of selection rules. The vibration needs to change both the dipole μ as well as the polarizability (α) along the vibrational coordinate Q:[111–115]

$$\frac{\partial \mu}{\partial Q}\frac{\partial \alpha}{\partial Q} \neq 0 \qquad \text{(eqn. 3)}$$

This means that the vibration needs to be both IR- and Raman-active. The signal is related to the microscopic hyper-polarizability of the molecules and hence is described as a product of IR and Raman selectrion rules.[90,115–117] Even-order methods therefore employ combinations of vibrationally-resonant IR and non-resonant visible (VIS) light to generate a signal.

In addition, the presence of an interface provides a reference plane for the molecules under study, and the various spectroscopic methods can measure their orientation and alignment by employing different polarization-directions of the light. Most sensitive in this regard are even-order spectroscopies, which can distinguish by the sign of the signal whether a molecular group points towards or away from the surface (which, however, requires a special form of signal detection, *i.e.* heterodyne detection, see section 3.2.2).[106,107,109,118–121] This originates from the fact that the signs of the macroscopic susceptibility tensor-elements are related to linear combinations of several molecular hyper-polarizability tensor-elements.[106,107,111,115,118] Also odd-order spectroscopy can determine the average orientation of adsorbates via different signal strengths obtained from s- and p-polarized light.[122–125] In contrast to even-order spectrosocpy, however, they cannot distinguish parallel from anti-parrallel alignment. Covalently bound sample molecules have an average orientation at the surface, which strongly depends on the surface morphology of the substrates as well as on details of the interaction between the substrate and the sample. For instance, well-defined, crystalline surfaces and a low degree of structural heterogeneity within a surface-bound ML allow a close internal packing of the molecules. Contrasting to that, roughened surfaces with

nanostructured particles and weak interaction between the ML constituents result in a rather heterogeneous distribution of orientations.[19]

On highly polarizable metal substrates (in contrast to a dielectric such as a glas), additional selection rules become relevant in both even- and odd-order spectroscopy.[126–128] That is, a transition dipole aligned along a surface normal induces a mirror-dipole in the metal, which points in the same direction (Figure 1, left). These contributions add up constructively, resulting in a total non-zero transition dipole moment of the combined adsorbate/substrate system. In contrast, if the transition dipole is aligned perpendicular to the surface normal, the induced mirror-dipole in the metal points in the opposite direction (Figure 1, right). The two contributions then add up destructively, and the total transition dipole moment will be zero. The first case therefore results in a spectroscopically active vibration on the surface, while the latter case results in a non-active vibration. This is known as the "surface selection rule".[127,129–132] Although this rule is most widely known for metal surfaces, it practically applies also on semiconductor surfaces, such as Si.[3]

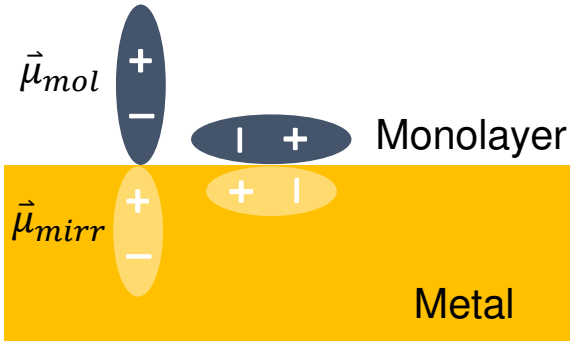

Figure 1. The surface selection rule. An electric dipole (μ) along the surface normal induces a mirror-dipole with the same magnitude in a highly polarizable substrate (e.g., a metal), which both add up constructively. In contrast, an electric dipole parallel to the surface induces a mirror-dipole of opposite direction, which both add up destructively and hence completely cancels the transition dipole of the combined adsorbate/substrate system.

2.1.2. Surface-Sensitivity *versus* Surface-Specificity

Consider a molecular ML as a sample, which is covalently bound at a solid surface (Figure 2 (a), blue). If the ML is in contact with a medium (*e.g.* a solvent, grey), which is non-absorbing at the frequency of the sample, in principle any even or odd-order spectroscopic method can be used to obtain a signal from the sample, *i.e.* any method can be *surface-sensitive*. By the chemistry of the adsorption process, it can still be guaranteed that only molecules at the surface are detected.

If, however, a comparable number of molecules of the same type as in the ML is present also in the bulk solution (Figure 2 (b), blue), odd-order spectroscopic techniques cannot easily discriminate them from the ML, unless the spectroscopic properties (*e.g.* band positions) are modified by the presence of the surface. In such a case, even-order methods are beneficial, since the non-linear susceptibilities are exploited to single out the response from only non-centro-symmetric systems, *i.e.* the oriented ML. Consequently, even-order methods are *surface-specific*, as only molecules with a net polar orientation result in a signal. The same situation holds for a liquid-gas interface, where a preferentially oriented layer forms at the interface (Figure 2 (c)). The interfacial layer can then be discriminated by even-order spectroscopy from the subjacent isotropic bulk liquid as well as from evaporating isotropic gas-phase molecules. Note however that this does not necessarily imply that only a *single* layer of molecules bound to or located at the interface contributes to the even-order signal. It is rather all molecules that break the centro-symmetry. The presence of a surface may induce order up to several molecular layers away, which all contribute to an even-order signal.[50,133,134]

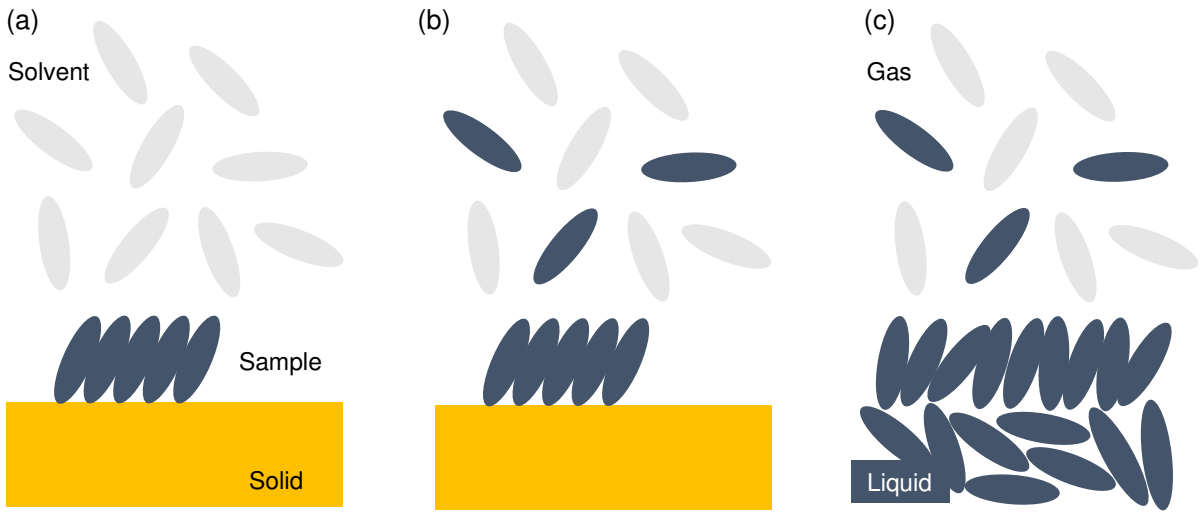

Figure 2. Schematic examples for systems, which can be investigated by surface-sensitive and surface-specific spectroscopy. (a) Example applicable for surface-sensitive spectroscopy (both even- and odd-order methods). Sample molecules (blue) arranged in a surface ML in contact with a non-absorbing solvent (grey). (b) and (c) Samples for which a surface-specific, even-order spectroscopy is required. In (b) a ML at a solid-liquid interface is in contact with an isotropic solution, which contains molecules that absorb at the same frequency as the ML. In (c) preferentially oriented molecules at a liquid-gas interface are in contact with a bulk liquid and gas-phase sample of the same type of absorbing molecules. Only a surface-specific spectroscopy can discriminate the preferentially oriented molecules in (b) and (c) from the isotropic environment.

2.1.3. 2D IR Spectroscopy at Surfaces

The differences in the underlying nonlinear susceptibilities have important consequences for the signal from both a theoretical and a technological point of view. Before moving to experimental aspects, we first briefly review the principles of 3rd- and 4th-order 2D IR spectroscopy.

2.1.3.1. 3rd-Order Spectroscopy

The relevant quantity for the lowest-order time-resolved spectroscopy considered here is the 3rd-order nonlinear polarization $P^{(3)}$, which is associated with $\chi^{(3)}$. In ultrafast spectroscopy, it is more convenient to use a time-domain instead of the frequency-domain representation of (eqn. 1). This reveals the time-domain polarization $P^{(3)}(t)$, (eqn. 4):[103]

$$P^{(3)}(t) \propto \left(\frac{i}{\hbar}\right)^3 \int_0^\infty dt_3 \int_0^\infty dt_2 \int_0^\infty dt_1 \, \mu_1 E_1(t-t_3)\mu_2 E_2(t-t_3-t_2)\mu_3 E_3(t-t_3-t_2-t_1) \cdot R^{(3)}(t_3, t_2, t_1)$$

(eqn. 4)

and the emitted signal field is given by:

$$E^{(3)}(t) \propto i \cdot P^{(3)}(t) \quad \text{(eqn. 5)}$$

$P^{(3)}(t)$ results from a convolution of the externally applied IR fields ($E_1(t)$, $E_2(t)$, $E_3(t)$) with the samples' response function $R^{(3)}(t)$. For all cases considered here, the applied IR fields are assumed to be resonant with a vibrational transition. Thus, they act three times on associated transition dipole moments $\mu_{1,2,3}$. The variables t_i are time intervals between successive light-matter interactions under the temporal envelope of the ultrashort laser pulses (Figure 3). In the limit of impulsive excitation, *i.e.* when the temporal duration of the pulses is short compared to the molecular dynamics, these variables can be substituted by experimentally controllable delay times between the pulses. These delay times are scanned to map the dynamics of the sample and to acquire multi-dimensional spectra.

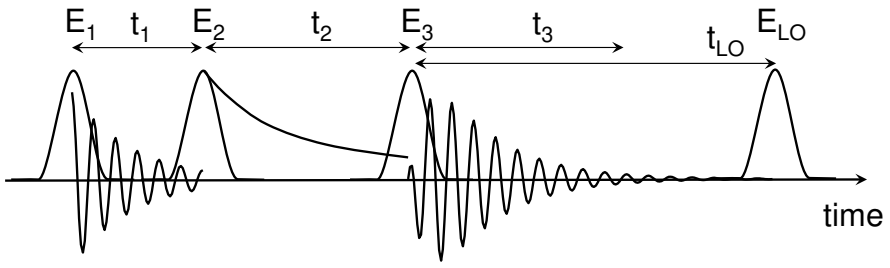

Figure 3. Pulse sequence for 3rd-order spectroscopy, including a LO field (E_{LO}) for heterodyne-detection (sections 2.1.4 and 2.1.5).[135] *Electric fields $E_{1,2,3}$ correspond to the input pulses, which induce the 3rd-order signal. Oscillatory lines correspond to vibrational free-induction decays (FID). The exponential decay following E_2 is associated with vibrational relaxation, for instance. Time runs from left to right and t_i correspond to intervals between light-matter interactions.*

The fourth field in Figure 3 is termed the local-oscillator (LO), which is employed in multi-dimensional spectroscopy in order to measure the signal field with its amplitude and phase, rather than just its intensity (sections 2.1.4 and 2.1.5). The response function $R^{(3)}(t)$ constitutes multiple pathways, through which the electric fields act on the sample and the signal is finally emitted.[71,103] To visualize the different pathways, we use energy-level diagrams (Figure 4) introduced by Albrecht et al.[136,137], in which horizontal lines represent vibrational states, and up-/down-pointing vertical arrows represent light-matter interactions with negative/positive (up) and positive/negative frequencies (down) for solid/dashed arrows, respectively. The fourth (wavy) arrow indicates signal generation and its interaction (μ_4) is included in $R^{(3)}(t)$ for simplicity (eqn. 4).

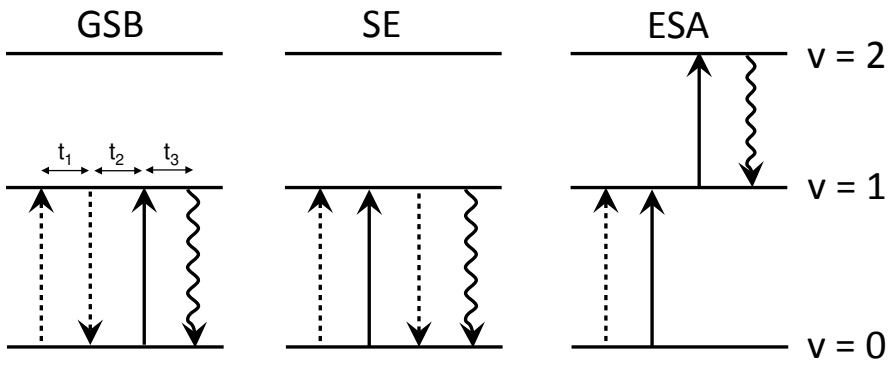

Figure 4. Energy level diagrams for 3rd-order IR spectroscopy. Only rephasing diagrams are shown for clarity. Vibrational states (v = 0, 1, 2) are represented by horizontal lines. Solid/dashed vertical arrows represent electric field interactions on the |ket⟩- and ⟨bra|-sides of the density matrix, respectively. Time runs from left to right in each diagram. Signal emission is indicated with a wavy arrow. GSB ≡ ground state bleach, SE ≡ stimulated emission, ESA ≡ excited state absorption.

2D IR involves two pump pulses and a single probe pulse. Since all vibrations considered here have frequencies with $\omega >> k_B T$, the entire population is present initially in the vibrational ground state (v = 0). For a standard 2D IR signal, one has to consider the three lowest vibrational levels, *i.e.* v = 0, 1, 2 (Figure 4). A first interaction with the field of one of

the pump pulses produces a vibrational coherence between the v = 0 and v = 1 states, which oscillates as a function of time t_1, which thus is often referred to as a "coherence time". The macroscopic polarization associated with the coherence of the many molecules from an ensemble will run out of phase over time (dephasing), resulting in a vibrational free-induction decay (FID, Figure 3).[71,103] The second pump interaction converts the initial 0-1 coherences to a population in v = 1 (Figure 4) or back in v = 0. Following the second interaction, the sample can undergo, *e.g.* vibrational relaxation from v = 1 back to v = 0 via energy dissipation to the environment, or to other parts of the same molecule through internal vibrational energy redistribution (IVR) during time t_2, which is referred to as the "population time". After a third interaction with the probe pulse, a vibrational coherence is again generated, the FID of which oscillates during the coherence time t_3 (Figure 3). The last coherence can be generated between the 0 and 1 levels, both as absorption as well as stimulated emission (Figure 4), or between the 1 and 2 levels as absorption. The 0-1 and 1-2 transitions result in different signs of the signal; that is, the 0-1 transition in a reduced absorption of the probe pulse, and the 1-2 transition in a newly induced absorbance. Therefore, these signals are termed ground state bleach/stimulated emission (GSB/SE) as well as excited state absorption (ESA), respectively. This description holds for the simple case of a single vibrational mode, which is not coupled to any other mode. In cases of coupled oscillators, more advanced descriptions apply, which have been worked out in detail elsewhere.[71,138–140] The total number of pathways can be grouped in "rephasing" as well as "non-rephasing" pathways[71,103], depending on the sequence of the positive/negative frequencies to generate the signal. These determine whether or not a vibrational echo is formed after the interaction of the third electric field.[140,141] For clarity, Figure 4 shows only the rephasing pathways for 3rd-order spectroscopy.

2D IR spectra are obtained after a 2D Fourier transformation of the emitted field as a function of coherence times t_1 and t_3.[71] This is done for a fixed population time t_2, and the shape of the

resulting 2D IR spectra will depend on t_2. To generate one frequency axis (ω_3), the signal can be dispersed in a spectrograph, effectively performing the Fourier transformation with respect to coherence time t_3. To generate the other frequency axis, the coherence delay (t_1) between the first two pump pulses has to be scanned in time.[71] This generates an oscillating signal in the time domain with respect to t_1, the Fourier transformation of which then results in the frequency axis ω_1.

The two spectral axes in a 2D IR signal are often called "pump" (ω_1) and "probe" axes (ω_3), and it is instructive to interpret a 2D IR spectrum as a pump-probe signal that is spectrally resolved with respect to both pump and probe frequencies.[142] Note, however, that the definition of pump and probe axes as horizontal and vertical axes is unfortunately not used in a unified way in the literature.[143] Although Figure 4 shows only rephasing pathways, all 2D IR spectra shown in this review represent *fully absorptive* spectra, which are generated experimentally from the sum of rephasing and non-rephasing pathways. Most 2D IR studies nowadays report on this type of signal.[71,103] The general concept of obtaining a 2D IR spectrum is similar for different experimental implementations of 3rd-order 2D IR, and technical details are discussed in Section 2.2.2.

2.1.3.2. 4th-order Spectroscopy

In order to make ultrafast 2D IR a strictly surface-specific method, one needs to go one order higher in nonlinearity, that is to $\chi^{(4)}$. This is done by addition of a fourth pulse to the three-pulse 2D IR sequence from Figure 3. The fourth electric field comes from a VIS pulse (green, Figure 5), which intercepts the FID of $P^{(3)}(t)$, and up-converts it to a VIS signal (blue). The VIS pulse is generally long in time, hence narrow in frequency, which defines the spectral resolution of the measurement (see 2.2.3 for details). Due to the summation of IR and VIS frequencies, the method is termed sum-frequency generation (SFG)

spectroscopy.[90,107,109,110,115,117,144,145] Note that in variance to 3rd-order 2D IR, the LO pulse for heterodyne detection (blue) also needs to be in the VIS spectral range.

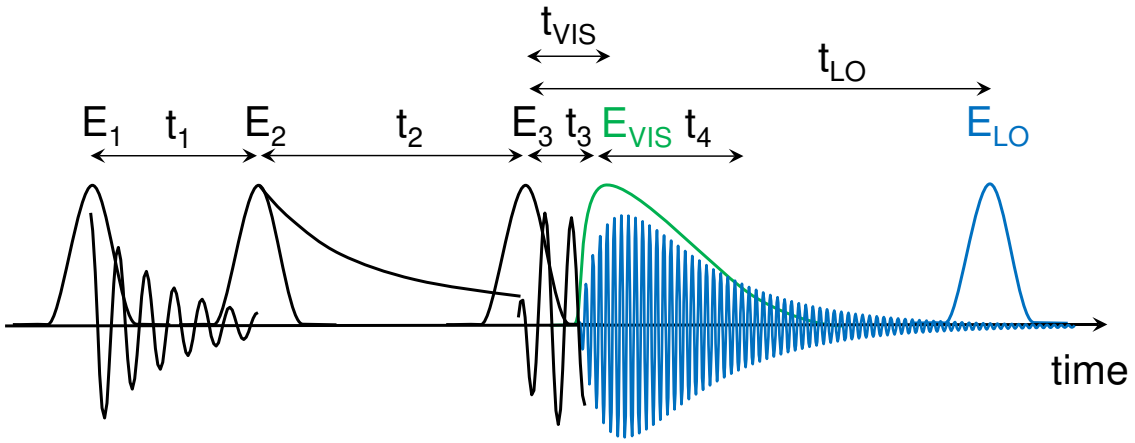

Figure 5. Pulse-sequence for 4th-order 2D SFG spectroscopy including a LO field (blue, E_{LO}) for heterodyne-detection. Electric fields $E_{1,2,3}$ (black) correspond to the input IR pulses. The green E_{VIS} pulse corresponds to the VIS up-conversion pulse, which generates a sum-frequency signal (blue). Oscillatory lines correspond to free-induction decay curves (FID). The exponential decay following E_2 is associated with vibrational relaxation, for instance. Time runs from left to right, and t_i correspond to intervals between light-matter interactions.

In analogy to (eqn. 4), the 4th-order polarization reads in a time-domain representation:

$$P^{(4)}(t) \propto \left(\frac{i}{\hbar}\right)^4 \int_0^\infty dt_4 \int_0^\infty dt_3 \int_0^\infty dt_2 \int_0^\infty dt_1 \, \mu_1 E_1(t-t_4)\mu_2 E_2(t-t_4-t_3)$$
$$\cdot \mu_3 E_3(t-t_4-t_3-t_2)\alpha E_{4,VIS}(t-t_4-t_3-t_2-t_1)R^{(4)}(t_4,t_3,t_2,t_1)$$

(eqn. 6)

A fourth integral enters the calculation of $P^{(4)}(t)$ from the corresponding response function $R^{(4)}(t)$. The frequency of the up-converting VIS pulse is generally tuned off-resonance to any molecular (*e.g.* electronic) transition. The laser pulses interact with the sample either through the transition dipole moments (IR, $\mu_{1,2,3}$) or the molecular polarizability (VIS, α). As above, the final signal generation interaction is included in the response function $R^{(4)}(t)$ for clarity. Since the VIS-interaction with a non-resonant (virtual) level is very short-lived (≈ 1 fs) in

comparison to the IR response (a few hundreds of femtoseconds to picoseconds), it is generally approximated as δ-shaped in the time domain.[135] The 4th-order response then reduces to:

$$R^{(4)}(t_4, t_3, t_2, t_1) = R^{(3)}(\, t_3, t_2, t_1) \cdot \delta(t_4) \qquad \text{(eqn. 7)}$$

Under this assumption, the integral over the VIS field collapses, and the expression for $P^{(4)}(t)$ simplifies to a three-fold integral over the IR fields:

$$P^{(4)}(t) \propto \left(\frac{i}{\hbar}\right)^4 \alpha E_{4,VIS}(t) \int_0^\infty dt_3 \int_0^\infty dt_2 \int_0^\infty dt_1 \, \mu_1 E_1(t - t_3) \mu_2 E_2(t - t_3 - t_2)$$
$$\cdot \, \mu_3 E_3(t - t_3 - t_2 - t_1) R^{(3)}(t_3, t_2, t_1)$$

(eqn. 8)

Again, $P^{(4)}(t)$ creates a signal field $E^{(4)}(t)$, which is emitted from the sample:

$$E^{(4)}(t) \propto i \cdot P^{(4)}(\, t) \qquad \text{(eqn. 9)}$$

According to (eqn. 8), the information content of $P^{(4)}(t)$ is very similar to $P^{(3)}(t)$, except that the polarizability (α) now enters. As a consequence, the sign of the signals in SFG now also depends on the orientation of the molecules with respect to the surface (see sections 2.1.1 and 3.2.2),[106,107,111,118,119] that is, GSB/SE and ESA can both result in positive or negative signals.

The 4th-order 2D SFG response functions can again be visualized in terms of energy level diagrams (Figure 6, only rephasing pathways are shown). Here, dashed horizontal lines represent the short-lived virtual states. In general, the 2D SFG energy level diagrams are very similar to 3rd-order 2D IR (Figure 4), except for the fourth, VIS field (green) for up-converting the signal (blue wavy arrow). The response function also comprises GSB/SE as well as ESA pathways. One has to keep in mind, however, that selection rules of the pump and probe processes are different due to the additional up-conversion process.

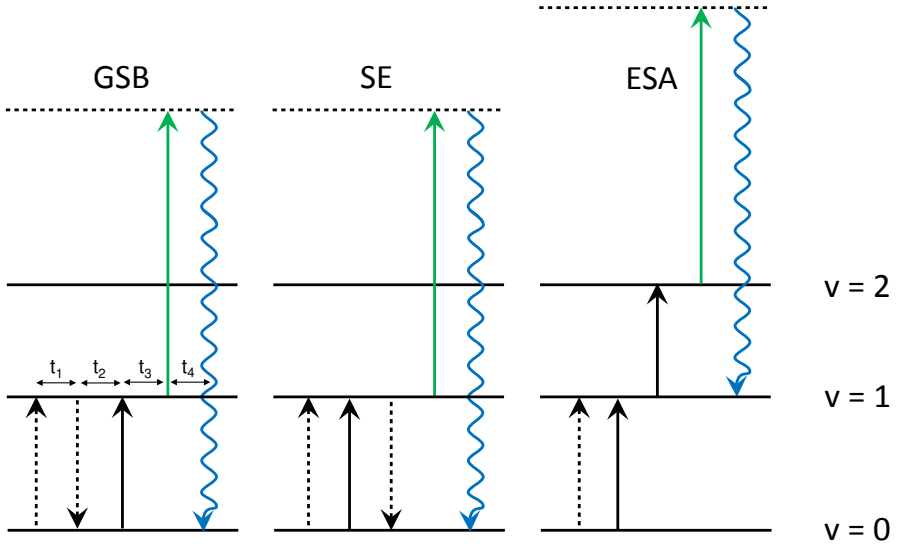

Figure 6. Energy level diagrams for 4th-order 2D SFG. Only rephasing diagrams are shown for clarity. Vibrational states (v = 0, 1, 2) are represented by solid horizontal lines, while virtual states are represented by dashed horizontal lines. Solid/dashed vertical arrows represent electric field interactions on the |ket⟩- and ⟨bra|-sides of the density matrix, respectively. Black arrows correspond to IR fields while green and blue arrows correspond to VIS fields. Time runs from left to right in each diagram. Signal emission is indicated with a wavy arrow. GSB ≡ ground state bleach, SE≡ excited state emission, ESA ≡ excited state absorption.

To generate a 4th-order 2D SFG signal, one needs to do exactly the same as for the generation of a 3rd-order 2D IR spectrum. That is, dispersion of the signal field $E^{(4)}(t)$ in a spectrograph results in the "probe" spectral axis. A Fourier transformation of the oscillating signal along t_1, which needs to be scanned explicitly, again gives the "pump" frequency axis. The final signal field encountered by the detector is located in the VIS spectral range and obeys the relationship $\omega_{sig} = \omega_{vis} + \omega_{vib}$. Knowing the spectrum of the VIS up-conversion pulse, the 2D SFG spectrum is commonly shifted back to the IR spectral range by subtracting the VIS center frequency from the signal frequency.

3rd- and 4th-order 2D IR spectra generally contain very similar information and have similar appearance. To highlight this, Figure 7 (a) shows an example of a 3rd-order 2D IR signal of a bulk solution sample of an α-helical peptide in bulk solution acquired in the spectral region of

the amide-I band (1635 cm^{-1}).[121] The different spectral contributions of GSB/SE (blue/cyan) and ESA (red/yellow) exhibit specific pattern and separation, which reports on molecular properties (as discussed in section 3).[121] Figure 7 (b) shows the same peptide as in (a), however, now immobilized on a Gold (Au) surface and measured with surface-specific 2D SFG.[121] Again, the signal exhibits GSB/SE as well as ESA contributions, which are of similarly high signal to noise ratio as compared to the 3rd-order 2D IR data. However, the features are spectrally shifted and different in shape due to the immobilization of the sample at the Au surface.[121] In many cases, 2D IR and 2D SFG spectra can be interpreted in a similar manner since they contain information from the same molecular parameters.

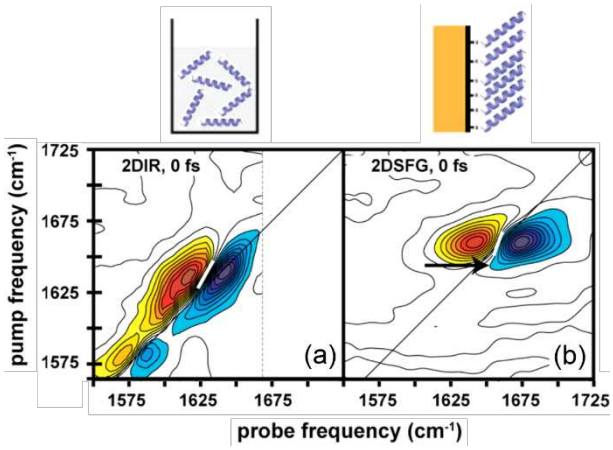

Figure 7. 2D IR (left) and complementary 2D SFG (right) spectrum from an α-helical peptide in either (a) solution or (b) as ML on an Au surface in the spectral region of the amide-I band. Both spectra show GSB/SE (cyan/blue) as well as ESA signals (yellow/red), however, with different frequencies due to the immobilization of the sample. Adapted with permission from ref.[121]*. Copyright (2014) American Chemical Society.*

2.1.4. Signal Field Detection

The emitted signal can be detected in two ways. First, it may be measured by a detector that records simply its intensity (homodyne detection), in which case all phase information is lost. While homodyne detection is practically non-existent in 3rd-order 2D IR spectroscopy, it is in use for 4th-order 2D SFG, as its experimental realization is much easier.[146–149] Alternatively, interferometry can be applied, where a so-called local oscillator (LO, Figure 3 and Figure 5)

with known field is overlaid with the signal field on the detector (heterodyne detection).[150–152] This results in the measured signal:

$$S = \left|E_{LO} + E_{sig}\right|^2 = |E_{LO}|^2 + \left|E_{sig}\right|^2 + 2\left|E_{LO}E_{sig}\right|\cos(\phi_{LO} - \phi_{sig}) \qquad \text{(eqn. 10)}$$

The general concept of heterodyne detection is the same for 3rd- and 4th-order 2D IR, and it involves the isolation of an interference term (last term in (eqn. 10)) from two other contributions, which can be either subtracted ($|E_{LO}|^2$) or neglected ($\left|E_{sig}\right|^2$) in the limiting case of $E_{\mathrm{LO}} >> E_{\mathrm{sig}}$. As a key-point, heterodyne-detection allows obtaining both amplitude and phase information of the signal. The phase is especially powerful in multi-dimensional spectroscopy, where molecular information is contained in the sign of the various peaks.[71]

2.1.5. Phasing of 2D IR Signals

In order to obtain interpretable 2D IR spectra after Fourier transformation, the spectra need to be "phased" in order to result in the sought absorptive response. Phasing is an important aspect in 2D IR spectroscopy, since it has an impact on spectral lineshapes.[71] Inaccurate phasing results in a mixing between absorptive and dispersive features in the 2D IR lineshapes. The quantity of interest is the phase difference between two pairs of electric fields, *i.e.* E_1/E_2 and E_3/E_{LO}.[71,151,153] Established phasing procedures are *e.g.* the signal projection onto the probe axis to match a reference pump-probe spectrum (projection slice theorem)[142,154], acquisition of an interferogram of spatially separated beams at the sample position[155,156], an interferogram from collinear pump pulse-pairs[157,158], or the application of a mid-IR phase-modulator to generate known and fixed phase differences of the electric field[159,160].

For heterodyne-detected even-order spectroscopy, different phasing methods have been developed as well, which rely on interferometry of a LO with the signal.[106–108,161–165] Phasing

in SFG is a considerably more difficult task, since the detected signal is in the VIS range, implying more stringent requirements regarding phase-stability of the setup. Despite tremendous technical development in heterodyne-detected VIS techniques[166], the short wavelength is still a challenge. The major differences between the various developed schemes for heterodyne-detected SFG 2D IR lie in the generation and the origin of the LO. The corresponding experimental layouts will be discussed in section 2.2.3.

2.2. Experimental Implementations

2.2.1. Overview

We start with an overview of the different layouts implemented by various research groups designed to obtain 2D IR signals from solid-liquid/gas interfaces. All 2D IR variants require three light-matter interactions between the IR pulses and the sample, which are controlled by two time delays. The basic difference between the methods lie in the way in which the signal is generated and detected. This is the origin of the different orders on nonlinearity ($\chi^{(3)}$ *vs.* $\chi^{(4)}$) and different degrees of experimental complexity. Each technique exhibits benefits and shortcomings, which need to be evaluated on a case-by-case basis in view of the specific application one has in mind. A schematic overview of the experimental configurations discussed here is shown in Figure 8.

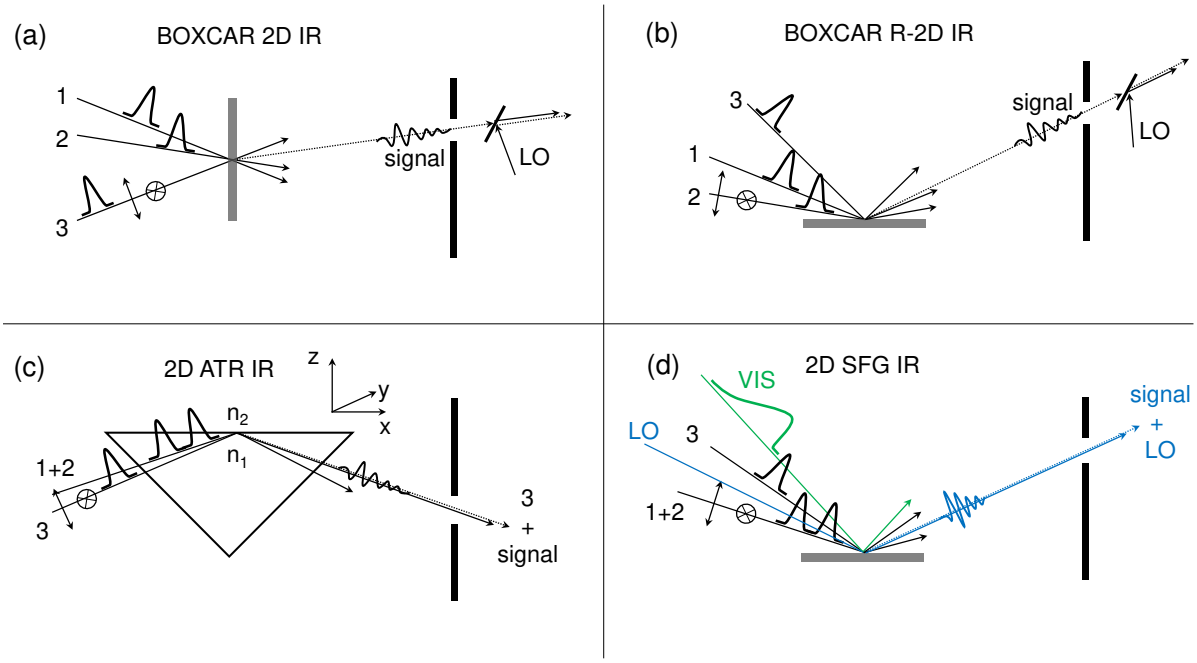

Figure 8. Experimental layouts for 2D IR spectroscopy at surfaces. (a) – (c) 3rd-order methods, (d) 4th-order spectroscopy. (a) BOXCAR 2D IR geometry in transmission mode. (b) BOXCAR geometry in reflection mode (R-2D IR). (c) 2D attenuated total reflectance (ATR) IR geometry. (d) 2D sum-frequency generation (SFG) IR spectroscopy. General definitions of s- and p-polarization with respect to the surface plane of the sample are indicated as arrows pointing to the paper plane and in the paper plane, respectively.

The three configurations for 3rd-order 2D IR (Figure 8 (a) – (c)) use up to three independent mid-IR beams, and work either in transmission or reflection mode. Figure 8 (a) shows the typical BOXCAR arrangement for 3rd-order 2D IR (section 2.2.2.1).[71,167–169] The three input beams are focused and spatially overlapped on the sample, and the signal light is emitted in the fourth corner of the box-arrangement defined by the input beams. The direction of emission is determined by the phase-matching of the incoming pulses.[103] All three input pulses (1, 2, and 3) have similar intensities and contribute a single light-matter interaction to the signal generation. Following spatial filtering, phase-sensitive detection of the signal light involves heterodyning with a LO. The BOXCAR technique can also be operated in an "external" reflection mode[170] (R-2D IR, Figure 8 (b)). In this case, the input beams are focused from the top onto the reflecting plane of a substrate, *e.g.* a metal layer, which is also

used for sample immobilization (section 2.2.2.2). As in transmission BOXCAR 2D IR, the signal is generated at the interface, however, it is now reflected from the surface, spatially filtered and again externally heterodyne detected. R-2D IR thus allows investigations on non-IR-transparent substrates. The BOXCAR geometry exhibits the highest sensitivity among all existing forms of 3rd-order 2D IR, since all three incident pulses exhibit the same intensity, and the LO intensity can be adjusted independently.[171]

The second form of reflective implementations of 3rd-order 2D IR exploits internal attenuated total reflectance (Figure 8 (c), 2D ATR IR).[172–177] 2D ATR IR (section 2.2.2.3) is designed as a two-beam pump-probe type[157,158,160] spectroscopy, in which an intense IR pump beam and a weak IR probe beam are spatially overlapped at a small angle (< 10°) at the sample interface. The pump pulse contributes two interactions and contains a collinear pump pulse pair (1 + 2), while the probe pulse contributes a single interaction. Contrasting to the external reflection arrangement (Figure 8 (b)), the two beams are incident from the bottom of the sample. The substrate-sample interface is a single reflecting plane of an ATR substrate with a refractive index (n_1), which is higher than that of the sample (n_2). The sample molecules are immobilized at the reflecting ATR interface, and can be in contact with any medium that has a lower refractive index than the ATR material. The intensity of pump and probe beams is strongly different, and the intensity of the intrinsic LO (the probe beam itself) relative to the signal cannot be adjusted independently. As such, 2D ATR IR generally has a lower sensitivity as compared to the BOXCAR arrangements. It is nevertheless used, since it is experimentally simpler, in essence avoids the application of an external LO for phasing, and enables a smaller angle between the two beams.

Finally, 2D SFG (Figure 8 (d), see section 2.2.3) is considered as the only truly surface-specific method among the four presented layouts. 2D SFG employs three beams for signal generation that are focused on the interface at small angles (< 10°), and angles relative to the

surface normal of about 60 – 75°. These are the two IR beams (black, Figure 8 (d)) for excitation and probing, and one VIS beam for spectral up-conversion (green). As in R-2D IR spectroscopy, all current implementations for 2D SFG enter the sample-substrate interface from the top. The excitation pulse contributes two interactions and contains a collinear pump pulse pair (1 + 2), while the probe and VIS up-conversion pulses each contribute a single interaction. Phase-matching of the input beams determines the direction of signal emission (dashed blue) and the signal is spatially filtered from the excitation beams. The LO pulse (solid blue) for heterodyne signal detection is incident on sample with an angle, such that it spatially overlaps with the signal field.[135]

In the following sections, we will discuss the various schemes, and their specific strengths and weaknesses, in more detail.

2.2.2. Details on 3rd-Order Methods of 2D IR

2.2.2.1. BOXCAR Transmission Configuration of Surface-Sensitive 2D IR

Due to its high sensitivity, the BOXCAR geometry (Figure 8 (a)) is often considered advantageous for surface-sensitive 3rd-order 2D IR in transmission, since the number of contributing molecules is low at the interface (section 1.2).[19] BOXCAR 2D IR moreover allows and requires measuring the rephasing and non-rephasing response signals separately, from which an absorptive 2D IR spectrum is obtained as the sum of the two. Furthermore, one may also collect complimentary time-domain signals such as from heterodyne-detected transient gratings or photon-echo peak-shifts.[151,152,178–180]

In the standard transmission BOXCAR geometry, only IR transparent samples can be measured. In order to minimize the background from strongly absorbing solvents, experimental geometries generally require a very thin (< 50 μm) path-length of the sample cells. For the immobilization of molecules with established chemistry of surface-

functionalization, one often coats an IR-transparent window (*e.g.* CaF_2) with a thin layer of another substrate material such as SiO_2. To that end, plasma-enhanced chemical vapor deposition (PECVD) has been used.[181–183] The requirement of high IR transmission of that layer demands thicknesses on the order of a few tens up to about hundred nanometers. SiO_2 can afterwards be functionalized by chloro-silanes or acidic groups (carboxylic acids or phosphonic acids).

The average alignment of the sample molecules at the interface can be determined from the dichroic ratio of polarization-dependent experiments.[181–184] As the polarization of all three incident beams can be independently controlled, the polarization-dependent vibrational dynamics (*e.g.* anisotropy) can be measured.[183,185–187] Also the relative orientation of the sample with respect to the beam propagation can be adjusted in an angular range in which the substrate does not exhibit too high reflectance. However, most experiments so far have been performed using either the Brewster angle of the window material, or normal incidence of the beams.[23,181–183,185] The strengths of transmission BOXCAR 2D IR have been demonstrated by Fayer et al. in a series of studies employing MLs, which contained metal-carbonyl complexes with strong extinction coefficients ($> 1000\ M^{-1}\ cm^{-1}$).[181,188,189] Experiments have been performed under different experimental conditions, also elucidating the impact of sample immobilization by in-depth comparison between bulk solution and ML dynamics (section 3.2.1.1).

2.2.2.2. External Reflectance 2D IR Spectroscopy

Very recently, 3rd-order BOXCAR 2D IR has been realized in external reflection geometry (R-2D IR) also by Fayer et al.. In this variant, pump and probe pulses are incident on the sample from the top (Figure 8 (b)).[170] The experimental layout was used to study ultrafast dynamics of organic MLs on single crystal surfaces of Au at the solid-gas interface. The

polarization in BOXCAR R-2D IR is always perpendicular to the surface, allowing the observation of vibrational bands with transition dipole components along the surface normal.[170,190] This is due to the approximately π phase-change upon reflection for in-surface-plane field components, nearly independent of the angle of incidence (AOI). The polarization component along the surface normal is enhanced also in external reflection,[190] however, in a way that strongly depends on the AOI. Thus, an optimization of this parameter is beneficial in order to enhance the signal, the details of which have been worked out theoretically.[170,190,191] In general, a larger AOI increases the electric field components normal to the surface, and an approximately two-fold enhancement of the signal (compared to a transmission geometry layout) has been achieved.

2.2.2.3. 2D Attenuated Total Reflectance IR Spectroscopy

The ATR geometry can largely eliminate the background problem from strongly absorbing solvents and is therefore used extensively for linear FTIR spectroscopy.[1,122,192–197] Recently, the approach has been extended towards 3rd-order 2D ATR IR spectroscopy in order to elucidate the vibrational dynamics at solid-liquid/gas interfaces.[172–177] Ultrafast vibrational dynamics have been resolved from carbon monoxide (CO) bound to different types of metal nanoparticles[172] and under electrochemical conditions[175], or from self-assembled organic MLs on metal surfaces[173,174]. In addition to this, surface-enhancement effects from the presence of metal nanoparticles have been resolved[176] and optimized towards multi-photon vibrational ladder-climbing on a surface[177].

While the methods described in the previous sections, *i.e.*, 2D IR in transmission and external reflection, do not differ much from 2D IR in solution phase in terms of the optical design, ATR spectroscopy brings about a couple of new aspects, which originate from the total internal reflection. In general, total internal reflection occurs when light coming from an

optically denser medium encounters an interface to an optically rarer medium at an AOI that exceeds the so-called critical angle (θ_c):[1,72,122,192,193]

$$\theta_c = arcsin\left(\frac{n_2(\omega)}{n_1(\omega)}\right) \quad \text{(eqn. 11)}$$

The AOI is defined with respect to the normal of the surface plane (*x*-*y*, Figure 8 (c)). The critical angle θ_c depends on the ratio ($n_2(\omega)/n_1(\omega)$), with $n_2(\omega)$ and $n_1(\omega)$ being the frequency-dependent refractive indices of the optically rarer medium (the sample) and the optically denser medium (the ATR substrate), respectively; that is $n_2(\omega) < n_1(\omega)$ (Figure 8 (c)). (eqn. 11) implies a large range of acceptable AOIs when the difference between the two refractive indices ratio is high.[122,193,194,198] At the interface, the electric field of the incident wave generates an evanescent wave (E_{ev}) in the medium of lower refractive index, which decays exponentially with increasing surface distance *z*,

$$E_{ev}(z) = E_0 exp\left[-\frac{z}{d_p}\right] \quad \text{(eqn. 12)}$$

where E_0 is the electric field strength at the interface and d_p the penetration depth.[72,194,198] The exponential decay of E_{ev} results from the fact that the wave-vector of the incident electric field becomes imaginary beyond the interface.[199–201] The evanescent wave E_{ev} is the central quantity in ATR spectroscopy, which is in variance to transmission experiments, where plane waves are considered. Due to its non-propagating nature in the *z*-direction, a few differences exist with respect to the local electric fields between ATR spectroscopy and transmission experiments, as discussed in the following.

The polarization of E_{ev} may for instance differ from the polarization of the incident fields.[176,202] That is, an incident p-polarized wave results in both *x*- and *z*-components in the sample, *i.e.*, an elliptically polarized E_{ev}, whose degree of ellipticity depends on the AOI.[176,202,203] Contrasting to that, s-polarized light generates an exclusive *y*-component of E_{ev}.

Due to the elliptically-polarized E_{ev} for p-polarized light, determination of orientational dynamics of adsorbates at interfaces is not as straightforward as in transmission experiments.[202,204] A common strategy in ATR absorption experiments is to work close to the critical angle[204] in order to generate a linearly polarized E_{ev}. However, this has not been implemented yet in 2D ATR IR, because of occurring lineshape distortions for AOIs too close to θ_c (*vide infra*).

The penetration depth depends on multiple experimental parameters, *i.e.* the two refractive indices at the interface, the frequency of the incident light and its polarization, as well as the AOI.[205,206] It is convenient to consider two penetration depths ($d_{s,p}$) for s/p-polarizations.[205] The $d_{s,p}$ values can be tuned selectively for different substrates. To illustrate this, Figure 9 shows three different substrate/sample systems, which can be employed in 2D ATR IR (ZnSe (2.43) / ZrO_2 (2.01) / CaF_2 (1.40)). The sample medium is assumed to have a refractive index n_2 = 1.35 (*e.g.* water, at a wavelength of 5 µm). In general, the penetration depth of p-polarized light (red) is larger than that for s-polarized light (black), and all curves approach zero for AOIs near 90°. Near θ_c, the penetration depths steeply increase. Moreover, the difference in $d_{s,p}$ curves is larger for substrates with a larger refractive index (ZnSe > ZrO_2 > CaF_2).

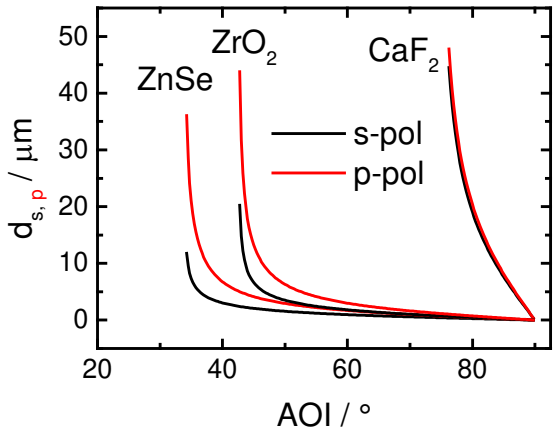

Figure 9. Dependence of the penetration depth for s- and p-polarization ($d_{s,p}$) as a function of the AOI for ZnSe, ZrO_2, and CaF_2 in contact with a medium of refractive index n_2 = 1.35,

calculated for radiation of λ = 5μm. Red curves correspond to p-polarization, while black curves correspond to s-polarization.

The interfacial electric field strength is enhanced due to overlapping incoming and outgoing electric fields as well as the generation of a surface polarization by the incident field.[200,207] The electric field vectors in all three dimensions ($E_{0,x,y,z}$, Figure 8 (c)), however, exhibit different dependences on the AOI and the $n_{1/2}$ values. The highest field strengths occur near θ_c, while close to an AOI of 90° all field intensities approach zero.[203,205,199,205] Furthermore, in case of absorbing media, the refractive index of the sample (n_2) becomes complex-valued. As a result, θ_c is not sharply defined anymore and a more gradual increase of the reflectivity occurs with AOIs farther away from θ_c.[199] High reflectivity of the ATR interface is, however, strongly desired due to the generally weak intensity of the probe pulse in pump-probe-type 2D ATR IR.[172] Thus, it is advantageous to work with AOIs exceeding θ_c by about 10° or more.

In the existing reports on 2D ATR IR[172–177], CaF_2 has been used as an ATR material despite its low refractive index in the mid-IR spectral range (n = 1.4 at 5 μm). CaF_2 exhibits distinct advantages for applications in ultrafast IR spectroscopy over more commonly used ATR materials such as Ge, Si. The limitation of these semiconductor materials is their low band gap, which can easily be excited by the intense IR pulses via multi-photon absorption. CaF_2, in contrast, is highly transparent in a very broad spectral range from the mid-IR to the UV, and furthermore is a cheap, non-toxic and easily available material that is much less susceptible to mechanical stress compared to, *e.g.* BaF_2, as another example for a widely used IR-transparent material in ultrafast IR spectroscopy. Other ATR materials exist (ZrO_2, ZnSe), which exhibit a higher refractive index than CaF_2 and thus support a broader range of solvents with higher refractive index (*e.g.*, DMSO, DMF, decane). Also ZnSe is a semiconductor with a fairly low band gap, but if the pump power is kept below a certain threshold (≈500 nJ with a 200 μm beam diameter), multiphoton absorption is negligible. ZrO_2 would be ideal in terms

of its optical properties, but is not a common material, so prisms need to be custom made and thus are significantly more expensive than CaF_2 or ZnSe.

Due to the smaller number of beams, which allows smaller AOIs, it is advantageous to implement 2D ATR IR in pump-probe geometry[157,158,160]. Compared to the BOXCAR geometry, the pump-probe 2D IR layout has a lower sensitivity due to the fact that the LO intensity cannot be adjusted independently.[157,160,166,171] Its inherent heterodyne-detection (Figure 8 (c)) however greatly simplifies the phasing procedure, since the relative phase of the signal light and the probe pulse is automatically set. Therefore, only the phase difference of the pump pulse pair defines the phase of the 2D IR signal, which in turn can easily be monitored and measured during a scan for obtaining the 2D data.[158] Finally, 2D ATR IR in the pump-probe geometry automatically measures purely absorptive spectra without the need to independently measure the rephasing/non-rephasing signals and add them.

Traditionally, ATR IR absorption spectroscopy is performed in multi-reflection geometries in order to increase the signal strengths and S/N ratio.[193,194,208] Contrasting to that, ultrafast 2D ATR IR has to be implemented in a single reflection mode[172–177] due to the required spatial overlap of pump and probe pulses. The much smaller ATR prisms then also reduce the dispersion of the ultrashort pulses inside the prism, which can be pre-compensated.[176,209]

Sputter-coated, ultrathin (< 10 nm) metal layers haven been employed as substrates in 2D ATR IR spectroscopy for the straightforward immobilization of molecules with thiol-linkers[19] in analogy to immobilization techniques known from external reflection and ATR IR absorption spectroscopy.[122,210–212] Such nano-structured layers enhance the nonlinear signal by plasmonic effects, and thus enable the measurement of ML of even very weak absorbers with extinction coefficients $\varepsilon < 200\ M^{-1}\ cm^{-1}$.[173,174] Figure 10 (a) and (b) shows an example of 2D ATR IR spectra of *para*-mercaptobenzonitrile on sputtered Au surfaces (average thickness 1 nm) and immersed in diethylether. Despite the only low extinction coefficient of the nitrile

label ($\varepsilon \approx 170\ M^{-1}cm^{-1}$), vibrational dynamics can be recorded over multiple integers of the corresponding vibrational lifetime (~ 8 ps)[174] due to an approximately 50-fold signal enhancement.[176] Enhancement factors from the nano-structured surfaces can be tuned with the metal layer thickness (section 3.4)[177], but metal layers of > 10 nm have not been used in 2D ATR IR so far, mainly to avoid lineshape distortions and intrinsic absorption of the metal layer (*vide infra*). Other deposition techniques such as electrochemical deposition, or chemical vapor deposition (CVD) are applicable as well, which also result in nano-structured surfaces. Regarding the preparation of crystalline surfaces for 2D ATR IR, atomic layer deposition (ALD) of layers with nm-thickness[213] could in principle be used, but has not been tested as of yet.

Signal-enhancing metal layers are, however, not necessary to resolve interfacial vibrational dynamics of adsorbates with 2D ATR IR. The surfaces from semiconductor oxides can be functionalized with carboxylic[214] or phosphonic acids[215] and are similarly suited for 2D ATR IR spectroscopy. Figure 10 (c) and (d) shows as an example 2D ATR IR spectra from a ML of Re(4,4′-dicarboxyl-2,2′-bipyridine)$(CO)_3Cl$ immobilized at sputter-coated Indium-Tin-Oxide (ITO) surfaces with a thickness of 5 nm and in contact with Methanol. The 2D ATR IR spectra show well-resolved diagonal and cross-peaks from the symmetric (~2025 cm^{-1}) and asymmetric (1880 – 1940 cm^{-1}) stretching vibrations of the tricarbonyl ligands. These features report on intramolecular vibrational coupling and energy transfer of the adsorbate molecules, similar as known from metal tricarbonyl complexes in bulk solution.[216,217]. The vibrational dynamics can again be followed over multiple integers of the vibrational lifetime (here: about 20 ps)[22].

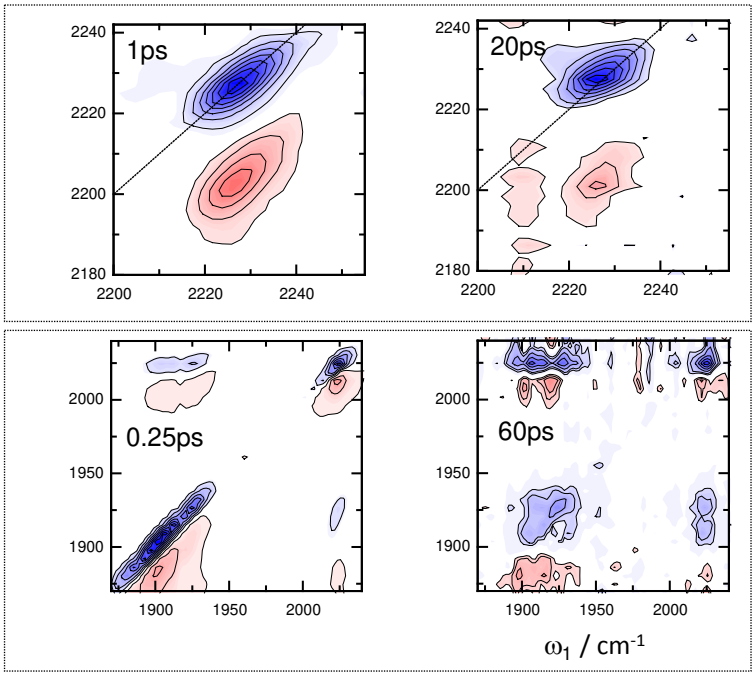

Figure 10. (a) and (b) Surface-enhanced and (c) and (d) non-surface enhanced 2D ATR IR spectra for different samples at solid-liquid interfaces and at the indicated population delays. (a) and (b) para-mercaptobenzonitrile (p-PhCN) on 1 nm Au immersed in Diethylether, and (c) and (d) Re(4,4'-dicarboxyl-2,2'-bipyridine)(CO)$_3$Cl on 5 nm ITO and immersed in Methanol.

An important effect in 2D ATR IR spectroscopy is related to distortions of the vibrational lineshapes for AOIs close to θ_c.[205,218–220] This effect originates from the wavelength-dependence of the samples` refractive index, which induces a wavelength-dependent penetration depth in the vicinity of a resonance. This is of particular importance when working close to θ_c, where a minimal change in the refractive index results in a large variation of the penetration depth.[205] In addition, the variation of the penetration depth becomes stronger with increasing extinction coefficients of the sample.[205] As both absorption and dispersion of the sample contribute to the refractive index n_2, this effect can result in the presence of dispersive contributions to the measured spectrum (anomalous dispersion).[205,218–220] To illustrate this effect, Figure 11 shows 2D ATR IR spectra of a strongly absorbing model compound, *i.e.* $Cr(CO)_6$ dissolved in bulk acetonitrile, on a CaF_2 prism for two different AOI values. When working far away (*i.e.*, ~ 85°) from θ_c, which is about 75° for this sample

substrate system, the 2D ATR IR spectra exhibit only GSB/SE (blue) as well as ESA bands (red) (Figure 11 (a)). A reduction of the AOI (~ 80°) closer to θ_c, the presence of anomalous dispersion induces spectral changes to the 2D ATR IR signals. These are discernible by dispersion-induced contributions on the high-frequency side of the GSB/SE band (arrow in (b)). Such changes might be artificially interpreted as ESA-like signal contributions.[221–223] Therefore, an optimization of the AOI in a 2D ATR IR experiment involves removing the anomalous dispersion effect in the spectra.

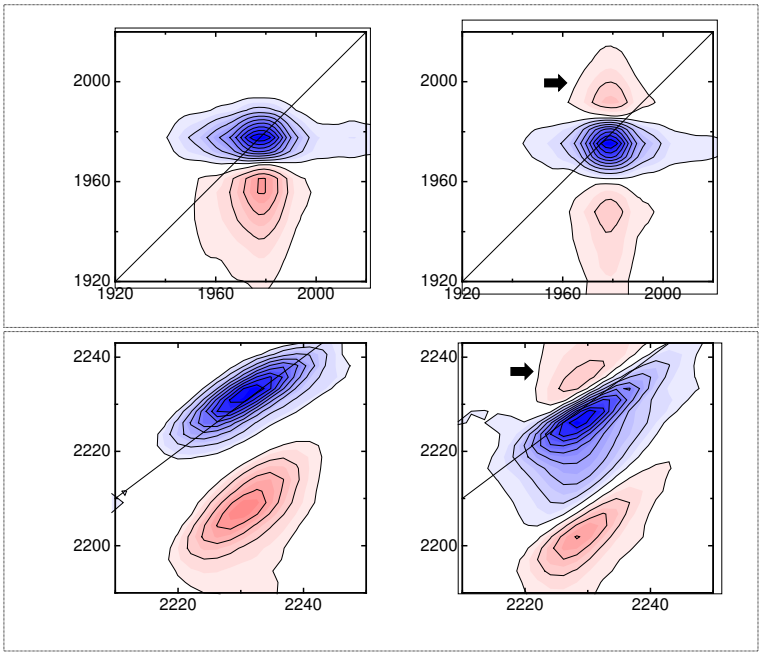

Figure 11. Two sources of lineshape distortions in 2D ATR IR spectroscopy. (a) and (b) Influence of the AOI for a bulk solution sample. 2D ATR IR spectra of an isotropic solution of $Cr(CO)_6$ in MeCN on a CaF_2 prism with an AOI of (a) ~ 85° (absent distortion) and (b) ~ 80° (present distortion). (c) and (d) Influence of a plasmonic metal layer. 2D ATR IR spectra of a ML on para-mercaptobenzonitrile on sputter-coated Ag layers of (c) 1 nm (absent distortion) and (d) 1.5 nm thickness (present distortion) on CaF_2 prisms. Effects of lineshape distortions are marked with arrows. All spectra are measured with s-polarization.

A second source of lineshape distortions in 2D ATR IR can occur for adsorbates at nano-structured, plasmonic metal layers, which are often used for sample immobilization.[224–229] Here, the distortion originates from the involvement of enhanced optical near-fields around the polarizable nano-structures in the excitation process of the adsorbate (see also section 3.4).

The optical near-fields are interpreted as scattering of the incident IR light from the highly polarizable nano-structure.[229–231] The resulting adsorbate spectra often exhibit so-called Fano-type asymmetric lineshapes, which result from the interference between the discrete resonances from the adsorbate with a broadband continuum from the metal layer.[229,230,232–235] The band shapes can thus be tuned experimentally by controlling the dielectric function of the metal layer, which is determined by the type of the metal, its thickness or microscopic morphology.[227,228] The distortion effect can contribute even for experimental geometries, for which the AOI has been optimized to eliminate anomalous dispersion as discussed above. To illustrate this, Figure 11 (c) and (d) show 2D ATR IR spectra of a ML samples of para-mercaptobenzonitrile (p-PhCN) adsorbed on ultrathin silver (Ag) layers of (c) 1 nm and (d) 1.5 nm average thickness. For the 1 nm thickness, the GSB/SE and ESA signals of the CN stretch vibration appear undistorted, whereas slightly thicker Ag layers of 1.5 nm result in the appearance of dispersive signals on the blue-detuned side of the GSB/SE band (arrow). For the reported 2D ATR IR studies, this effect has been eliminated by tuning of the metal layer thickness of the substrate.[172–177]

It is important to note that Fano-type lineshapes are not unique to ATR IR spectroscopy. In a very general sense, such lineshape distortions can occur for various vibrational spectroscopic methods, which involve plasmonic and or metallic sample substrates[236], thus also for SFG[237–241], SERS[242–245] transmission[227–229], ATR[220,224,225] and even more specialized methods such as high-resolution electron energy loss (HREEL)[246,247] spectroscopy.

2.2.3. 2D Sum-Frequency Generation Spectroscopy

In its initial implementation, 2D SFG was used as a homodyne-detected method for investigations of liquid-air interfaces.[146–149,248] These experiments have been the first to demonstrate that multi-dimensional vibrational spectroscopy can be extended to monolayer

thin samples at interfaces. The implementation of heterodyne-detection (Figure 8 (d)) afterwards considerably advanced 2D SFG regarding interpretation of the obtained spectra. 2D SFG at solid-liquid interfaces has a broad range of applications and has been used to study surface-specific signals of CO adsorbed to Platinum electrodes[135], surface-bound peptides[121] and DNA strands[249], amyloid fibers[250] as well as metal-carbonyl electro-catalysts[49,251,252].

Most conveniently, an 800 nm VIS pulse from a Ti:S amplifier is used for the up-conversion, which is spectrally narrowed to approximately 1 nm bandwidth (~15 cm^{-1}) by use of an interference filter, for instance. Alternative methods are available for producing the up-conversion pulse[163] such as notch filters, etalons or grating-slit combinations. The spectral filtering stretches the pulse significantly in time and typically generates an asymmetric temporal profile with a single-sided exponential decay.[253,254] The temporal delay between the IR probe and the VIS pulse is often set to zero in order to cover the complete temporal range of the vibrational FID for up-conversion. However, applications for non-zero delays exist as well for SFG spectroscopy, mostly aiming at reducing short-lived non-resonant background signal contributions, but such delays also alter the vibrational lineshape artificially.[163,253]

It is well known from $\chi^{(2)}$ SFG spectroscopy that the signal spectrum depends on the temporal shape of the up-conversion pulse.[163] The single-sided exponential decay temporal profile of the VIS pulse leads to slight spectral distortions of a 2D SFG spectrum. This was demonstrated for the case of CO adsorbed to polycrystalline Platinum (Pt) electrode.[135] Figure 12 (a) and (b) show model calculations, assuming a VIS pulse profile with a 600 fs single sided exponential decay (panel (a)) or an infinitely spectrally narrow, continuous wave (cw) VIS field (panel (b)). The latter gives the direct 2D IR response, since it covers the entire vibrational FID. While both simulations reveal the same response in the ω_1 direction, the ω_3 response is slightly broadened in Figure 12 (a). This is due to the VIS pulse acting as a window function on the FID.[135]

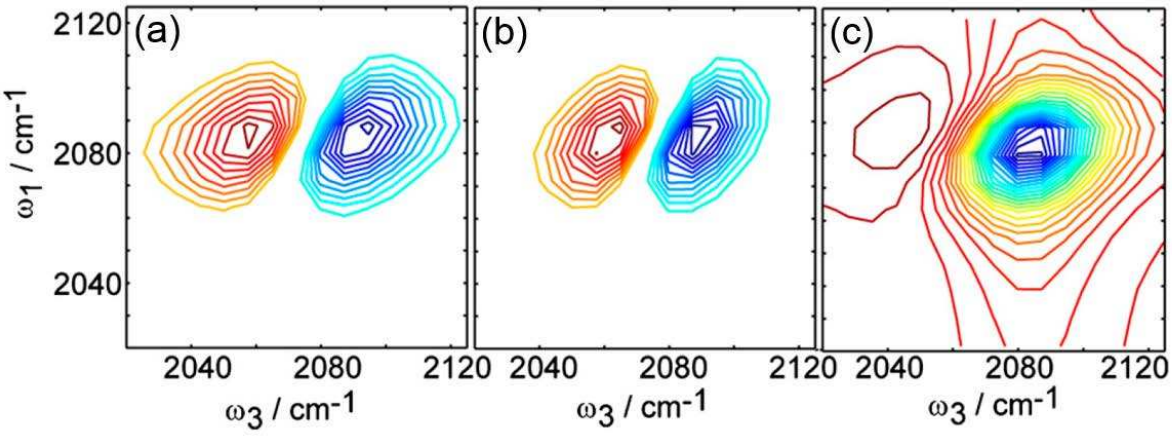

Figure 12. Effect of the LO on the shape of simulated 2D SFG spectra for CO on a Pt surface.[135] *The VIS up-conversion pulse is simulated as a single-sided exponential with decay time 600 fs in (a) and as cw-light in (b). Panel (c) shows a simulated 2D SFG spectrum with the intrinsic* $\chi^{(2)}$ *SFG FID as LO. Adapted with permission from ref.*[135]*. Copyright (2011) National Academy of Sciences.*

Experimentally, a compromise has to be found between the intensity of the up-conversion pulse, spectral resolution and distortions of the spectra. Regarding intensity of the up-conversion pulse, it is important that the signal intensity depends on the pulse duration.[255] A narrower VIS spectrum results in a better frequency resolution and less spectral distortion, but at the same time in lower signal magnitudes. Alternative methods for up-conversion also exist, which directly sample the vibrational FID in the time domain.[163] The latter method therefore circumvents spectral distortion in the ω_3 axis. However, an additional temporal delay needs to be scanned in this case, which is time consuming and has only been implemented for $\chi^{(2)}$ SFG so far.

Initial studies of 2D SFG without an external LO beam employed intrinsic heterodyne-detection by use of the $\chi^{(2)}$ SFG signal, which co-propagated with the $\chi^{(4)}$ signal in case of the experimental geometry depicted in Figure 8 (d).[148,149] This approach leads to more complicated signals, whose analysis requires detailed simulations.[135,146] To demonstrate this, Figure 12 (c) shows a calculated 2D SFG spectrum of CO on Pt with the $\chi^{(2)}$ SFG response

used as intrinsic LO, instead of external (broadband) heterodyning (Figure 12 (a) and (b)). Since the $\chi^{(2)}$ SFG spectrum exhibits only the spectral width of the 0-1 transition, it is not broad enough to cover both the 0-1 and 1-2 transitions with equal intensity. Thus, the 0-1 response is strongly enhanced over the red-shifted 1-2 transition. This highlights the necessity for 2D SFG to get rid of the $\chi^{(2)}$-based SFG spectrum and to employ an external LO.

An external LO beam can be generated by frequency mixing of a part of the IR light with a portion of the spectrally-narrowed VIS pulse in a nonlinear crystal (*e.g.* 5% Mg:$LiNbO_3$).[135] This LO is then overlaid on the sample with an angle, such that the reflected LO beam matches the direction of the signal emission beam (Figure 8 (d)). The signal and the LO beams co-propagate to the detector and the delay between the two can be adjusted by a pair of ZnSe wedges.[135] Regarding the phase-stability between the LO and the signal in SFG spectroscopy, realizations exist, which can be as good as only a few degrees over the course of up to ten hours.[161]

As an alternative to the external generation of a LO field, non-resonant signals from substrates such as reflecting metal layers have been used as "intrinsic" LOs.[119,121,249] Due to the instantaneous response of the metal, non-resonant background signals are temporally short (and thus spectrally broad), and have a defined phase with respect to the signal.[256] Although this method is experimentally much easier compared to the implementation of an external LO, application of intrinsic LO fields always requires a careful validation of the phase relationship with respect to the signal. Phasing of the 2D SFG signal sign can afterwards be done by comparison with reference samples.[249] Independent of that, optimization of the LO intensity can be used to control the signal magnitude of the heterodyned term (eqn. 10).

In order to remove unwanted signal contributions (*i.e.* the $\chi^{(2)}$-response or light scattering), to speed up data acquisition, and to facilitate phasing, some 2D SFG works at solid-liquid/gas interfaces have employed a mid-IR pulse-shaper (acousto-optic modulator, AOM) to generate

phase-stable coherent pairs of pump pulses in a single IR excitation beam (Figure 8 (d)). The application of an AOM is beneficial since it allows facile generation of t_1 delays, as well as easy phase-cycling for scatter-suppression and data collection in the rotating frame.[135,163] In a pump-probe configuration, which is most commonly used, the signal beam contains both the sought $\chi^{(4)}$ response as well as the $\chi^{(2)}$ response. Due to two orders lower nonlinearity, the latter is much stronger than the former,[135,165] but it can be eliminated by phase-cycling.[135] Alternatively, the two pump interactions may be spatially separated,[257] resulting in different directions of the emitted $\chi^{(2)}$ and $\chi^{(4)}$ signals.

The AOI as well as polarizations of the incident beams determine the signal intensity also in 2D SFG.[115,258] Typically, the IR beams exhibit a more grazing AOI (in the order of 60-75°) as compared to the VIS beam (Figure 8 (d)). Depending on the substrate, it is advantageous to use p- or s-polarized incident light in external reflection 2D SFG. For instance, intensity maximization on strongly polarizable substrates, such as metal surfaces, occurs for p-polarized light[121,135,249,250], while s-polarized contributions are suppressed.[170,190] Contrasting to that, weak dielectric surfaces exhibit very low reflectivity of p-polarized light.[161,258] In most implementations of 2D SFG at for instance solid-liquid interfaces, all pulses exhibit p-polarization owing to the application of metal surfaces for immobilization.[121,135,249,250] A full control of the polarization in 2D SFG is a powerful tool to study the sample orientation and the SFG-activity of certain modes.[111,161] Note that the metal-surface selection rule (section 2.1.1) applies for 2D SFG as well, which prevents measuring transition dipole components of samples that are parallel to a highly polarizable surface.[121]

Compared to 3rd-order 2D IR methods, some practically relevant differences exist for 2D SFG. For instance, the high intensity of the incident beams, especially the VIS up-conversion beam, can make it necessary to spatially translate the sample in order to prevent sample degradation.[49,119] This is particularly important for thermally susceptible samples, such as

biological molecules, or for substrates that absorb in the spectral region of the up-conversion pulse. In addition, 2D SFG requires multiple optical frequencies and at least three input beams, resulting in a rather complex setup. Moreover, the signal is generated in the VIS spectral range, which requires an about tenfold higher phase-stability between the LO and the signal compared to the mid-IR range. Finally, when the IR beams impinge on the sample in external reflection, the mid-IR beam may need to travel through an absorbing solvent. This reduces the IR intensity at the interface, just as in case of transmission and external reflection 2D IR.

Although all 2D SFG spectra from solid-liquid/gas interfaces reported so far have been acquired in an external reflection configuration (Figure 8 (d)), the method should in principle be applicable in internal reflection geometry as well, or even in a combined internal/external reflection scheme.[50,114,258–262] It might therefore be possible in future extensions of 2D SFG to combine the advantages of truly surface-specific even-order spectroscopy with the benefits of avoiding to have to transmit the IR beams through strongly absorbing solvents.

Despite its experimental complexity, 2D SFG has been applied for a series of substrates and samples. In addition to liquid/air interfaces[147,148,263–269], strongly reflecting noble metal layers[49,121,135,249–251] have most commonly been used as surfaces, either for the formation of organic/biological MLs, or for use as electrode surfaces. Alternatively, easy-to-functionalize interfaces have been employed, such as semiconductor surfaces.[257] Although 2D SFG does in principle not require immobilization of the sample molecules at the surface, all of the reported studies at solid-liquid interfaces have exploited MLs that were covalently linked. To that end, thiol-containing linkers have been used either at evaporated metals on crystalline silicon wafers, or polycrystalline metal surfaces. In fact, the applicable range of samples is very broad, as demonstrated for 1D SFG studies.[22,50,133,134,161,162,270–274] The details of all

experimental as well as theoretical benefits and shortcomings need to be carefully considered in order to evaluate whether the strictly surface-specificity of 2D SFG is required.

3. Results and Discussion

3.1. Information from 2D IR Spectra at Surfaces

Many examples exist in literature, in which 3rd-order 2D IR was used to study molecular dynamics of samples in bulk solution.[71,75,83–86,138,275–280] More recently, a couple of works have been presented, in which properties and dynamics of molecules immobilized on surfaces have been analyzed in a similar manner.[23,50,133,134,147,148,173,174,181–183,185,263,269,274,281,282] It is of pivotal importance to elucidate the differences in molecular properties at interfaces compared to solution and relate them to the distinct properties of an interface. Here we present a first overview of recent examples from surface-sensitive and surface-specific 2D vibrational spectroscopy, which will then be discussed in more detail in the upcoming sections.

Significant interest lies in vibrational lineshapes and the underlying mechanisms of line-broadening.[71] Besides two extreme cases of purely homogeneously and inhomogeneously broadened bands, much attention has been paid in 2D IR spectroscopy to the intermediate regime of spectral diffusion, *i.e.* when different oscillators under the envelope of an IR band interconvert in vibrational frequencies.[71,103] Spectral diffusion can be caused by solvent-solute interactions such as hydrogen-bonding and solvent relaxation[138,169,283,284], or by chemical exchange, energy-transfer as well as intramolecular conformational changes.[91,92,181,283,285] Determination of spectral diffusion on the timescales of sub-picoseconds up to nanoseconds at solid-liquid interfaces is valuable, since it reports on intra- as well as intermolecular dynamics of the adsorbate. Comparison of the adsorbate dynamics with reference experiments in bulk solution indicates the impact of the interface directly. This concept has been employed for different samples with mainly third-order surface 2D IR spectroscopy.[173,174,181–183] A general

result that emerges from these studies is that the dynamics are considerably slower at the interface as compared to bulk solution. Impacts of surface-coverage, surface-structure or sample heterogeneity have been systematically investigated and report on purposely tuned vibrational dynamics at the interface, as shown in section 3.2.1.

Besides spectral diffusion, a further important aspect is that 2D IR methods can measure intermolecular interactions, which manifest themselves as cross-peaks between different vibrational transitions.[71] Cross-peaks are extremely valuable since they reveal the molecular structure due to the strong dependence of couplings and energy transfer rates on the distance between the corresponding molecular groups.[71,92,147,285] If two vibrational modes cannot be described by independent potential energy surfaces, they are considered to be "coupled".[71,138,140] Vibrational coupling can exist between vibrations within a given molecule, or between vibrations of different molecules, if they are in close enough proximity. 2D IR is ideal to study delocalized vibrations in closely-packed molecular MLs[121,249,286,287], and to investigate the effect of coupling in dependence of surface properties. Vibrational coupling between chromophores has for instance been identified in dye-sensitized systems[286,287] or in self-assembled MLs on Au nanoparticles[31], as discussed in section 3.2.3. Such interactions are likely to a play key-role in the performance of hybrid organic-inorganic devices in the fields of solar cells or heterogeneous catalysis.

Energy transfer between different vibrations results in the appearance of 2D IR cross-peaks as well. Again, energy transfer can take place between vibrational modes of the same molecule (through IVR), but also between different molecules such as a solute and a solvent or within a densely packed aggregates. Responsible mechanisms of energy transfer can involve (near) resonance energy transfer[92,281] or diffusive and ballistic transfer over sub-nm distances[288–290]. 2D IR at surfaces has been used to identify energy transfer pathways at solid-liquid interfaces in various systems and to elucidate its impact on spectral diffusion[92,173,181]. Both the

presence[287] or the absence[172,173,183] of energy transfer between adsorbate molecules have been discussed, as shown in section 3.2.3.

In addition to the dynamics of organic MLs on different surfaces, many recent works demonstrated future avenues, for which surface-sensitive 2D IR will become important. For example, it has been demonstrated by 2D ATR IR spectroscopy that ultrafast vibrational dynamics (spectral diffusion and vibrational relaxation) can be investigated in dependence of an electrochemical potential for adsorbates (*e.g.* CO) at electrode surfaces. These results are discussed in section 3.3. Another development is the use plasmonic structures to increase the signal strength and to improve surface-sensitivity. We refer here specifically to aggregates of plasmonic nanoparticles[31,172,173,175,176] as well as to more elaborate versions with explicitly tunable nano-antennas[291]. These approaches allow ultra-sensitive 2D IR spectroscopy at interfaces with signal enhancement of up to more than four orders of magnitude. In addition to this, strong near-field enhancement even enables multi-quantum IR excitations, which can be relevant for studying highly-excited vibrational states of adsorbates, as discussed in section 3.4.[177]

Another extension of surface-sensitive 2D IR aims at expanding the dynamical information to excited electronic states. This is done by adding an actinic UV/VIS pump pulse to a third-order 2D IR sequence in transient 2D IR spectroscopy. For instance, the charge-transfer dynamics between a dye and a substrate used in dye-sensitized solar cells has been investigated.[292] It has been shown that different binding configurations of the dye at the semiconductor surface exhibits different charge-injection efficiencies. This is expected to have a great impact on the deeper understanding of dye-sensitized solar cells, as discussed in section 3.5.

3.2. Ultrafast Dynamics of Adsorbates

3.2.1. Spectral Diffusion at Solid-Liquid/Gas Interfaces

3.2.1.1. Alkyl Monolayers Equipped with Metal-Carbonyl Headgroups

Extensive work on ultrafast vibrational dynamics of immobilized metal carbonyl complexes has been conducted by Fayer et al., who applied third-order BOXCAR 2D IR spectroscopy in transmission and in external reflection geometry. These experiments demonstrated that standard third-order 2D IR exhibits a high enough sensitivity to measure ultrafast vibrational dynamics from only ML thin samples. Transition-metal carbonyl complexes, as the ones employed in these studies, are widely known as catalysts for various chemical processes.[40,293,294] Concerning IR spectroscopy, such compounds offer the benefit of distinct and experimentally easily accessible vibrational bands, which sensitively respond to environmental changes. They have a high extinction coefficient along with vibrational lifetimes that are long enough to measure spectral diffusion over several tens of picoseconds.

In a series of papers, spectral diffusion dynamics of metal carbonyl headgroups embodied in different variants of self-assembled MLs have been investigated. The investigations systematically determined the impact of numerous experimental parameters on spectral diffusion, such as different solvent environments[182], surface coverages[23,183] , surface-structure and morphology[23,170], or the distance of the headgroup from the surface[185]. Figure 13 shows examples of different surface compositions used in these studies.[23]

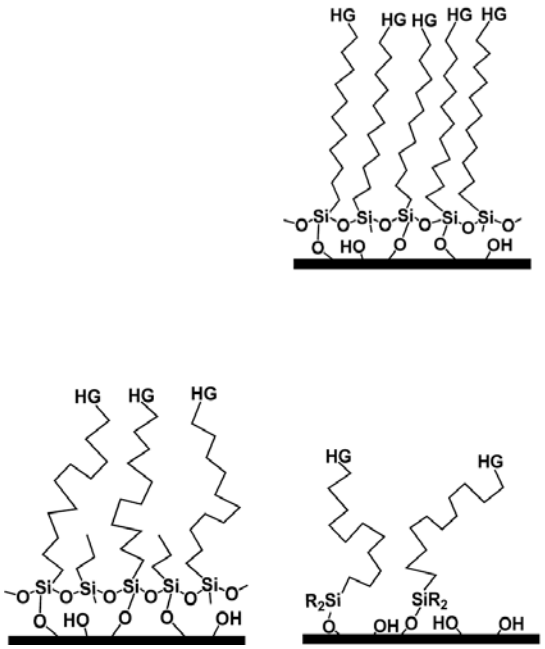

Figure 13. Structural variations of MLs studied with transmission BOXCAR 2D IR spectroscopy. (a) Scheme of the headgroup fac-Re(Phen)(CO)$_3$Cl. (b) A model for a ML with full coverage (100%). (c) A model for reduced surface coverage (50-25%), prepared from mixed ML of C3 and C11 alkyl chains. (d) A model for a ML with lowest surface coverage (15%). Adapted with permission from ref.[23]*. Copyright (2015) American Chemical Society.*

In a first report, the ultrafast dynamics of the Re-carbonyl headgroup in a ML with a C11-chain as a spacer between the headgroup and the surface was investigated (Figure 13 (a) and (b)) and compared to dynamics of only the headgroup (without the C11 chain) in bulk solution,[181] see Figure 14. Depending on experimental conditions, the headgroup dynamics are significantly different. For instance, bare MLs without any contact to solvent molecules (Figure 14 (a)) or MLs in contact with a solvent ($CHCl_3$) ("wet", Figure 14 (b)) show strongly elongated lineshapes of the GSB/SE (red-yellow) along the diagonal at early population times (0.5 ps), which evidence a large degree of inhomogeneity of the sample. The ML signals are drastically different from what is observed for the headgroup in bulk $CHCl_3$ (Figure 14 (c)), where the anti-diagonal width of the 2D IR band is significantly larger. The anti-diagonal width reports on the relative contribution of homogeneous line-broadening to the total

(diagonal) linewidth[71], indicating a largely homogeneous line broadening mechanisms in the latter case. Moreover, the signals from bare and wet MLs exhibit only very minor evolution in lineshapes with increasing population delay. Again, this is in sharp contrast to the bulk solution sample, where the signals evolve from slightly elongated signals to almost circularly shaped 2D IR signals within a few picoseconds after excitation, (c).

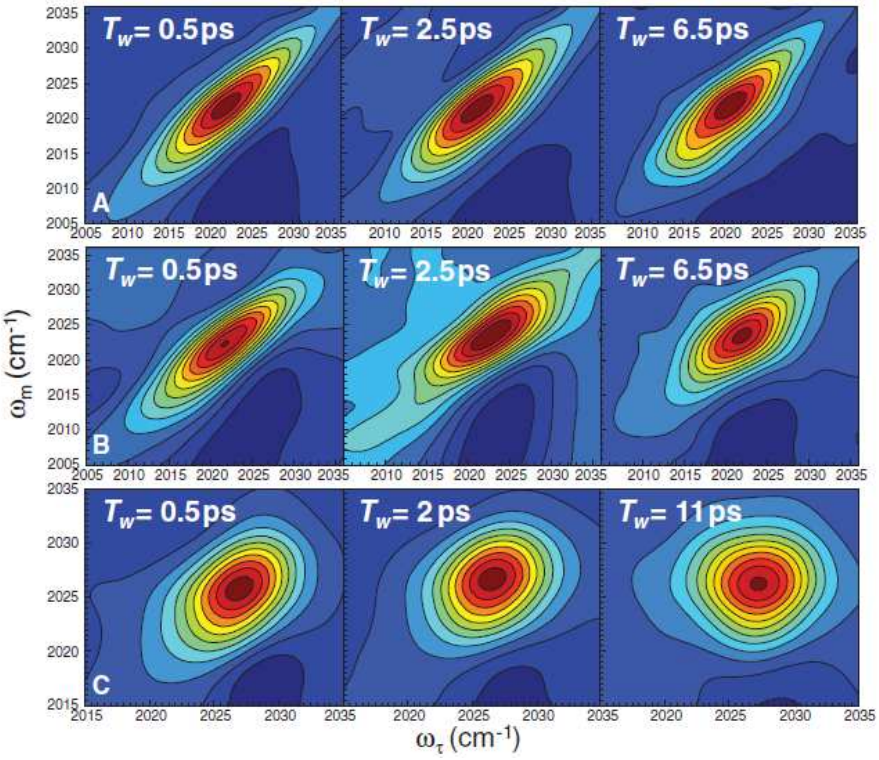

Figure 14. Transmission BOXCAR 2D IR spectra (GSB/SE) of the symmetric carbonyl stretching mode a fac-Re(Phen)(CO)$_3$Cl headgroup in different environments at indicated waiting times. (a) The headgroup incorporated in a bare ML (no solvent), and (b) in a solvent-incubated ML ($CHCl_3$, "wet"). MLs were formed from C11 alkyl-chains attached to silica surfaces. (c) The same from solely the headgroup (no C11-chain) as a bulk solution sample. Adapted with permission from ref.[181]*. Copyright (2011) AAAS.*

The central quantity used in the studies of ultrafast spectral diffusion is the center line slope (CLS) as a function of population delays.[181] The CLS is a measure of spectral elongation of 2D IR signals along the diagonal and therefore reports on structural heterogeneity of the sample. The temporal evolution of the CLS moreover resembles the normalized frequency-frequency correlation function.[295] A close analysis of the CLS dynamics extracted from the

2D IR signals of Figure 14 quantified that the structural dynamics slows down by a factor of 5 upon immobilization of the headgroup in a wet ML, and even more by a factor of 15 when the solvent is removed, *i.e.* the bare ML.[181] These differences between all three samples showed for the first time that both the structural dynamics of the ML as well as the solvent molecules are considerably slowed down at the interface. It is noteworthy, however, that even an immobilized and bare ML sample is not static, but exhibits inherent structural fluctuations on timescales of much less than a nanosecond. This is still significantly faster compared to for instance structural fluctuations in (pseudo)nematic domains of liquid-crystal samples with aromatic chain-structures.[296,297] MD simulations of structural fluctuations of similar aliphatic MLs with Re-carbonyl headgroups later on revealed that strong contributions to the structural fluctuation originate from dihedral flips in the aliphatic chains as well as flips in the triazole ring structure.[170] This indicates a high degree of structural flexibility in the chains even in the ML.

The systematic manipulation of the surface-composition of the MLs revealed clear trends in the spectral diffusion of the headgroup, which were largely attributed to motions of the alkyl chains in the absence of a solvent.[23] Figure 15 shows the decay of the CLS obtained from 2D IR spectra from samples with different surface-coverages of the headgroup. Experimentally, the headgroup surface-concentration has been controlled either by preparation of mixed MLs from short-chain and long-chain aliphatics (50-25%, Figure 13 (c)), or even further (15%, Figure 13 (d)) by an independent attachment procedure using a mono-chlorsilane linker.[23] By use of short- and long-chain mixed MLs, these experiments aimed at elucidating the effect of collapsing ML structures due to a local perturbation of the chain conformation. In the range of 100 – 50 % surface coverage (Figure 15, black/red), the dynamics can be described well by a single exponential decay and slows down only mildly when reducing the coverage. However, a breakup in two different timescales of spectral diffusion was observed for surface-coverages

below 50 % (blue and green). Here, exponential fitting required the introduction of a constant offset, which reflects a seemingly static process that much slower than the accessible experimental timescale, *i.e.* >> 80 ps. The increasing offset contribution with decreasing surface coverage was explained by collapsing ML structures at lower surface coverages (Figure 13 (c) and (d)), which resulted in high energetic barriers for the interconversion of chain structures.[23]

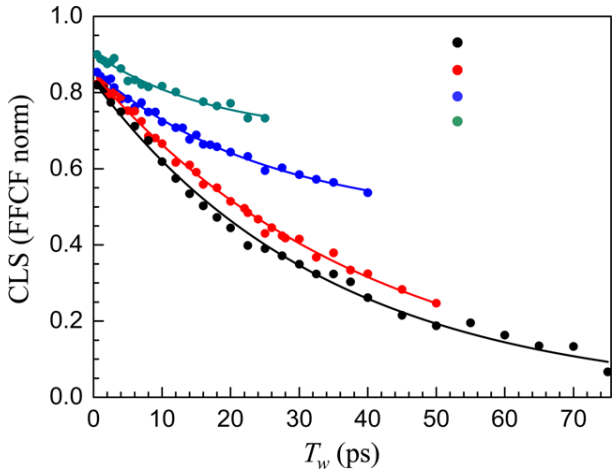

Figure 15. Center line slope (CLS) evolution in dependence of population delay (T_w) for the ML samples depicted in Figure 13 as bare ML. 100% coverage of the headgroup (black points), 50% coverage of the headgroup (red points), 25% of the headgroup (blue points), 15% coverage of the headgroup (green points). Symbols represent experimental data, while solid lines represent experimental fits. Adapted with permission from ref.[23]. Copyright (2015) American Chemical Society.

A similar slowdown of spectral diffusion with decreasing surface-coverage of the Re-carbonyl headgroup was observed by Fayer et al. on single-crystalline Au surfaces by use of R-2D IR spectroscopy, albeit with less drastic differences (Figure 16).[170] In this case, the effect was attributed solely to the dilution of the Re-carbonyl headgroups while keeping an overall upright orientation of both the labelled and the non-labelled C11 chains intact. The effect is thus distinctively different from the collapsing ML structures discussed in Figure 13 and Figure 15: Experimental data and accompanying MD simulations suggested that subtle structural defects are induced in the backbone structure of the C11 chains (Figure 16),[170]

Experimental data (red) and simulated (blue) spectral diffusion dynamics for 40% (HG_{high} (a)) and 20% headgroup surface-coverages (HG_{low} (b)) demonstrated that the presence of the Re-carbonyl headgroup causes an increasing amount of gauche-defects in the long alkyl chains along with triazole ring flips. These structural changes slightly (about 15%) accelerate the conformational fluctuations of the headgroup, which manifest themselves by an increased spectral diffusion rate. Such small effects can be better investigated on a mono-crystalline surface, which has a significantly smaller number of structural defects as compared to MLs on rough sputtered surfaces.[19,170]

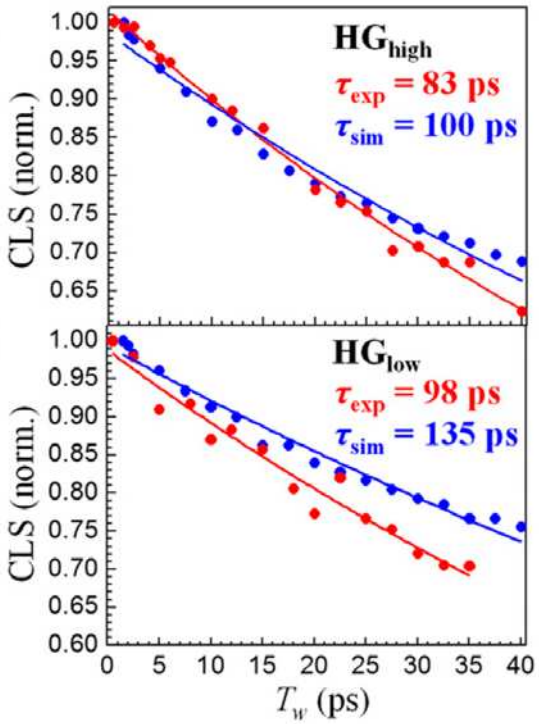

Figure 16. Normalized CLS dynamics from R-2D IR spectroscopy of MLs on Au surfaces. (a) HG_{high} refers to a high headgroup density, whereas (b) HG_{low} refers to a low headgroup density. Red and blue solid circles correspond to experimental and simulated data points (MD simulations). Solid lines correspond to exponential fits with indicated time constants. Adapted with permission from ref.[170]*. Copyright (2016) National Academy of Sciences.*

In addition to the ultrafast dynamics, spectral band positions of the IR labels also change upon adsorption (Figure 14) and in dependence of surface coverage.[23,170] This effect has been

attributed to the vibrational Stark effect[298,299], caused by interactions of a given molecular dipole with the total electric dipole field generated by all surrounding headgroups. As the surface-coverage is increased, the total electric field at each headgroup increases as well, thereby causing a frequency shift. Since the headgroups of the molecules fluctuate, the total electric dipole fields also become time-dependent, causing spectral diffusion.[23,170]

As the headgroup often is the part of a molecule, which is of chemical or physical importance for the application of a ML, another important aspect is its distance to the surface, since the substrate might impact the chemical properties of the headgroup. In this context, it is known that long hydrocarbon chains tend to form well-ordered MLs by extensive hydrophobic interaction between the aliphatic chains.[19,20] As such, the structural dynamics of the ML is expected to depend on chain length of the spacer between the headgroup and the surface, which has indeed been observed experimentally (Figure 17). A significantly slower timescale of spectral diffusion was observed for MLs with short alkyl-chains (C3, blue) as compared to long chains (C11, red), which was attributed to the lower number of internal degrees of freedom and the more rigid structure of the short alkyl chains.[185]

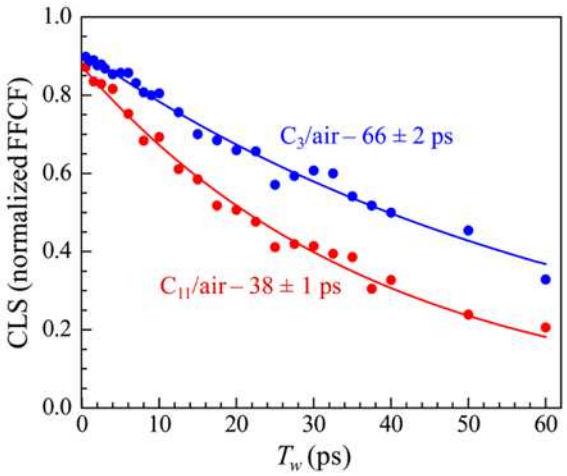

Figure 17. CLS evolution of the symmetric carbonyl stretching mode of a fac-Re(Phen)(CO)$_3$Cl headgroup in bare MLs with different chain lengths of 3 (C3, blue) and 11 (C11, red). Symbols represent experimental data, while solid lines represent experimental fits with indicated time-constants. Adapted with permission from ref.[185]. Copyright (2014) American Chemical Society.

Furthermore, detailed investigations have been performed on the impact of different chemical environments on the MLs, *e.g.* different solvents in contact with the MLs.[182] As a general observation, interaction of the MLs with solvents accelerated spectral diffusion of the headgroups. Strongly interacting solvents also evoked a separation of timescales for structural dynamics within the ML and solvent-related spectral diffusion, revealing multi-exponential spectral diffusion dynamics.[185]

3.2.1.2. Organic Monolayers with Weakly Absorbing IR Headgroups

The metal carbonyl groups exhibit extinction coefficients, which are among the highest available for IR-labels ($\varepsilon > 10^3\ M^{-1}\ cm^{-1}$).[181] Such high values facilitate the detection of nonlinear signals from a small numbers of molecules. Exploiting enhanced optical near-fields from thin metal layers (which will be discussed further in section 3.4) in 2D ATR IR facilitates the investigation of also vibrational labels with much smaller extinction coefficients.[176,177] Figure 18 shows examples of 2D ATR IR spectra obtained for vibrational headgroups with different extinction coefficients, *i.e.,* (a) and (b) an azide group ($-N_3$) with $\varepsilon \approx 550\ M^{-1}cm^{-1}$, and (c) and (d) a selenocyanate group (-SeCN) with $\varepsilon \approx 100\ M^{-1}cm^{-1}$, attached to different aliphatic or aromatic organic backbones and immobilized on an ultrathin (average thickness 1 nm) noble metal layer (Au or Ag). Such IR-labels are highly sensitive to their chemical environments and are widely used in ultrafast IR spectroscopy.[60,296,297,300–302] Their vibrational lifetimes, N_3 (~1.5 ps) << SeCN (~200 ps),[173,174,296,297,300,303] allow 2D IR measurements on a broad range of timescales, *i.e.* between a few picoseconds and up to a few hundreds of picoseconds. Spectral diffusion dynamics of MLs with such functional groups have been studied at noble metal surfaces in different chemical environments. It was shown that also at noble metal layers, vibrational lineshapes are dominated by inhomogeneous

broadening (Figure 18).[173,174] Similar to metal carbonyl samples, spectral diffusion was found to be much slower at interfaces as compared to isotropic samples by factors ranging between three to 20, depending on the chemical nature of the environment and the structure of the MLs.[173,174]

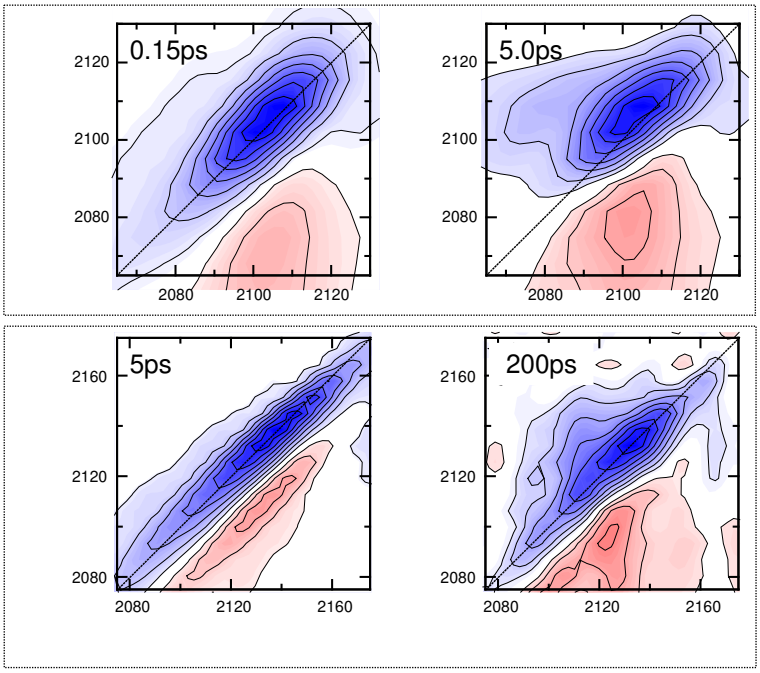

Figure 18. 2D ATR IR spectra at the indicated population delays for (a) and (b) 2-azidoethanthiol (2N3) on 1 nm Au immersed in Acetonitrile, (c) and (d) para-mercaptophenylselenocyanate (p-PhSeCN) on 1 nm Ag immersed in Methanol. Blue signals correspond to GSB/SE, while red signals correspond to ESA. Panels (a) and (b) are adapted with permission from ref.[173]*. Copyright (2015) AIP Publishing LLC.*

In contrast to the spectral diffusion dynamics, vibrational relaxation with lifetimes varying by only about ± 25% is not strongly dependent on the immobilization process, as demonstrated by several studies from all employed 2D IR methods.[121,173,174,176,182] This mild variation was interpreted by the weak interaction between the substrate and the headgroups. Thus, energy-transfer to the substrate is inefficient, and dominant vibrational relaxation occurs via IVR or energy transfer to the solvent environment.

3.2.1.3. Monolayers of Small Molecules

In addition to organic MLs equipped with different IR labels, strong interest also exists in the characterization of the vibrational properties of small molecules with only few atoms, such as carbon monoxide (CO)[89,135,172,304], adsorbed hydrogen[89,305–307], pseudo-halides (*e.g.* CN^-) [90,308–310], or water[50,52,311–314]. These adsorbates are important in heterogeneous catalysis and also allow one to address fundamental questions of substrate-adsorbate coupling and energy transfer. Small molecules often adsorb on metal surfaces via strong covalent bonds, which may significantly change their electronic properties, giving rise to frequency shifts and changes in the transition dipole moment.[130,315] They frequently exist in different binding configurations on the surface, which can be distinguished spectroscopically.

Similar to organic MLs, 2D IR signals of adsorbates from small molecules can reveal ultrafast spectral diffusion dynamics. Figure 19 shows 2D ATR IR spectra of CO adsorbed from aqueous solutions onto different types of metal surfaces, *i.e.* ultrathin (sub-nm) (a) Pt layers and (b) Gold/Palladium (Au/Pd, 80:20) alloys. CO exhibits spectral diffusion dynamics that are much faster (~6 ps, Figure 19 (c)) than those of organic ML systems (Figure 15 and Figure 17).[172] It is believed that spectral diffusion of surface-bound CO originates predominately from hydrogen-bond interactions with water molecules.[172] On the other hand, spectral diffusion is still rather slow as compared to typical timescales of, *e.g.* organic carbonyl compounds in water (< 2 ps).[80,283,316] This again indicates a rather confined nature of the water layer at the metal surface, slowing down the dynamics by hindered rotations or changes in hydrogen-bond strengths.

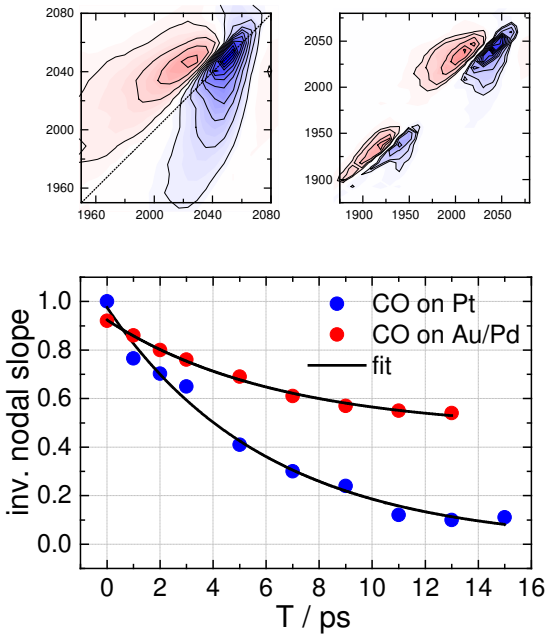

Figure 19. 2D ATR IR spectra of CO adsorbed to (a) Pt nanoparticles and (b) Au/Pd alloys on a CaF_2 ATR substrates at a population delay of 0 ps. Blue signals correspond to GSB/SE while red signals are due to ESA. Linearly-bound CO is observed with frequencies > 2000 cm^{-1}, while bridged-bound CO is observed at ~1975 cm^{-1} for Au/Pd and lies outside the observation window for Pt (~1820 cm^{-1}).[195] *(c) Spectral diffusion dynamics characterized by the CLS between GSB/SE and ESA signals. Circles correspond to experimental values, while solid lines are exponential fits including a static offset. Adapted with permission from ref.*[172]*. Copyright (2014) American Chemical Society.*

3.2.1.4. Spectral Diffusion at Liquid-Gas Interfaces

Also fourth-order 2D SFG may be used to investigate spectral diffusion, which has been demonstrated for water-air[147,148,263], water-lipid[264,265], water-surfactant[266–268] or salt-water-air interfaces[269]. The strength of fourth-order 2D SFG spectroscopy lies in the fact that such systems can also be investigated, in which the sample molecules are not linked covalently to the surface, owing to the true surface-specificity of the method (section 2.1.2). Both homodyne (without LO) and heterodyne-detected (with LO) 2D SFG has been used for that purpose.[147,148,263] Of particular interest is the impact of an interface on the intermolecular interactions and dynamics of water molecules.[147,263] For example, Figure 20 shows homodyne-detected 2D SFG spectra of the D_2O-air interface (white lines are the CLS) in the spectral region of the ground-state bleach of the OD-stretching bands at a series of population

delays together with the retrieved temporal evolution of the CLS (lower right panel).[147] The measurements show a rapid loss of spectral correlation on the sub-picosecond to picosecond timescale for surface water, which is, however, slower than in bulk water[317]. Isotope-dilution experiments were employed to proof that intermolecular energy transfer is the only relevant mechanism for spectral diffusion at the interface, and not the structural mobility of the water molecules. On the basis of a modified Förster-theory for resonant energy transfer at an interface with only one hemisphere of acceptor molecules, the experimentally observed temporal evolution could be modelled successfully without incorporating free fitting parameters (black line in the lower right panel).[147] It was inferred that the reduced number of water molecules at the interface alters the probability for intermolecular energy transfer, thereby slowing down the spectral diffusion.

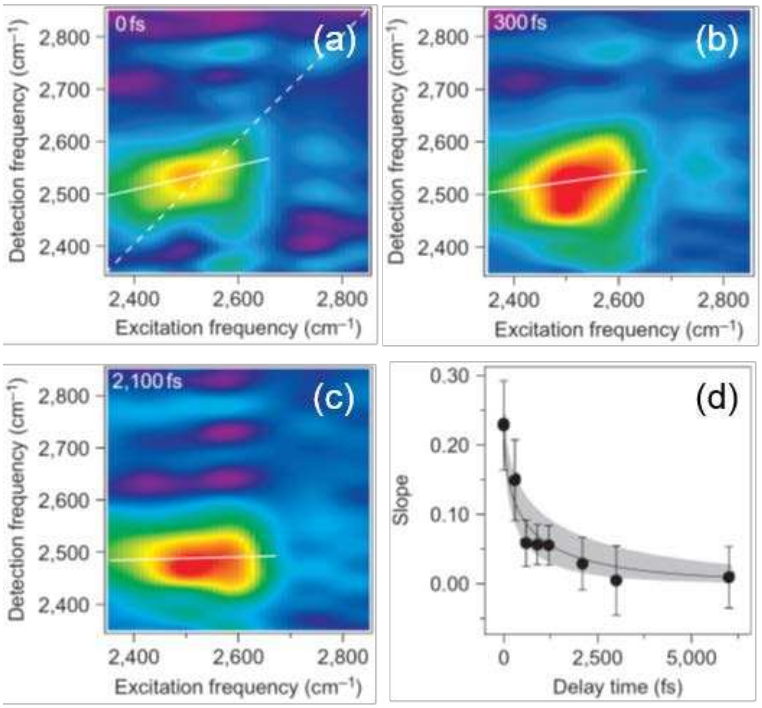

Figure 20. Homodyne-detected 2D SFG data of the D_2O-air interface at (a) 0 fs, (b) 300fs and (c) 2100 fs. White lines correspond to the CLS for the GSB signal of the OD-stretch vibration. (d) Shows the spectral diffusion dynamics obtained from the CLS at different waiting times. The solid, black line is based on a Förster energy-transfer model (the uncertainty from the Förster radius is indicated by the shaded region). Adapted with permission from ref.[147]*. Copyright (2011) Nature Publishing Group.*

Heterodyne-detected 2D SFG has been employed afterwards to study spectral diffusion at H_2O-air interfaces, resolving both the GSB and ESA features of the OH-stretching vibration (Figure 21). From the evolution of the nodal slope (black line ≡ experimental data, green line ≡ linear fit), a time constant for spectral diffusion of about 250 fs has been deduced.[263] The slowdown of the spectral diffusion with respect to bulk water[317] is very close to the expected factor of two, which is again explained by only half the number of adjacent molecules at the interface to which energy can be transferred.[263] The differences in dynamics between the D_2O and H_2O data (Figure 20 and Figure 21) are the result of lower transition dipole moment of the former, which results in a lower rate for intermolecular energy transfer.[147] Overall, the sub-picosecond energy-transfer dynamics of surface-water are more than one order of magnitude faster when compared to the structural dynamics of organic MLs discussed above. This reflects the persistent strong coupling of water even at the water-air interface, which results in energy transfer dynamics that are faster than the structural dynamics.[147]

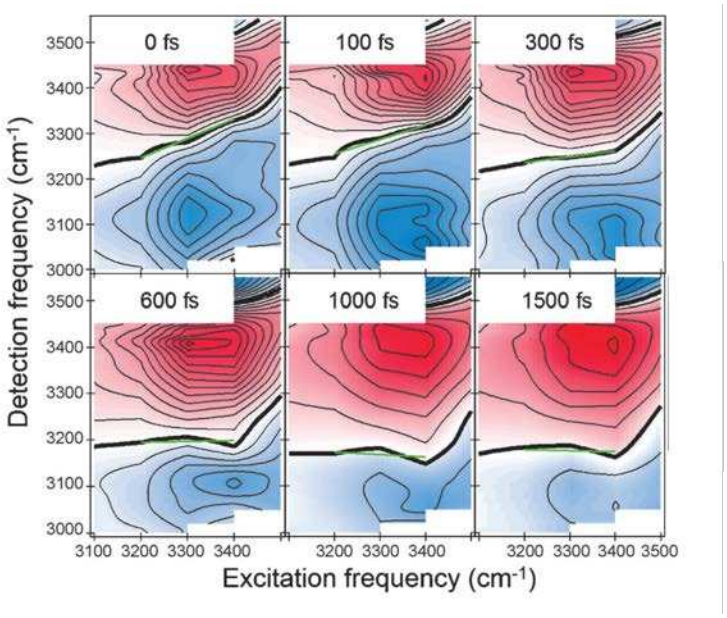

Figure 21. Heterodyne-detected 2D SFG spectra of the water (H_2O)-air interface at indicated population delays in the spectral region of the OH-stretch vibration. GSB/SE signals are shown in red, while ESA signals are shown in blue. Linear fits (green) to nodal slopes (black lines) have been used to determine spectral diffusion. Adapted with permission from ref.[263]*. Copyright (2014) John Wiley and Sons.*

The dynamics of surface water at liquid-air interfaces have also been studied dependent on the presence of either positive or negatively charged surfactants.[265,266,268,318] For instance, positively charged interfaces, generated by using Langmuir MLs of the cationic surfactant (cetyltrimethylammonium bromide (CTAB), Figure 22), have been investigated by use of heterodyne-detected 2D SFG. In this case, isotope diluted water has been used (HOD/D_2O) in order to eliminate the otherwise existing double band structures in the SFG spectrum of surfactant-water interfaces, which has been attributed to either Fermi-resonances or multiple water species.[263,266,268] Spectral diffusion is only slightly slower (~300 fs) than for the uncharged water-air interface (~250 fs, Figure 21). However, the cationic surfactant introduces a high degree of structural inhomogeneity in the surface-water, reflected by a comparatively high CLS value (black line) at early population times (0 ps). These experiments have demonstrated that the presence of surface-charge does not significantly alter the spectral diffusion dynamics of surface water.

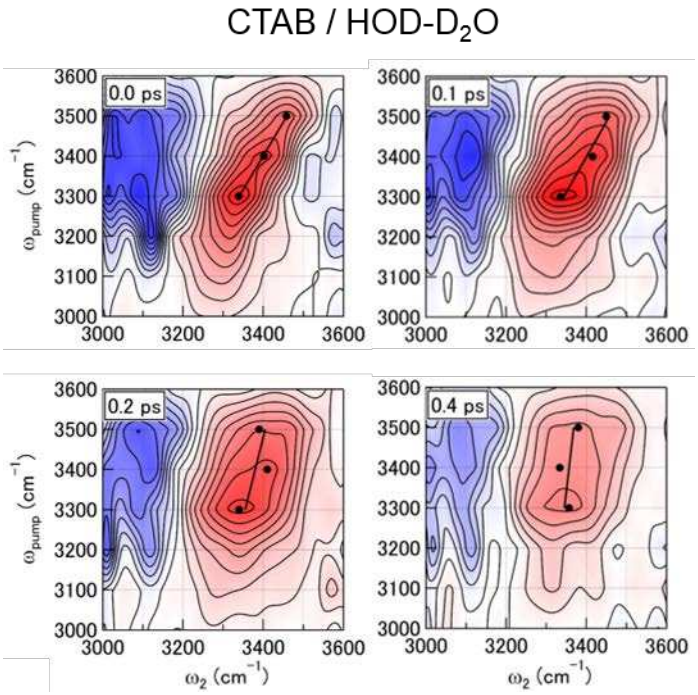

Figure 22. 2D SFG spectra in the OH-stretch region of the CTAB/(HOD in D_2O) interface at the indicated population delays. Black points indicate the center frequencies for specific pump frequencies, which are used to construct the CLS (black lines) of the GSB/SE signal (red).

Blue signals indicate ESA bands. Adapted with permission from ref.[268]*. Copyright (2015) AIP Publishing LLC.*

3.2.1.5. Summary on Spectral Diffusion Dynamics at Surfaces

As a general result from different sample systems, spectral diffusion is significantly slowed down at interfaces as compared to bulk solution. The examples furthermore demonstrate that different contributions to the ultrafast dynamics can be disentangled by comparative studies of the samples under different experimental conditions. The effect of the substrate, the inherent intramolecular contributions as well as the chemical environments have been studied in detail. Experiments even at low coverage (< 20%) are possible with the currently employed methods. The range of IR labels, which have been used, is broad, ranging from strongly absorbing metal carbonyls to labels with lower extinction coefficients, such as azides or nitriles and selenocyanates. The employed IR labels all absorb in a similar range of vibrational frequencies (~2300 – 1900 cm^{-1}), which is beneficial from an experimental point of view due to the low water absorption in this range. However, there is no intrinsic limitation that would not allow one to extend the technique over the entire spectral range of organic functional groups of interest (3500 – 1000 cm^{-1}). This has consequently been demonstrated by applications to OH and OD oscillators at liquid-gas interfaces.

3.2.2. 2D SFG for Studying Orientation of Functional Groups

3.2.2.1. Theoretical Considerations

Adsorbed molecules can orient with respect to the interface by different types of interactions with the surface. Such orientational effects can be investigated very sensitively by 2D SFG, since both the signal magnitudes and the signal sign are strongly dependent on molecular orientation (see also section 2.1.1). Zanni et al. have investigated in detail the impact of orientation of functional groups in 2D SFG.[111,121,249] Their studies emphasize the benefit of

fourth-order 2D SFG over second-order SFG via observable cross-peaks, which can appear between coupled oscillators or via energy transfer.

Figure 23 shows a theoretical case study of 2D SFG spectra (assuming that all pulses are p-polarized) of two coupled modes with frequencies ω_a and ω_b and different relative orientations and different absolute orientations with respect to the surface normal. Only 2D SFG spectra from rephasing response pathways have been considered for simplicity.[111] If the modes are coupled and aligned in parallel (Figure 23 (a), left panel), two sets of diagonal and cross-peaks appear in the 2D SFG spectrum with similarly high intensity. However, if the modes exhibit the same absolute orientation relative to the normal, but 90° relative to each other (Figure 23 (a), right panel), the diagonal peaks persist but the cross-peaks are strongly diminished. This is not due to a change of coupling between the modes, but originates from changes in the signs of distinct elements of the $\chi^{(4)}$ tensor, which cause partly destructive interference between response pathways.[111] The two cases demonstrate that cross-peak intensities relative to diagonal peaks can be used to determine the relative orientation of functional groups.

An additional effect comes into play when the orientational flexibility of functional groups is taken into account (Figure 23 (b), left panel). This is most prominent if the two transition dipoles enclose an angle of 90°, and the ω_b mode is isotropically distributed in angles ψ, in which case the corresponding diagonal peak averages out due to the changing sign of the signal with orientation.[111] Consequently, the ω_b mode is invisible in 2D SFG (Figure 23 (b), left panel). If, alternatively, ω_a and ω_b modes point in opposite directions, both diagonal peaks show up with opposite signs (Figure 23 (b), right panel).

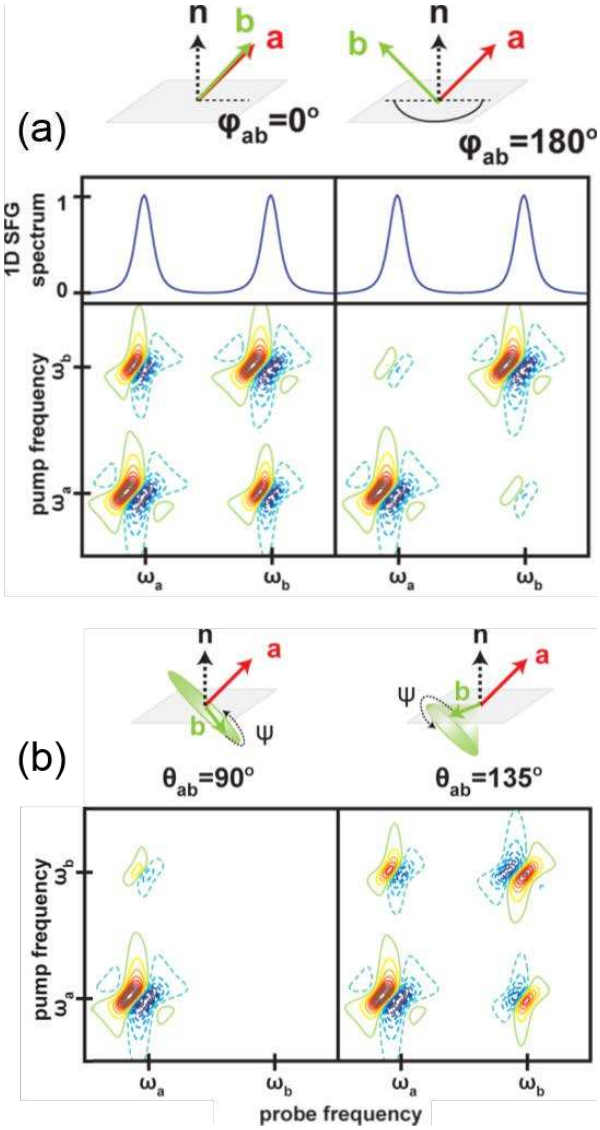

Figure 23. Impact of orientation in 2D SFG with all p-polarized pulses and rephasing pathways. Two coupled vibrations with frequencies ω_a and ω_b are oriented with respect to the surface normal n as sketched above the 2D SFG spectra. (a) Both vibrations have the same angles relative to the normal, but different angles with respect to each other. The top panels show second-order SFG spectra, which are identical, but the cross-peak intensity depends on relative angle between ω_a and ω_b. (b) Effect of orientational averaging in ψ of mode ω_b. Mode ω_a lies along the rotation axis. In the left panel, the ω_b diagonal signal is averaged out, since it is isotropically oriented in ψ. Cross-peaks between ω_a and ω_b are still visible. In the right panel, ω_b is not completely averaged out. Note the different signs of the diagonal peaks, which stem from opposite (average) orientation with respect to the surface. Adapted with permission from ref.[111]*.Copyright (2013) American Chemical Society.*

Interestingly, weak cross peaks may still persist despite the fact that the corresponding diagonal peaks disappear due to isotropic averaging (Figure 23 (b), left panel). Hence, an SFG-inactive, isotropic distribution of modes (ω_b) can still result in a 2D SFG signal at cross-

peak positions through coupling with an SFG-active mode (ω_a). This effect has been used to determine the orientation and structure of surface-bound oligo-nucleotides[249] or peptides[121] on Au surfaces, as discussed further below. Independent of that, a vibrational mode can also be invisible to SFG because of its Raman-inactivity (section 2.1.1),[111] but again, such a mode may contribute to 2D SFG spectra *via* a cross-peak as long as it interacts with the first three IR fields in the 2D IR sequence. This effect has been exploited in homodyne detected 2D SFG on Raman-inactive CH_2 modes in organic MLs at the water air interface.[146,149]

3.2.2.2. Practical Applications

As an example for the use of 2D SFG to determine molecular orientation, oligonucleotides on an Au surface have been investigated.[249] Such samples are of interest in the fields of molecular recognition and drug delivery.[319–321] Figure 24 (a) shows a 2D SFG spectrum of a poly(thymine) ML with a chain length of 25 nucleotides on Au in the spectral region of mainly the C=O and C=C stretching vibrations. The 2D SFG spectrum exhibits diagonal peaks from the 0-1 transitions (T_i) and 1-2 transitions (O_i) along with cross-peaks (C_{ij}) between the different modes i and j. Note the inversion of sign of the diagonal peaks T_1 vs. T_2, which reflects the opposite orientation of the corresponding groups relative to the surface (see Figure 23). Intra-base cross-peaks (C_{21} and C_{23}) are observed, for which the C_{23} peak lacks a diagonal counterpart (*i.e.* T_3), which has been attributed to orientational averaging.[249] The presence of this cross-peak has thus been taken as an experimental indication for the theoretical prediction shown in Figure 23 (b).

As a second important observation, a distinct off-diagonal feature (*i.e.* C_{11}) could not be explained by coupling between any of the modes T_1-T_3. Also the C_{11} cross-peak has no diagonal counterpart and was thus suggested to report on a previously unresolved inter-base coupling between bright and dark T_1 modes of neighboring thymine bases, induced by base-

stacking.[249] This interpretation has been confirmed by DFT calculations of a reduced model system with four thymine bases (Figure 24 (b)), from which an excitonic Hamiltonian has been deduced that describes the inter-base coupling. From this model, the experimental 2D SFG spectrum could be reproduced qualitatively (Figure 24 (c)), including the C_{11} cross-peak. From the observed inter- and intra-base cross-peaks in the 2D SFG spectrum and the theoretical model, the absolute orientation of the oligo(thymine) chain with respect to the Au surface could be determined, as well as the relative orientation between bases. An in-depth comparison of 2D SFG data from different samples was furthermore used to show that the order in the poly(thymine) chains increases with chain-length over a range of up to 25 nucleotides.

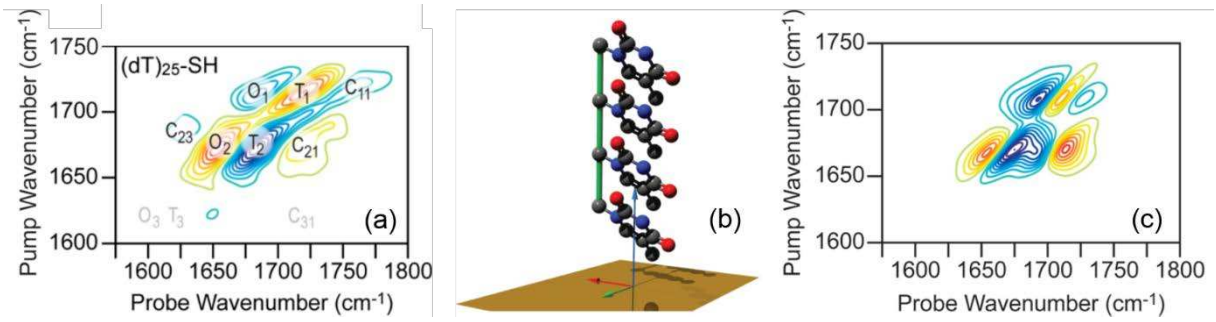

Figure 24. (a) 2D SFG spectrum of poly(thymine) $(dT)_{25}SH$ at a population delay of 0 fs in the spectral region of the carbonyl-stretching vibrations. (b) A molecular model with four stacked and coupled bases on an Au surface. (c) Simulated 2D SFG spectrum for the model shown in (b), which qualitatively describes the experimental spectrum in (a). Adapted with permission from ref.[249]. Copyright (2015) American Chemical Society.

3.2.2.3. Summary on Orientation at Surfaces

The discussed example demonstrates the extraordinary sensitivity of 2D SFG to determine both the absolute orientation relative to the surface and the relative orientation between modes. The results have been supported by similar observations made for peptides on Au surfaces.[121] The same level of orientational resolution can probably not be achieved with third-order 2D IR techniques, since in that case only the signal magnitude, and not its signs, depends on orientation. Although most reported 2D SFG studies so far employed all pulses

with p-polarization, other polarization condition should enhance the orientational resolution power even more.[111] For instance, the cross-peak intensity might be increased relative to often dominating diagonal peaks,[111] in analogy to what has been implemented for third-order 2D IR[322]. Note, however, that (i) s-polarized components of the incident light are diminished in a reflective geometry on metal surfaces (section 2.1.3) and (ii) also for 2D SFG the "surface selection rule" (section 2.1.1) applies, which prevents measurements on vibrations with transition dipole moments oriented parallel to the surface of immobilization.

3.2.3. Vibrational Coupling and Energy Transfer at Interfaces

Since molecules in a ML are in very close proximity, one might expect to observe intermolecular interactions via 2D IR cross-peaks between vibrational modes of different molecules, induced by either direct coupling[119,121,249,286,287] or by excitation energy transfer[92,173,181,183]. The search for such cross-peaks has been expedited with all currently available methods for 2D surface vibrational spectroscopy. The interest in intermolecular cross-peaks is reasoned by the fact that the underlying interactions are strongly distance and orientation-dependent.[71] Cross-peaks and their dynamics should therefore be a measure of intermolecular structure.

As a first example, third-order transmission 2D IR studies on organic capping layers of isolated Au nanoparticles have shown that vibrations on different molecules in a ML can indeed couple.[31] Figure 25 shows 2D IR spectra of symmetric (υ_s) and anti-symmetric stretch vibrations (υ_a) from a carboxylate group (COO^-) of either acetate dissolved in bulk D_2O/NaOD ((a) and (c)) or as a ML of marcaptoundecanoic acid (MUA) on Au nanoparticles. Both the υ_s and υ_a exhibited only a single band in bulk solution (unbound, Figure 25 (a) and (c)) with GSB/SE (blue) as well as ESA contributions (red). In contrast, the vibrations are coupled within the ML due to close packing of the long (C11) alkyl-chains, manifested by a

splitting of the υ_s band into a doublet structure (at 1450 cm^{-1} and 1420 cm^{-1}, Figure 25 (b)). Moreover, cross-peaks appear between the two bands in the 2D IR (indicated by an arrows), which were attributed to excitonic coupling of the υ_s modes on the ML. Interestingly, the υ_a band remains uncoupled even though the same functional groups contributes to the signal (Figure 25 (c) and (b)). This suggests that the coupling mechanism is strongly dependent on the orientation of the transition dipole moment, which is different for the υ_a and υ_s bands.

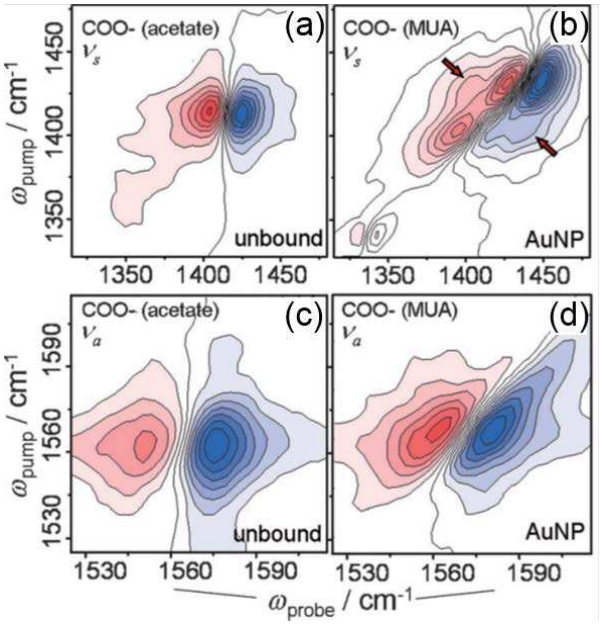

Figure 25. Observation of excitonic coupling in a ML on Au nanoparticles. (a) 2D IR spectrum of the symmetric stretch vibration υ_s from acetate dissolved in bulk solution (unbound). (b) 2D IR spectrum of υ_s in a mercaptoundecanoic-acid (MUA) ML on Au nanoparticles. (c) and (d) same as (a)/(b), however, for the asymmetric stretch vibration υ_a. Cross-peaks (arrows) appear only for υ_s of MUA ML on Au nanoparticles. All measurements were performed at a population delay of 300 fs in D_2O/NaOD as a solvent to deprotonate the carboxylic acids. Adapted with permission from ref.[31]*. Copyright (2013) John Wiley and Sons.*

Interactions between adsorbate molecules is far from universal in MLs and can strongly depend on the functional group under study, despite the close packing of molecules. For instance, 2D ATR IR signals from the azido-groups in MLs of 11-azidoundecanthiol (11N3) on an Au surface have not revealed any indication of excitonic coupling.[173] Excitation energy transfer between neighboring azide labels has been ruled out as well with the help of isotope-

dilution experiments. Isotope-dilution is a preferred tool to study the interaction of adsorbates, since the chemical properties of the ML is not changed. To illustrate this, Figure 26 (a) and (b) shows 2D ATR IR spectra of all-^{15}N (2027 cm^{-1}) and all-^{14}N (2095 cm^{-1}) terminated MLs co-adsorbed with a ratio of 2.4:1 at early (0.15 ps) and at late (3 ps) population delays. No cross-peaks can be detected, indicating the absence of vibrational excitation energy transfer. Due to the spectral separation of the ^{15}N and ^{14}N bands, such energy transfer would have to be non-resonant. But also resonant (*e.g.* Förster-type) excitation energy transfer can be ruled out, since the spectral diffusion dynamics of the isotope-mixed (MML) samples is the same as that of the isotope-pure samples (ML, Figure 26 (c)).

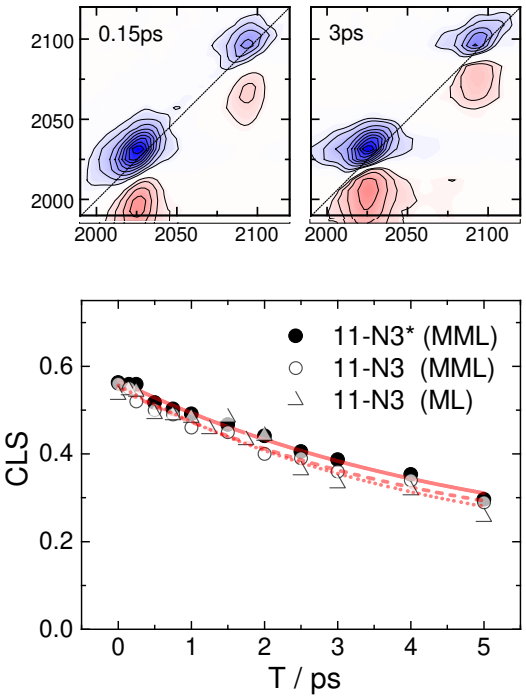

Figure 26. Absent excitation energy transfer in mixed MLs (MML) of isotope-labelled (all-^{14}N (11N3) vs. all-^{15}N (11N3)) 11-azidoundecanethiol. (a) and (b) 2D ATR IR spectra of a 1:2.4 mixed ML at early (0.15 ps) and late (3 ps) population delays. (c) CLS decay curves of both peaks in the 2D IR spectrum (11N3 (MML) and 11N3*(MML)) compared to an isotope-pure sample (11N3 (ML)). Symbols are experimental data while red lines correspond to single exponential fits including an offset. Adapted with permission from ref.*[173]*. Copyright (2015) AIP Publishing LLC.*

The same observation has been reported for MLs with Re-carbonyl headgroups with different surface coverages on a SiO_2 surface.[183] In that case, C11-chains with and without Re-carbonyl headgroups were co-immobilization on the surface, without any change in the spectral diffusion kinetics in dependence on surface coverage of the labelled compound. Energy-transfer or coupling between different molecules is thus not always present in a ML, probably since the interaction between the adsorbates requires distinct chemical or electrostatic effects, which strongly depend on the chemical nature of the sample.

In another example of a Re-carbonyl without any spacer between the headgroup and the linker (Figure 27 (a)), on the other hand, energy transfer between adjacent molecules was indeed observed.[286,287] This type of molecules undergoes charge-injection into a semiconductor substrate after VIS photo-excitation.[323] It has been suggested that the dyes form domains of mono-, di- and trimers on a sapphire surface, which are identified by multiple peaks the 2D IR spectrum. Initially (0 ps, (b)), only GSB/SE and ESA diagonal peaks (red) exist in the transmission 2D IR signal, which correspond to the different dye aggregates. Increasing population delays, however, reveal cross-peaks (dashed circles in Figure 27 (c) and (d)), indicating excitation energy transfer among the adsorbate molecules.

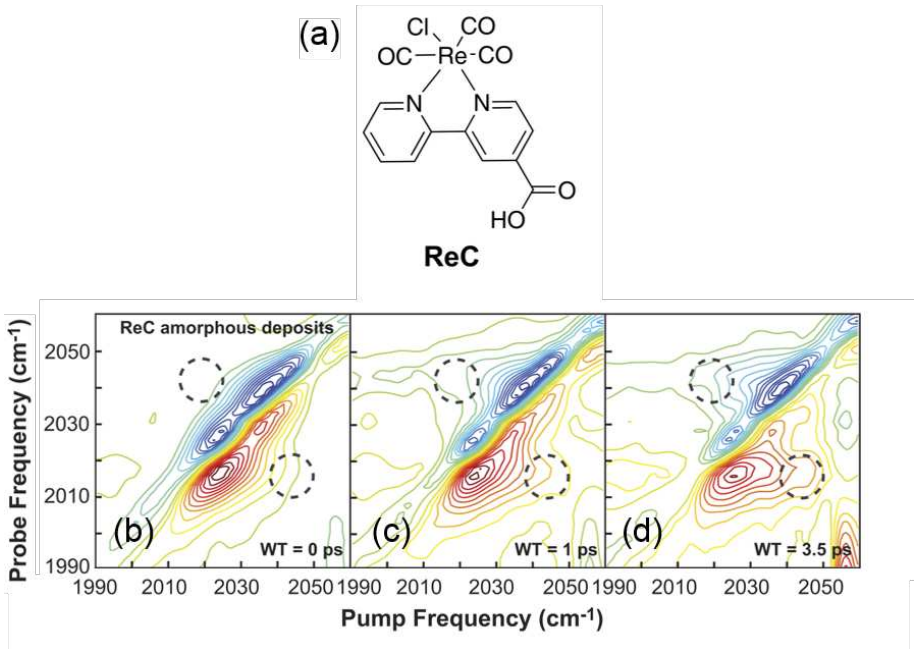

Figure 27. Third-order transmission 2D IR reveals interaction of Re-carbonyl dyes on sapphire substrates. (a) Structure of the employed dye. (b) – (d) Waiting time dependence of the 2D IR spectra; the dashed circles indicate the formation of a cross-peak. Adapted with permission from ref.[287]*. Copyright (2015) AIP Publishing LLC.*

Vibrational coupling and energy transfer has also been investigated at a charged liquid-air interface by use of 2D SFG spectroscopy,[266] revealing intermolecular interactions between non-immobilized molecules in the vicinity of the interface. Figure 28 shows homodyne-detected 2D SFG spectra of water in contact with a surfactant (sodium dodecyl sulfate, SDS). Two diagonal peaks are clearly observed, which are assigned to water molecules directly hydrogen-bonded to SDS (2510 cm^{-1}) and aligned water molecules below the surfactant (2380 cm^{-1}). The cross-peaks between the two sub-ensembles of water molecules reveal an ultrafast energy transfer process. The different intensities for the upper and lower diagonal cross-peaks were suggested to originate from different transfer efficiencies between the two subsets of water molecules, possibly including entropic contributions, which make transfer in one direction more likely than in the other direction. These experiments thus gave unprecedented insight into the mechanisms with which different water molecules can interact near charged surfaces.

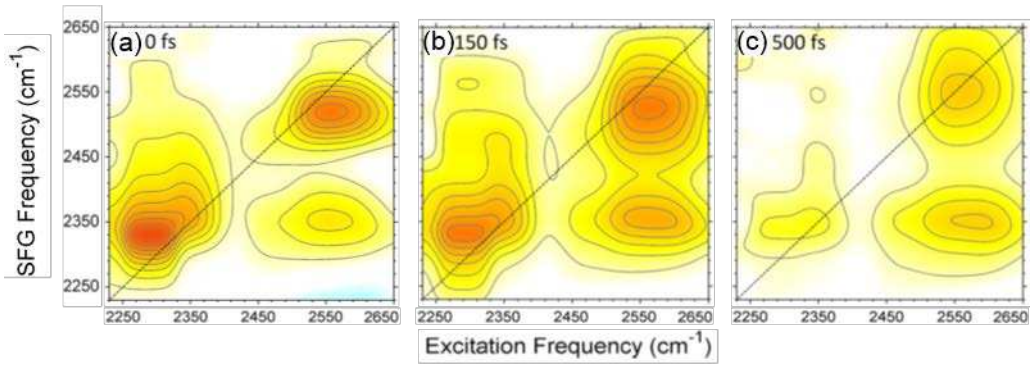

Figure 28. Homodyne-detected 2D SFG spectra of the water-surfactant interface (SDS) in the spectral region of the OD-stretching vibration at population delays of (a) 0 fs, (b) 150 fs, and (c) 500 fs. Upper and lower diagonal peaks correspond to water molecules in contact with SDS versus aligned water molecules below the surfactant, respectively. The cross-peaks report on an energy-transfer between these species. Adapted with permission from ref.[266]*. Copyright (2015) American Chemical Society.*

3.2.4. Substrate-Adsorbate Interactions

The interaction of an adsorbate from Re(diCN-bpy)$(CO)_3Cl$ with an Au substrate has been investigated by 2D SFG.[49,251] Figure 29 (a) and (b) show fourth-order 2D SFG of the immobilized molecule and complementary third-order 2D IR spectra in bulk solution at a population delay of 80 fs. Clear features of GSB/SE and ESA diagonal peaks were observed at about 1930 cm^{-1}, and at 2025 cm^{-1}. In the case of the 2D SFG spectrum, the diagonal features exhibit opposite signs, indicating different orientations with respect to the surface, with the carbonyl groups dominating the lower-frequency mode being closer to the surface (see section 3.2.2).[49] The emphasize here lies in the amplitude of the intra-molecular cross-peaks, which oscillates as a function of population time with a period of about 330 fs (100 cm^{-1}, see Figure 29 (d)), which reflects the inter-state coherences between different carbonyl stretching modes within each of the adsorbed molecules.[49] This low-frequency oscillation matches well the difference frequency of the diagonal peaks (Figure 29 (c)).[139,140] The dephasing of that coherence is faster for the immobilized molecule, which has been attributed to the interaction with the metal substrate via its mirror-dipoles.[324] This conclusion is supported by the fact that other origins of dephasing (*e.g.* intermolecular coupling of the adsorbed catalysts, or coupling to low-frequency substrate phonons) could be ruled out.[49,251] Substrate-adsorbate coupling hence might influence molecular dynamics even though the IR-label is not in direct contact with the surface. That mechanism is believed to be relevant as long as the functional group under study is in close enough proximity to the surface (<< 10 nm).[49]

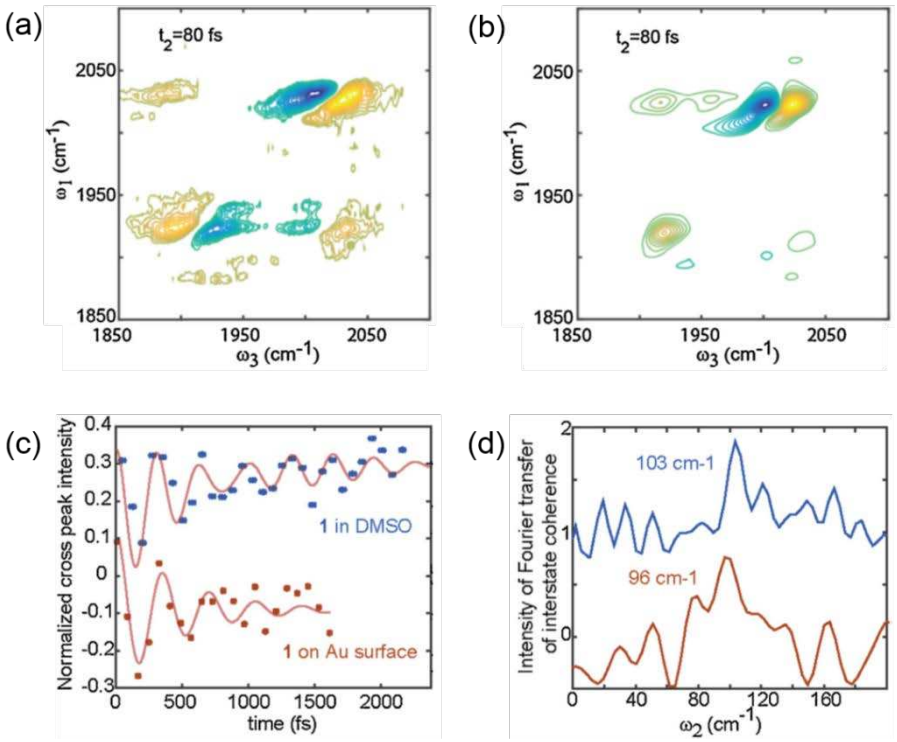

Figure 29. (a) 2D SFG spectrum of a Re(diCN-bpy)(CO)$_3$Cl ML on Au and (b) 2D IR spectrum of Re(diCN-bpy)(CO)$_3$Cl in bulk solution (DMSO). Both spectra are for a population delay of 80 fs and with all pulses p-polarized. (c) Oscillations in integrated cross-peak amplitudes in dependence of population delays. The coherences for the surface-bound molecules dephase faster than in bulk solution. (d) Fourier-transformation of the oscillations in (c). Adapted with permission from ref.[251]*. Copyright (2016) Elsevier.*

3.2.5. Summary on Intermolecular and Substrate-Adsorbate Interactions

Overall, the different forms of surface 2D IR spectroscopies are well-suited to investigate intermolecular interactions of adsorbates. Being able to determine such interactions is one of the strengths of 2D IR spectroscopy compared to techniques revealing only a single spectral dimension. Interactions between adsorbates is one of the major research directions in surface 2D vibrational spectroscopy, since many physical or chemical properties of a ML are expected to depend on such effects. These include for instance dissipation of excess vibrational energy among different adsorbate molecules, structural re-arrangements within the MLs, the order of packing within the MLs, the ability to intercalate host molecules, or interactions between functional groups in a ML and their accessibility by the surrounding.

These points are relevant regarding, *e.g.* the thermal stability and the thermal conductance of molecular surfaces, chemical sensing or molecular recognition, as well as electrical conductance of holes, electrons or ions and electron injection dynamics after photo-excitation. Especially for the latter, one of the major questions has been raised by Zanni et al.[286,287] regarding the possible relationship of electronic *vs.* vibrational interaction of aggregated photosensitizer on semiconductor interfaces. It has been suggested that aggregation will not only lead to energy transfer and coupled vibrational states, but also between electronic states. As the electronic dynamics are relevant for, *e.g.* charge-injection into the semiconductor substrate, delocalized electronic states might have an impact on the performance of a functional device. It is therefore desirable to advance the current investigations from model systems to working devices in order to test the impact of intermolecular interactions on their performance *in-situ*.

A clear picture of whether or not intermolecular interactions occur at surfaces has not yet emerged from the currently available spectroscopic data. We expect that details of the sample preparation contribute to the observation of such effects. Knowing precisely the substrate structure and adsorption geometry will be a promising starting point to further investigate the open questions.

3.3. 2D ATR IR at Electrode Surfaces

Charged interfaces are of significant importance due to their involvement in heterogeneous catalysis[38,193,196,325], biochemical processes[326–328] or solar cell materials[60,329,330]. Regarding catalysis, a particularly important field of research concerns the spectro-electrochemistry at solid-liquid electrode interfaces. It is therefore highly desirable to resolve ultrafast vibrational dynamics of adsorbates at electrode surfaces, since these can report on how interfacial charges influence intermolecular and environmental interactions. The different substrate materials

used for sample immobilization at surfaces, *e.g.* metals or semiconductors, often exhibit high electrical conductivity, which allows one to use such layers as the working electrode of an electrochemical cell. By applying an electrochemical potential to that electrode and adding a counter and a reference electrode, it is therefore possible to transform the sample cell into a spectro-electrochemical device.[135,293,331–333] However, the intrinsic IR-absorbance of a metal layer on the order of a few nanometer, the electrolyte solution, as well as the geometrical arrangements of working-, counter- and reference-electrodes impose experimental challenges.[175]

We have recently devised surface-sensitive third-order 2D ATR IR in combination with spectro-electrochemistry in a way that reduces these constraints.[175] In this approach, the totally-reflecting interface of a CaF_2 prism was made conductive by deposition of a 5 nm Indium-Tin-Oxide (ITO) layer. The use of ITO instead of metal layers is beneficial due to the low intrinsic IR absorbance of the material.[175] CO has then been bound to an additional Pt layer, which was so thin (average thickness of 0.1 nm) that it would not be conducting by itself, since it forms disconnected Pt nanoparticles. Figure 30 (a) – (c) shows 2D ATR IR spectra of that configuration with varying electrochemical potential. In a potential range of -1 V to +0.4 V, the frequency of the stretching mode of linearly-bound CO changes due to a vibrational Stark-shift with a tuning rate of 24 cm^{-1} V^{-1} (Figure 30 (d)), in good agreement with earlier reports obtained by other methods.[271,310,334] The Stark-effect is commonly explained by two combined effects, *i.e.* (i) potential-dependent changes in electron densities in the molecular orbitals of the adsorbate[332,335,336], and (ii) potential-dependent changes in energetic positions of vibrational states relative to each other due to slightly different dipole moments in these levels[337,338].

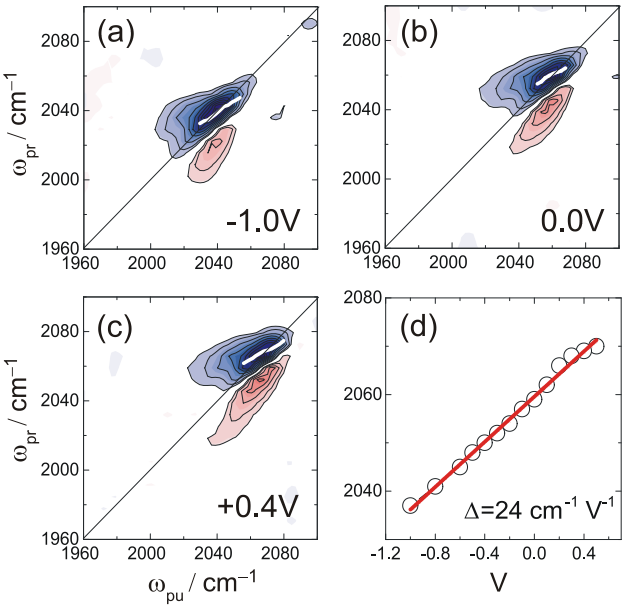

Figure 30. 2D ATR IR spectra of CO on sputter-coated Pt nanoparticles (average thickness 0.1 nm) on an ultrathin ITO electrode (average thickness 5 nm) in a potential region of (a) -1 V, (b) 0 V, and (c) +0.4 V. Blue signals correspond to GSB/SE, while red signals are due to ESA. White lines in the regions of GSB/SE correspond to the CLS. (d) The frequency of the CO stretching vibration shifts with a tuning rate of 24 cm^{-1} V^{-1}. Open circles represent measured data while the red solid line is a linear fit. All potentials were measured against a Ag/AgCl reference electrode. Adapted with permission from ref.[175]*. Copyright (2016) American Chemical Society. Copyright (2016) American Chemical Society.*

In addition, the spectral diffusion dynamics of the CO have been measured in dependence of the applied potential.[175] The CLS (white lines in Figure 30 (a) – (c)) at a series of population times revealed that the spectral diffusion of the CO molecule accelerates, if at all, only marginally from ~9.7 ps to ~8.6 ps when increasing the potential from -1.0 V to +0.4 V, respectively (Figure 31).[175] This indicates that the electrostatic potential induced by the surface charge has only a minor effect on the hydrogen-bonding network and the re-orientation dynamics of water molecules at the interface. This nearly absent surface-charge dependence is in contrast to water dynamics at other inorganic oxide-water interfaces (*e.g.* SiO_2), where the formation of hydrogen-bonds between water and the charged surface oxides strongly influences the network of water molecules and the associated vibrational dynamics.[50,133,134]

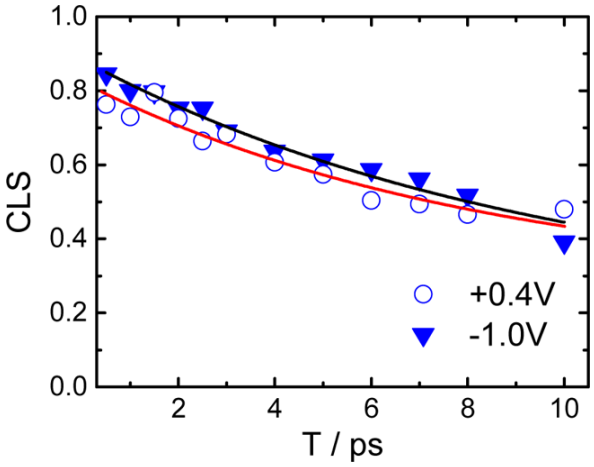

Figure 31. Spectral diffusion obtained from CLS from 2D ATR IR data of CO on an ITO/Pt electrode for electrochemical potentials of +0.4 V (circles) and -1.0 V (triangles). Solid lines correspond to single exponential fits including an offset. The potentials were measured against a Ag/AgCl reference electrode. Adapted with permission from ref.[175]*. Copyright (2016) American Chemical Society.*

The combination of 2D IR methods with electrochemistry allows one to study potential-dependent ultrafast dynamics near the electrodes of electrochemical devices. Many important phenomena can be investigated, including potential-dependent re-orientation of adsorbates[339,340], redox-active samples and electro-catalysts[308,341–343], structural dynamics within the Helmholtz double layer[344,345], or the origin of overpotentials for electrochemical reactions[343,346]. The possible range of applications is broad, ranging from catalytic water-splitting[347–349] and CO_2-reduction[293,343,350,351] to biologically-relevant redox-active proteins[326,327].

3.4. Surface-Sensitivity Through Surface-Enhancement

A common approach to gain surface sensitivity is based on short-ranged optical near-field effects generated in plasmonic nanostructures.[31,73,130,352,353] Despite lacking strict surface-specificity, this method has proven its use in $\chi^{(1)}$ FT-IR spectroscopy for various samples.[130,230,233,353–360] The basis is the generation of enhanced near-fields at interfaces from

plasmonic nanostructures such as noble metal particles[73,130,226,354,360,361] or nano-antennas[231,234,235,362–364], similar to surface-enhanced Raman spectroscopy (SERS).[365–368] The near-field enhancement extends to distances of only a few nanometers (< 20 nm) from the surface[31,73,130,352,353], and artificially enhances the sensitivity of the spectroscopic method to molecules at the interface by concentrating the interaction volume of the light and the sample. In this section, we give an overview on the strategies and results, which have been developed to exploit these surface-enhancement effects in the field of 2D IR spectroscopy at surfaces.

3.4.1. Enhancement from Noble Metal Nanoparticles

Using plasmonic Au nanoparticles as a source of near-field enhancement, we have characterized enhancement factors (EFs) for organic MLs under various experimental condictions,[31,176,177] The EF is defined as the enhancement for linear absorption, which scales as $\langle \mu_{eff} \rangle^2$, where μ_{eff} is the effective (*i.e.*, possibly enhanced) transition dipole and $\langle .. \rangle$ denotes an orientational average. On isolated Au nanoparticles in solution, comparatively small EFs of about 5 have been observed.[31] The dominant effect is the polarizability of the metal nanoparticles, which induces an enhanced radial electric field around the particle that can be lumped into μ_{eff}. This effect acts twice, *i.e.* for the excitation of the molecules transition dipole via the external field of the laser as well as for the resubmission of a free induction decay. In addition, also the orientational alignment of the transition dipoles on the metal surface relative to the local field contributes to the signal enhancement. Since the 2D IR signal scales as $\langle \mu_{eff} \rangle^4$, it in fact scales with EF^2, [31,176] implying that an EF^2-fold smaller number of molecules is needed to reveal the same 2D IR signal strength as a comparable non-enhanced signal.

The EFs can be significantly larger on sputter-coated substrates, which consist of aggregated of nanoparticles on the surface as long as the average metal layer thickness is small (≈1 nm). These aggregates result in a concerted action of near-fields from neighboring nanoparticles

that increases the local field in so-called "hot spots"[176,226], *i.e.*, the gaps between particles (Figure 32 (a) and (b)). By the polarization of the measurement light, one can select which parts of the nanoparticles are addressed. That is, s-polarized light generates an evanescent wave with a y-component at the interface, which polarizes the nanoparticles in the prism-plane and hence generates a strongly enhanced field in these gaps between the nanoparticles (shaded regions in Figure 32 (b)).[176,202] In contrast, p-polarized light generates an evanescent wave, which is predominately z-polarized at the interface,[176,202] and hence polarizes the nanoparticles along the normal of the prims surface (z-direction, Figure 32). In that case, the highest fields (shaded regions in Figure 32 (a)) are generated on the top of the nanoparticles,[176,226] which however are significantly smaller than for s-polarization. The shape of the nanoparticles is known to also have an effect on the near-field enhancement. That is, ellipsoidal particles have a long and a short axis, with the polarizability being larger along the long axis.[72] This effect increases the enhancement for s-polarized light even further, when the particles are flattened on the surface.

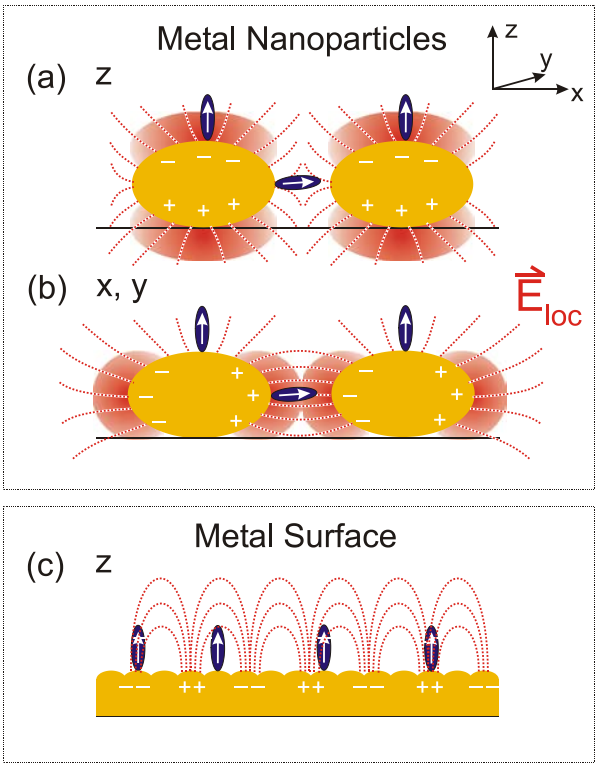

Figure 32. Surface-enhancement by (a) and (b) metal nanoparticles and (c) by a continuous surface. The predominant polarization of the nanoparticles for p-polarized and s-polarized light is shown in panels (a) and (b), respectively, with the dashed lines plotting the local electric fields around the nanoparticles and the red shades indicating regions of highest field strengths. (c) Excitation of a surface plasmon polariton, which is possible only for p-polarization. Adapted with permission from ref.[177]*. Copyright (2016) Published by the PCCP Owner Societies.*

For a continuous metal layer surface, a different enhancement mechanism dominates. p-Polarized light then can excite a surface plasmon polariton (SPP), which results in polarization of the metal layer along the z-direction (Figure 32 (c)).[200,369–373] Such a SPP can travel along the interface and generate local fields, which are perpendicular to the prism surface plane and are responsible for signal enhancement. For a perfect metal layer, the SPP can be excited only with p-polarized light, however, if the surface is structured on nanometer dimensions, it is still possible to obtain signals with s-polarized light due to the excitation of hot-spots between these nanostructures.[31,176,177,226]

The discussed near-field excitation mechanisms have been explored by polarization-resolved 2D ATR IR for MLs from para-mercaptobenzonitrile (p-PhCN) on Au surfaces.[176,177] Figure 33 shows the observed signal enhancement factors in dependence of the average metal thickness. Starting at EFs well below 100 for ≤ 1 nm (s-polarization), the EF increases continuously up to about 470 (3 nm) and afterwards decreases again due to the increasing IR absorbance of the metal layer itself. The gradual increase of EFs with average metal thickness results from the growth of the nanoparticles and the formation of hot-spots between the aggregates.[176] Contrasting to that, EFs for p-polarization stay low below 3 nm (< 10), but increase abruptly for a layer thickness of about 3.5 nm. That abrupt rise coincides with the percolation threshold, where the gold layer starts to become macroscopically conductive, and hence a SPP can form.[200,369–372] Enhancing 2D IR signals by plasmonic substrates is a

powerful tool to measure dynamics from MLs with very only low extinction coefficients (here: ε(p-PhCN) ≈ 170 M^{-1} cm^{-1}).

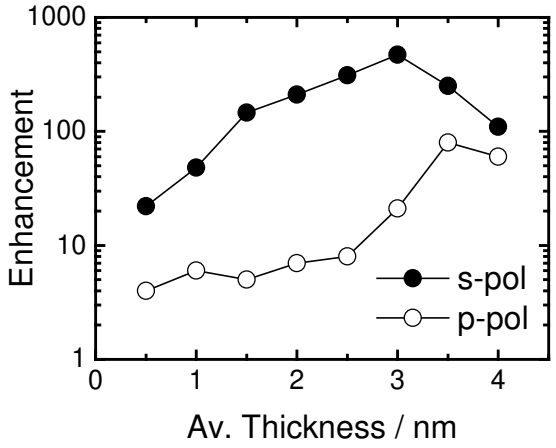

Figure 33. Dependence of the polarization-resolved EF for the CN stretch vibration of p-PhCN MLs on the average Au metal layer thickness. Solid circles are for s-polarization, open circles for p-polarization. Adapted with permission from ref.[177]*. Copyright (2016) Published by the PCCP Owner Societies.*

3.4.2. Vibrational Ladder Climbing in Surface-Enhanced 2D ATR IR Spectroscopy

With large EFs, the probability of multiple light-matter interactions between the excitation pulses and the sample increases. We have examined this effect[177] by employing an almost continuous Au layer (average thickness 3.5 nm) for the preparation of MLs. As shown in Figure 34, 2D ATR IR signals from MLs of p-PhCN exhibit clear signatures of multi-photon excitation pathways, which are absent for molecules in solution but otherwise measured under the same conditions. While the bulk signals exhibited a GSB/SE signal along with only a single red-shifted ESA bands, the surface-enhanced signal shows a series of increasingly red-shifted ESA bands, which correspond to the 2-3, 3-4 and even 4-5 transitions (Figure 34 (c) and (f)). Excitation with s-polarized light reveals a longer progression of ESA signals as compared to p-polarization, since the EF is larger (Figure 33).

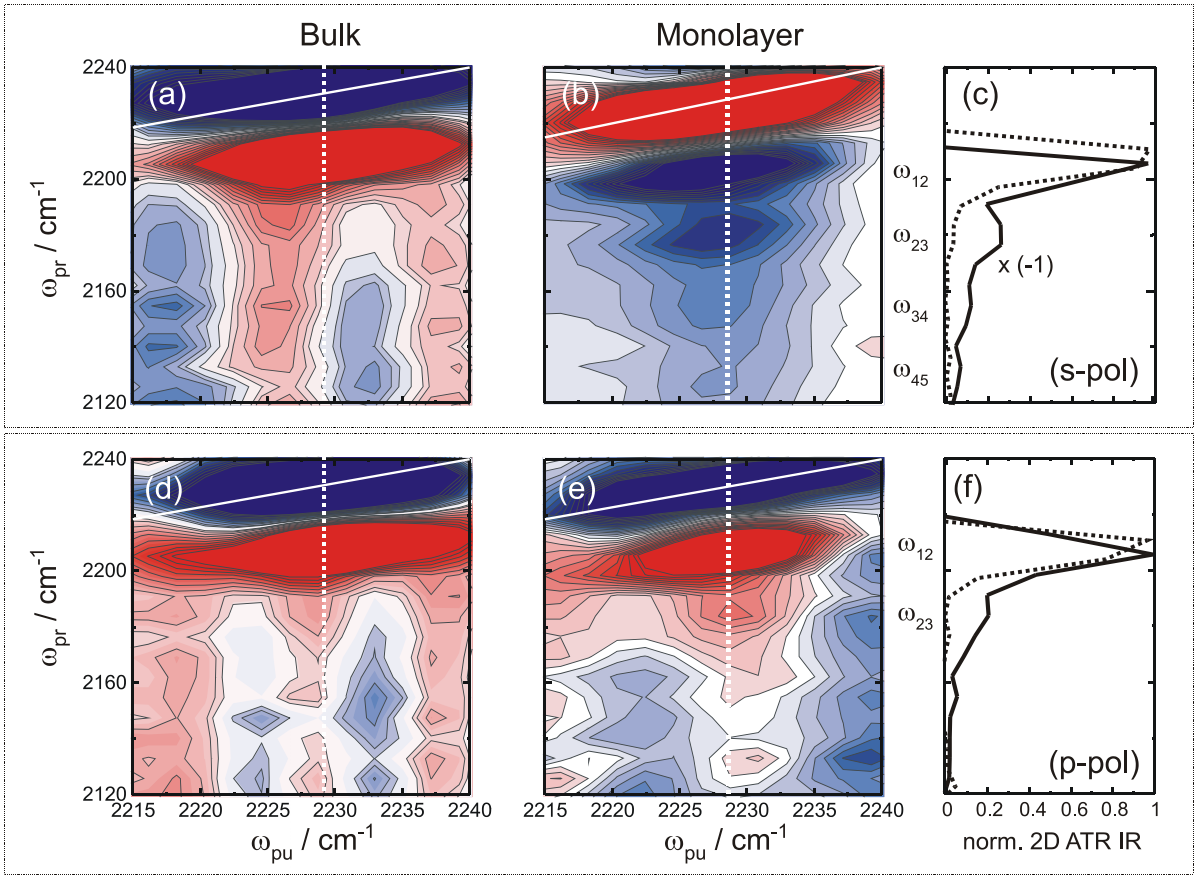

Figure 34. Vibrational ladder-climbing in 2D ATR IR for p-PhCN on a 3.5 nm thin Au layer. Panels (a) and (c) used s-polarized light, panels (d) and (f) p-polarized light, the left column was measured in bulk solution, the center column as a ML, and the right column contains cuts along the probe axis at the center frequency of the transition (indicated as white lines in (a)/(b) and (d)/(e)). Adapted with permission from ref.[177]*. Copyright (2016) Published by the PCCP Owner Societies.*

Significant interest exists in the characterization of highly excited vibrational states from different experimental and theoretical perspectives, since this represents a concentration of a large amounts of vibrational energy in a single chemical bond.[55,89,90,305,374–381] A particular focus lies on the mechanism of preparation of these states and how highly excited molecules dissipate the excess energy to the environment. The energy can for instance be transferred to the substrate and its phonon bath, leading to an increase in the sample temperature.[52,90] The energy can also be transferred to other adsorbed molecules *via* Förster-type energy transfer, or via intra- and intermolecular energy dissipation to lower-frequency modes.[90] Other

applications can be envisioned in the direction of mode-selective chemistry[382–384] at surfaces. Highly-excited molecules may be prepared in the vicinity of transition states of chemical reactions such as isomerization[385–387], surface-desorption reactions[306,388–393], or bond dissociation reaction[13,382,384,394–397]. Especially 2D IR methods are very powerful in this regard, since they allow one to directly observe energy transfer processes and couplings via cross-peaks and their associated kinetics.[71] Vibrational ladder-climbing on a surface therefore opens up a series of exciting applications regarding the investigation of vibrational dynamics in high energy regions of the ground state potential, which are not accessible by direct IR excitation.

3.4.3. Antenna-Enhanced Surface Spectroscopy

Purposely tailored nano-antennas with different size and shapes to enhance weak signals from very low numbers of molecules are widespread in ultra-sensitive IR spectroscopy.[229–234,362,363,398–400] This concept has recently been extended to ultrafast 2D IR spectroscopy by Rezus et al..[291] The plasmon-resonance for the metal nano-structures can be shifted from the VIS spectral range to the mid-IR by tuning of the size and shape of the antenna.[229–234,362,363,398–400] Figure 35 (a) and (b) show antenna-enhanced transmission 2D IR signals from the CO stretch vibration of 5 nm thin polymethylmetacrylate (PMMA) layers atop of randomly-positioned Au antennas (Figure 35 (c)).[291] The antennas have been randomly positioned to average out coupling between the antennas. The two given antenna lengths corresponded to plasmon resonances that are spectrally red- (a) or blue-shifted (b) with respect to the carbonyl-band of PMMA (1730 cm^{-1}). In this case, EFs as high as 60000 have been estimated,[291] which are much larger than what has been observed for sputter-coated metal surfaces.

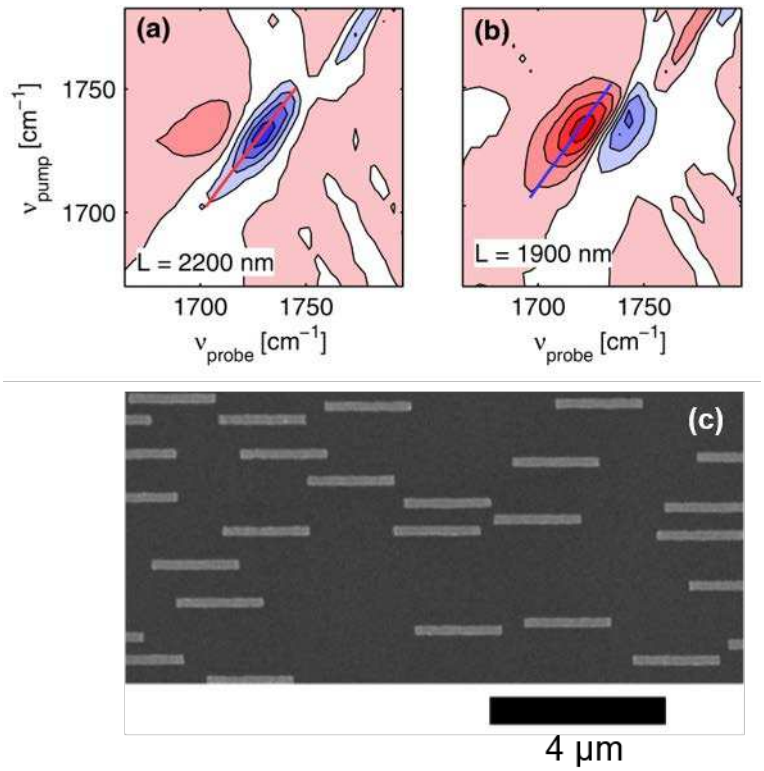

Figure 35. (a) and (b) 2D IR signals from a 5 nm layer of polymethylmetacrylate (PMMA) on Au nano-antennas of lengths L = 2200 nm and 1900 nm, respectively. Blue bands correspond to GSB/SE signals and red bands to ESA signals. The blue and red lines correspond to the center lines of the bands. (c) Scanning electron microscopy image of a random array of Au nano-antennas. Adapted with permission from ref.[291]*. Copyright (2015) American Physical Society.*

In this case, the optical near-fields are excited resonantly with the incident IR light.[233,234] Such surface-enhanced signals have been interpreted by a coupled-dipole model, which assumes a multiple scattering process for signal generation.[231,401] The near-resonance of vibrational transition and plasmon resonance results in a Fano-type lineshape (see also section 2.2.2.3), *i.e.* an interference between the sharp resonance of the vibrational transition with a broadband continuum.[229,232,234,235,402–404] Its asymmetric line profile can be discerned from the 2D IR signals by the different relative amplitudes of the GSB/SE and ESA bands (Figure 35 (a) compared to (b)).

3.4.4. Summary on Surface-Enhanced 2D IR Spectroscopy

Metal surfaces, metal nanoparticles at surfaces as well purposely designed nano-antennas at surfaces reveal significant EFs for 2D IR signals, which enable many possible applications. For example, peptides and proteins[121,326,327,398,405] or other biomolecules[249,406], as well as organic thin films[24,407,408] exhibit a variety functional groups with only low to intermediate absorption coefficients (~100 - 1000 M^{-1} cm^{-1}). Such systems can nevertheless be investigated with surface-enhanced 2D IR. Applications may be found in label-free diagnostic tools for chemical sensing[409–411] or molecular recognition[319,412,413].

Surface-enhanced 2D IR spectroscopy is currently applied in transmission and ATR geometry. However, similar electromagnetic signal enhancement effects can contribute in SFG as well[259], but have not been discussed so far in multi-dimensional signals. When using continuous metal layers for immobilization of the samples, it is noteworthy that a SPP cannot be excited under external reflection conditions due to missing wave-vector matching.[132,369,371,372] This would require an ATR techniques in surface-enhanced 2D SFG. Alternatively, periodic structures such as gratings may still excite a plasmon-polariton,[369] or local surface plasmons from nanoparticles can be exploited.[31,176]

3.5. Transient 2D IR at Interfaces

The majority of 2D IR studies at interfaces explored the equilibrated electronic ground state of the sample. Predominately in the fields of light-to-energy conversions[60,62,329,330,414] and photo-catalysis[38,42,415–421], significant interest also exists in non-equilibrium dynamics induced by either the transient formation of new chemical species or electronically excited states. We consider here transient 2D IR spectroscopy obtained by the implementation of an extra pulse to the 2D IR sequence, *i.e.* a UV-VIS actinic pump pulse.[83,217,277,292,422–424]

One example in this regard is the study of the excited electronic state of a metal-carbonyl dye following charge-injection into a semiconductor surface (TiO_2).[292] IR spectroscopy is a powerful method for studying such reactions, since vibrational frequencies of metal-carbonyl complexes sensitively respond to changes in oxidation states of this type of photo-sensitizers.[216,277,423,424] Figure 36 shows a comparison of (a) third-order 2D IR data along with (c) and (d) transient 2D IR data, and (b) the relevant pulse sequences for obtaining the spectra. The 2D IR signals of the symmetric carbonyl stretch vibration (top row sequence in (b)) were characterized by three GSB/SE (blue) and ESA (red) signals, which corresponded to different binding configurations and aggregates of the dye, similar as in Figure 27 (section 3.2.3).[286,287]

UV excitation followed by a 2D IR sequence (Type I, middle row in Figure 36 (b)) revealed excited state features (2060 cm^{-1}) in the 2D IR spectra, and the depletion of the electronic ground state of the dye (Figure 36 (c)). The formation of spectrally-shifted excited state features occurred since the CO stretch vibration is influenced by the oxidation state of the metal center.[217,423–425] However, from the transient 2D IR signal in Figure 36 (c) it is not directly clear if all existing adsorbate conformations contribute to the formation of the charge-injected species. This was determined from an additional transient 2D IR sequence, *i.e.* by placing the UV excitation pulse after the two first IR interactions (Type II, bottom row in Figure 36 (b)). Such a sequence is used to spectrally correlate the ground-state vibrational signature excited by the IR pump pulses with the excited state vibrational signature encountered by the IR probe pulse.[424,426] Figure 36 (d) shows that for this pulse sequence, a cross peak appears only for the lower frequency ground state absorption band (< 2035 cm^{-1}), but not for the other one. A more careful analysis of the cross-peak intensities revealed that the different conformations exhibit different efficiencies for electron injection.[292]

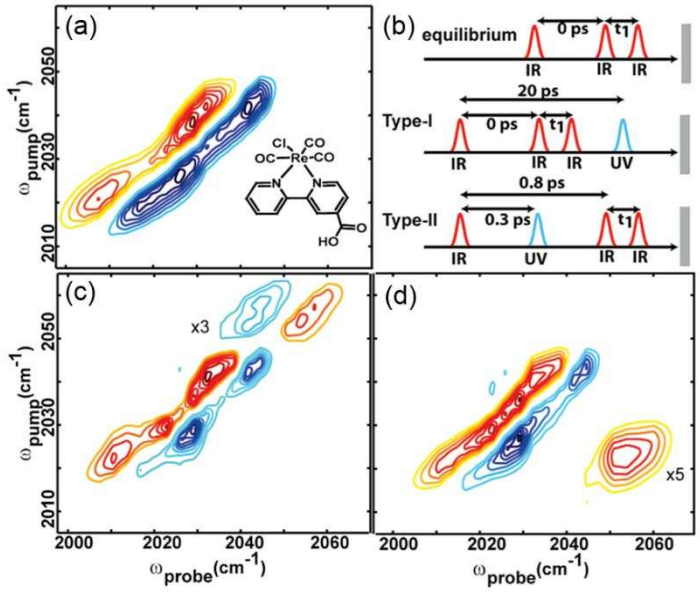

Figure 36. Comparison of 2D IR and transient 2D IR signals of a Re-carbonyl dye on a nano-particulate TiO_2 film. (a) Equilibrium 2D IR for the Re-dye (inset). (b) pulse sequences used for equilibrium and transient 2D IR. (c) and (d) Transient 2D IR spectra of the Re-dye for the Type I and Type II sequences in (b), respectively. Adapted with permission from ref.[292]*. Copyright (2009) American Chemical Society.*

Although reports on surface-sensitive transient 2D IR are still rare, with applications currently being limited to only strong IR-labels (*i.e.* metal carbonyls) and micrometer thicknesses of samples, its development is a significant advance for time-resolved surface spectroscopy. Charge injection between organic or inorganic dyes and semiconductors is an intense field of research[292,427–436], to which transient 2D IR can contribute by resolving adsorption geometries for optimal charge-injection dynamics, as shown above. Additional valuable information concerns degradation mechanisms, long-time performance, along with dye migration and restructuring of the surface. Other possible applications exist regarding isomerization reactions of molecular switches at surfaces,[385] or the impact of surface electronic states on adsorbates.[46–48,437–443] We expect that third-order 2D IR is going to be advantageous as a starting point for implementing transient 2D IR over a broader range of sample systems, since 2D SFG is already a higher-order nonlinear method with even weaker signals.

4. Conclusions and Outlook

4.1. General Remarks

Third-order 2D IR spectroscopy for samples in solution is an established method in time-resolved spectroscopy. After almost two decades of technological development, 2D IR is capable for routinely resolving, for instance, ultrafast conformational changes[88], structural diversity of bio-molecules[159,279], drug-binding to enzymes[444] or multi-ion configurations in K^+ channels[445]. Application of 2D IR methods to molecules at interfaces is, however, much less common as of now. Since the initial reports of 2D IR at surfaces less than ten years ago[135,149,181], three techniques have emerged, which we have discussed here. These are in chronological order of development: (i) 2D SFG, (ii) transmission 2D IR, and (iii) internal (ATR) and external reflection 2D IR spectroscopy. We have defined surface-sensitivity as the capability of a method to measure 2D IR spectra from only ML thin samples at solid-liquid interfaces. The methods can be further divided into truly *surface-specific* (2D SFG) and *surface-sensitive* versions (transmission and reflection 2D IR). This is based on the involvement of even- and odd-order nonlinear susceptibilities. It has been demonstrated that all three methods reveal similar molecular information with comparable temporal (sub-picosecond) and spectral resolution ($< 10\ cm^{-1}$). Fourth-order 2D SFG, however, offers the benefit of being specific to only the molecules at the interface, and to allow determining molecular orientation. At the same time, 2D SFG is experimentally more demanding as compared to third-order 2D IR methods (transmission and reflection).

The extraordinary sensitivity of all described methods, *i.e.* being able to generate a nonlinear signal from a very low number of molecules in a monolayer or less, is a major experimental achievement. Such sensitivity-levels would have been considered "out-of-reach" during the early days of ultrafast multi-dimensional infrared spectroscopy about eighteen years ago,[77]

and for a long time, concentrations of ≳10 mM were needed to measure a 2D spectrum and meaningful temporal evolution thereof. With the current experimental layouts, the investigation of ultrafast equilibrium dynamics at solid-liquid/gas interfaces is almost routine and it should be rather straightforward to extend them also to non-equilibrium processes.

Each of the surface 2D IR methods have proven to be useful for certain aspects of ultrafast vibrational dynamics at interfaces. The number of investigations is constantly expanding and the methods hold promise to create a fundamentally new view of surface-related phenomena in the near future. The current scope of 2D IR methods at solid-liquid/gas interfaces includes (i) the elucidation of ultrafast structural dynamics of ML samples and interfacial molecular orientation, (ii) intermolecular interactions (energy transfer and vibrational coupling), (iii) strategies of enhancing the signal magnitude by plasmonic interactions, (iv) ultrafast dynamics at charged interfaces in electrochemistry, and (v) transient investigations of non-equilibrium dynamics. Thus, the different forms of 2D IR spectroscopy have emerged as powerful tools for surface-science revealing information that could not be obtained by other methods.

Taking spectral diffusion dynamics of MLs as an example, a general result from the studies reported so far is that structural fluctuations of molecules at interfaces are significantly slowed down when compared to similar systems in bulk solution. This slow-down originates from the confined environment of the MLs at the interface, as well as from reduced interactions of the ML constituents with the solvation environment induced by packing effects. With the different methods developed so far, ultrafast structural dynamics of MLs can routinely be investigated, even for low surface coverages (< 20%) and for weakly absorbing functional groups ($\varepsilon \approx 100\ M^{-1}\ cm^{-1}$).

Concerning interactions of molecules at surfaces, a surprisingly low number of studies have identified intermolecular cross-peaks in 2D IR spectra. Despite the close contact and short

intermolecular distances in a ML, the rare observation of cross-peaks indicates inefficient energy transfer pathways between adsorbate molecules at solid-liquid/gas interfaces. Intramolecular energy redistribution, or in some cases energy transfer to the substrate, is much more efficient.

In order to enhance 2D IR signals from surfaces with a limited number of weakly absorbing molecules, plasmonic near-field effects from nano-structured substrates have been exploited in different experimental layouts. In the extreme case, tailored noble metal nano-antennas may increase the signal magnitude by more than four orders of magnitude. The only low number of molecules in a ML is thus no limitation.

Finally, ongoing method developments revealed ultrafast, 2D IR signals under electrochemical conditions or of non-equilibrium processes. The former was accomplished by designing the ATR surface as the working electrode of an electrochemical cell. Non-equilibrium dynamics were studied by incorporating an additional actinic pump pulse to a standard transmission 2D IR sequence in order to induce a perturbation of the sample (transient 2D IR). These developments are important steps towards making a broad range of future investigations available, as further outlined below.

Based on the studies that have appeared over the last few years in the field of 2D IR surface spectroscopy, we summarize the relevant points in Table 1. The biggest difference between the methods clearly lies in the odd- (transmission 2D IR, R-2D IR and 2D ATR IR) *versus* even-order nonlinear susceptibilities (2D SFG). A particular feature of 2D SFG is its possibility to discriminate molecular alignment from orientation, and 2D SFG can be performed even when molecules are not, or cannot be covalently bound to an interface, *e.g.*, at a liquid-gas or a liquid-liquid interface. Conversely, third-order methods are only applicable for immobilized samples on solid-liquid/gas interfaces, since the chemical step of surface binding is needed to discriminate the sample from the bulk solution. The probably most

prominent benefit of the odd-order methods is the comparatively easy operation based on well-established setups that can extended in a straightforward manner to a transient version for the investigation of excited electronic states. Apart from these aspects, all methods are in principle capable to resolve very similar information of molecular dynamics. With the current status of experimental methods, a powerful toolbox has already been developed that holds promise to tackle many relevant questions of surface science. In the remainder of the paper, we will give an outlook of where we think the field will go from here on.

Table 1. Overview on the presented surface spectroscopic techniques, their characteristics, applicability, benefits, challenges.

Method (Year)	Surface-...	Applied samples	Demonstrated Information	Demonstrated Benefits	Challenges/Limitations	Refs.
transmission 2D IR (2009)	sensitive ($\chi^{(3)}$)	chemi-sorbed monolayers IR-transparent semiconductors solid-liquid/gas interfaces µm-thick layers	spectral diffusion vib. relaxation energy transfer alignment excited state spectra	BOXCAR-sensitivity orientational dynamics non-enhanced and enhanced signals facile implementation	thin solvent layers transparent substrates sample immobilization	23,31,181–183,185,286,287,291,292
R-2D IR (2016)	sensitive ($\chi^{(3)}$)	chemi-sorbed monolayers reflective surfaces solid-gas interfaces	spectral diffusion vib. relaxation alignment	BOXCAR-sensitivity crystalline surfaces facile implementation	thin solvent layers sample immobilization	170
2D ATR IR (2014)	sensitive ($\chi^{(3)}$)	chemi-sorbed monolayers nanostructured metal layers IR-transparent semiconductors solid-liquid/gas interfaces	spectral diffusion vib. relaxation ladder-climbing vib. Stark-shift energy transfer vib. coupling	non-enhanced and enhanced signals minimal and tunable solvent background facile implementation	pump-probe sensitivity refractive indices of prism/sample sample immobilization polarization of evanescent waves thin metal layers	172–177
2D SFG (2008)	specific ($\chi^{(4)}$)	chemi-sorbed or physi-sorbed samples solid-liquid/gas interfaces liquid-gas interfaces	orientation vs. alignment spectral diffusion vib. relaxation energy transfer vib. coupling	surface-specificity orientation *vs.* alignment sensitivity to SFG-inactive modes via cross-peaks	phase-stability VIS- and mid-IR light sources intensity of VIS pulse thin solvent layers	49,111,119,121,135,146–149,248–252,257,263,265,266,268,318

4.2. Advancements of Sample Systems

Most of the examples discussed in this review have employed a sample covalently immobilization at the interface. While this is essentially unavoidable for any third-order order 2D IR method (transmission as well as reflection), 2D SFG is intrinsically able to resolve signals not only from chemisorbed species, but also from non-covalently bound samples (physi-sorption).[50,117,133,134] Future works are thus likely to involve applications of 2D SFG to solid-liquid interface and non-immobilized samples, similar as recently performed for, *e.g.* liquid-air interfaces.[107,263,268] Interesting applications in this direction are for instance dynamics of the solvation shell of adsorbates at interfaces. As an example, surface layers of water molecules exhibit different properties as compared to bulk water.[446–449] 2D SFG could be used to address hydrogen-bond networks at surfaces, and resolve analogies and differences to confined water molecules.[450–453] Elucidating the environmental dynamics around MLs might be an additional crucial step in establishing an understanding of the function of, *e.g.* heterogeneous catalysts. Here, dynamics and accessibility of the active sites is expected to play a key-role in their performance.

The reports on the different forms of 2D vibrational spectroscopy reviewed here employed "traditional" IR labels, which have also been used extensively in ultrafast IR spectroscopy in bulk solution.[300] While these labels are well-suited to obtain distinct information on ultrafast dynamics, such functional groups cannot always be incorporated in any sample. In addition, the labels often simply perform as "spectator" groups, being only indirectly related to the process under investigation (*e.g.* a metal-carbonyl group in a catalyst or a sensitizer). It is therefore highly desirable to expand the applicability of all types of 2D IR at surfaces to study active vibrations over a much broader spectroscopic range as considered so far. Interesting expansions might involve systems such as metal-oxygen bonds[454], oxygen-oxygen bonds[455], adsorbed atoms[456], small ions[457] and small molecules[458,459]. Similarly interesting would be the

collective intermolecular response of ML chains and solvent molecules at the interface. Modes with very low frequencies (< 1000 cm^{-1}), however, will require a combination of surface-sensitive spectroscopy with light sources from the THz spectral range.[460–463]

Another major point is the application of the surface 2D IR methods in conjunction with *in-situ* or *in-operando* working samples and devices. The most striking examples are related to vibrational dynamics in catalysis. Photo- and electro-catalysis[38,308,325,343,415,419,420,464,465], in the larger framework of "light-to-energy-conversion", are currently among the most intensely expedited fields of chemical research today. Here, countless molecular systems have been developed for potential applications regarding, *e.g.* water-splitting[41,465–468], CO_2-reduction[293,343,350,351] or waste-water treatment[418,419,469]. These systems exhibit considerably different degrees of catalytic activity, efficiency, and lifetime, for reasons that are often not clear. Establishing a correlation of the sample performance with *in-situ* structural and dynamical information is likely to help gaining a fundamental understanding of the systems and the underlying catalytic mechanisms.

4.3. Advancements of Experimental Methods

The currently existing experimental layouts are likely to undergo further technological development. A major up-coming trend will be the simplification of experimental setups, which will beneficially result in a more facile and rapid as well as in a possibly even automated data-acquisition[159,160,279]. The goal of such a development is to make 2D IR spectroscopy at interfaces routinely available as an analytical tool also to non-experts in other research fields that deal with surface-related phenomena.

In order to investigate chemical reactions at surfaces, *e.g.* catalytic cycles, an external trigger will be needed that starts the process. These triggers can be the sudden a change in interfacial temperature (T-jump)[470], surface-potential at an electrode (V-jump)[471,472], interfacial proton

concentration (pH-jump)[473], or electron-hole pair excitations[421,474–476]. Since the direct induction of such changes by electrical methods is often too slow for applications in time-resolved spectroscopy, different variants exist to produce these perturbations with the help of ultrafast laser pulses and the absorption of a photon. Optimally, the photon-induced changes in the sample are then monitored over many orders of magnitude in time (*e.g.* from femtoseconds to minutes or longer) to cover all possible responses of the sample and the formation of reaction products. This includes diffusion-related processes, energy dissipation between the sample and the environment, and the recovery of the initial state.

Finally, most studies reported here have employed heterogeneous surfaces, composed of nano-structured metal-, metal-oxide or semiconductor layers. It is expected that there exists a broad distribution of surface-binding configurations of the sample molecules, their interfacial orientation and consequently also possible intramolecular dynamics and intermolecular interactions.[22] Future developments of 2D IR at interfaces will thus need to work on resolving such spatial variations and their relevance regarding the ultrafast dynamics of the sample by the application of ultrafast nanoscopy.[477,478] This might require applications of currently developed more advanced mid-IR light-sources with for instance high (>100 kHz) repetition rates.[479–481] Employing conventional IR optics for focusing of the excitation and probing beams, the best spatial resolution that can be achieved is a few micrometers.[482] In contrast, optical near fields, generated by plasmonic nanostructures such as nano-tips, allow a considerably higher spatial resolution down to the regime of a few tens of nanometers.[483,484] In any case, the resolution of spatial differences and the establishment of an in-depth understanding of the processes at surfaces will additionally require a considerable involvement of theoretical signal analysis by help of quantum chemical calculations and MD simulations in order to interpret the results.[170,485–489]

To conclude, 2D vibrational spectroscopy at surfaces has opened up a completely new way of measuring ultrafast dynamics and spectral correlations in highly interesting and relevant samples. 2D vibrational at surfaces therefore allows the direct investigation of molecular interactions in highly heterogeneous environments. We have highlighted here the most recent technological developments in this research field along with detailed applications, which already at this point span a wide range of sample systems from biological molecules to catalysts. Starting from the current state of the art, the range of future applications for ultrafast 2D vibrational surface spectroscopy is very broad and the possible impact of the methods can hardly be overrated.

5. Author Information

‡*philip.kraack@chem.uzh.ch*

Phone: +41 44 63 544 77

**peter.hamm@chem.uzh.ch*

Phone: +41 44 63 544 31

Fax: +41 44 63 568 38

6. Author Biographies

Jan Philip Kraack obtained his Diploma degree in Chemistry from the Philipps-University of Marburg/Lahn (Germany) in 2008, working on ultrafast four- and six-wave-mixing spectroscopy on retinal proteins, under the supervision of Marcus Motzkus. He obtained his doctoral degree in 2013 (Dr. rer. nat.) from the Ruprecht-Karls-University Heidelberg (Germany), working on multi-dimensional ultrafast spectroscopy of vibrational coherence dynamics in excited electronic states of polyenes. In 2013 he joined the research group of

Peter Hamm at the University of Zürich (Switzerland), working on the development and application of new experimental methods for ultrafast, two-dimensional infrared spectroscopy at solid-liquid interfaces.

Peter Hamm studied physics at the Technical University of Munich (Germany), were he received his Diploma degree in Physics. He carried out his PhD studies under the supervision of Wolfgang Zinth at the Ludwig-Maximilians-University of Munich (Germany) between 1991 and 1995. He then moved to the University of Pennsylvania, Philadelphia and worked as a postdoc with Robin Hochstrasser. In 1999, he was appointed as an independent group leader at the Max Born Institute in Berlin (Germany). In 2001, he moved to University of Zürich (Switzerland) as Associate Professor at the Department of Physical Chemistry, and was promoted to Full Professor in 2007.

7. Acknowledgements

This research was funded by the Swiss National Science Foundation through grant number CRSII2_160801/1 and by the URRP LightChEC of the University of Zürich. Experimental support by the Center of Microscopy and Imaging at the University of Zürich (ZMB) with regard to the preparation and characterization of the metal layers is gratefully acknowledged.

8. References

(1) Zaera, F. Probing Liquid/solid Interfaces at the Molecular Level. *Chem. Rev.* **2012**, *112*, 2920–2986.

(2) Madey, T. E.; Yates Jr, J. T. *Vibrational Spectroscopy of Molecules on Surfaces*; Springer Science & Business Media: New York, 2013; Vol. 1.

(3) Ibach, H. *Physics of Surfaces and Interfaces*; Springer Berlin Heidelberg, 2006.

(4) Whitesides, G. M.; Laibinis, P. E. Wet Chemical Approaches to the Characterization of Organic Surfaces: Self-Assembled Monolayers, Wetting, and the Physical-Organic Chemistry of the Solid-Liquid Interface. *Langmuir* **1990**, *6*, 87–96.

(5) Somorjai, G. A.; Li, Y. Impact of Surface Chemistry. *Proc. Natl. Acad. Sci. U. S. A.* **2011**, *108*, 917–924.

(6) Castner, D. G.; Somorjai, G. A. Surface Structures of Adsorbed Gases on Solid Surfaces. A Tabulation of Data Reported by Low-Energy Electron Diffraction Studies. *Chem. Rev.* **1979**, *79*, 233–252.

(7) Somorjai, G. A. Modern Surface Science and Surface Technologies: An Introduction. *Chem. Rev.* **1996**, *96*, 1223–1236.

(8) Whitesides, G. M.; Ostuni, E.; Jiang, X.; Ingber, D. E. Soft Lithography in Biology. *Annu. Rev. Biomed. Eng.* **2001**, *3*, 335–373.

(9) Yates, J. T. Surface Chemistry at Metallic Step Defect Sites. *J. Vac. Sci. Technol. A Vacuum, Surfaces, Film.* **1995**, *13*, 1359–1367.

(10) Hiemenz, P. C. *Principles of Colloid and Surface Chemistry*; M. Dekker New York, 1986; Vol. 188.

(11) King, D. A. *The Chemical Physics of Solid Surfaces and Heterogeneous Catalysis*; Elsevier: Amsterdam, Oxford, New York, Tokyo, 2012; Vol. 5.

(12) Ertl, G. Reactions at Surfaces: From Atoms to Complexity (Nobel Lecture). *Angew. Chemie - Int. Ed.* **2008**, *47*, 3524–3535.

(13) Zambelli, T.; Wintterlin, J.; Trost, J.; Ertl, G. Identification of the “Active Sites” of a Surface-Catalyzed Reaction. *Science* **1996**, *273*, 1688–1690.

(14) Hess, C.; Funk, S.; Bonn, M.; Denzler, D. N.; Wolf, M.; Ertl, G. Femtosecond Dynamics of Chemical Reactions at Surfaces. *Appl. Phys. A Mater. Sci. Process.* **2000**, *71*, 477–483.

(15) Kolasinski, K. W. *Surface Science: Foundations of Catalysis and Nanoscience*; 3rd ed.; John Wiley & Sons: Chichester, UK, 2012.

(16) Adamson, A. W.; Gast, A. P. *Physical Chemistry of Surfaces*; 6th ed.; John Wiley & Sons, Inc.: New York, 1967.

(17) Somorjai, G. A.; Li, Y. *Introduction to Surface Chemistry and Catalysis*; 2nd ed.; John Wiley & Sons: Hoboken, New Jersey, 2010.

(18) Zaera, F. Surface Chemistry at the Liquid/solid Interface. *Surf. Sci.* **2011**, *605*, 1141–1145.

(19) Love, J. C.; Estroff, L. A.; Kriebel, J. K.; Nuzzo, R. G.; Whitesides, G. M. Self-Assembled Monolayers of Thiolates on Metals as a Form of Nanotechnology. *Chem. Rev.* **2005**, *105*, 1103–1169.

(20) Ulman, A. Formation and Structure of Self-Assembled Monolayers. *Chem. Rev.* **1996**, *96*, 1533–1554.

(21) Anatoli Davydov. *Molecular Spectroscopy of Oxide Catalyst Surfaces*; John Wiley & Sons, Inc.: Hoboken, New Jersey, 2003.

(22) Calabrese, C.; Vanselous, H.; Petersen, P. B. Deconstructing the Heterogeneity of Surface-Bound Catalysts: Rutile Surface Structure Affects Molecular Properties. *J. Phys. Chem. C* **2016**, *120*, 1515–1522.

(23) Yan, C.; Yuan, R.; Nishida, J.; Fayer, M. D. Structural Influences on the Fast Dynamics of Alkylsiloxane Monolayers on SiO 2 Surfaces Measured with 2D IR Spectroscopy. *J. Phys. Chem. C* **2015**, *119*, 16811–16823.

(24) Ulman, A. *An Introduction to Ultrathin Organic Films: From Langmuir-Blodgett to Self-Assembly*; Academic Press, Inc.: San Diego, 2013.

(25) Barth, J. V; Costantini, G.; Kern, K. Engineering Atomic and Molecular Nanostructures at Surfaces. *Nature* **2005**, *437*, 671–679.

(26) Chechik, B. V.; Crooks, R. M.; Stirling, C. J. M. Reactions and Reactivity in Self-Assembled Monolayers. *Adv. Mater.* **2000**, *12*, 1161–1171.

(27) Badia, A.; Lennox, R. B.; Reven, L. A Dynamic View of Self-Assembled Monolayers. *Acc. Chem. Res.* **2000**, *33*, 475–481.

(28) Talapin, D. V.; Lee, J. S.; Kovalenko, M. V.; Shevchenko, E. V. Prospects of Colloidal Nanocrystals for Electronic and Optoelectronic Applications. *Chem. Rev.* **2010**, *110*, 389–458.

(29) Boles, M. A.; Ling, D.; Hyeon, T.; Talapin, D. V. The Surface Science of Nanocrystals. *Nat. Mater.* **2016**, *15*, 141–153.

(30) Häkkinen, H. The Gold-Sulfur Interface at the Nanoscale. *Nat. Chem.* **2012**, *4*, 443–455.

(31) Donaldson, P. M.; Hamm, P. Gold Nanoparticle Capping Layers: Structure, Dynamics, and Surface Enhancement Measured Using 2D-IR Spectroscopy. *Angew. Chemie-International Ed.* **2013**, *52*, 634–638.

(32) Templeton, A. C.; Wuelfing, W. P.; Murray, R. W. Monolayer-Protected Cluster Molecules. *Acc. Chem. Res.* **2000**, *33*, 27–36.

(33) Kasemo, B.; Lausmaa, J. Material-Tissue Interfaces: The Role of Surface Properties and Processes. *Environ. Health Perspect.* **1994**, *102*, 41–45.

(34) Chan, V.; Graves, D. J.; Fortina, P.; Mckenzie, S. E. Adsorption and Surface Diffusion of DNA Oligonucleotides at Liquid / Solid Interfaces. *Langmuir* **1997**, *28*, 320–329.

(35) Mahon, E.; Salvati, A.; Baldelli Bombelli, F.; Lynch, I.; Dawson, K. A. Designing the Nanoparticle-Biomolecule Interface For “targeting and Therapeutic Delivery.” *J. Control. Release* **2012**, *161*, 164–174.

(36) Gomer, R. Diffusion of Adsorbates on Metal Surfaces. *Rep. Prog. Phys.* **1990**, *53*, 917–1002.

(37) Barth, J. V. Transport of Adsorbates at Metal Surfaces: From Thermal Migration to Hot Precursors. *Surf. Sci. Rep.* **2000**, *40*, 75–149.

(38) Fox, M. A.; Dulay, M. T. Heterogeneous Photocatalysis. *Chem. Rev.* **1993**, *93*, 341–357.

(39) Somorjai, G. A.; Contreras, A. M.; Montano, M.; Rioux, R. M. Clusters, Surfaces and Catalysis. *Proc. Natl. Acad. Sci. U. S. A.* **2006**, *103*, 10577–10583.

(40) Bailey, D. C.; Langer, S. H. Immobilized Transition-Metal Carbonyls and Related Catalysts. *Chem. Rev.* **1981**, *81*, 110–144.

(41) Maeda, K.; Domen, K. Photocatalytic Water Splitting: Recent Progress and Future Challenges. *J. Phys. Chem. Lett.* **2010**, *1*, 2655–2661.

(42) Schneider, J.; Matsuoka, M.; Takeuchi, M.; Zhang, J.; Horiuchi, Y.; Anpo, M.; Bahnemann, D. W. Understanding TiO2 Photocatalysis : Mechanisms and Materials. *Chem. Rev.* **2014**, *114*, 9919–9986.

(43) Bahnemann, D. Photocatalytic Water Treatment: Solar Energy Applications. *Sol. Energy* **2004**, *77*, 445–459.

(44) Kamat, P. V. Photophysical, Photochemical and Photocatalytic Aspects of Metal Nanoparticles. *J. Phys. Chem. B* **2002**, *106*, 7729–7744.

(45) Pichat, P. Representative Examples of Infrared Spectroscopy Uses in Semiconductor Photocatalysis. *Catal. Today* **2014**, *224*, 251–257.

(46) Auwärter, W.; Écija, D.; Klappenberger, F.; Barth, J. V. Porphyrins at Interfaces. *Nat. Chem.* **2015**, *7*, 105–120.

(47) Mette, G.; Sutter, D.; Gurdal, Y.; Schnidrig, S.; Probst, B.; Iannuzzi, M.; Hutter, J.; Alberto, R.; Osterwalder, J. From Porphyrins to Pyrphyrins: Adsorption Study and Metalation of a Molecular Catalyst on Au(111). *Nanoscale* **2016**, *8*, 7958–7968.

(48) Nguyen, S. C.; Lomont, J. P.; Caplins, B. W.; Harris, C. B. Studying the Dynamics of Photochemical Reactions via Ultrafast Time-Resolved Infrared Spectroscopy of the Local Solvent. *J. Phys. Chem. Lett.* **2014**, *5*, 2974–2978.

(49) Wang, J.; Clark, M. L.; Li, Y.; Kaslan, C. L.; Kubiak, C. P.; Xiong, W. Short-Range Catalyst–Surface Interactions Revealed by Heterodyne Two-Dimensional Sum Frequency Generation Spectroscopy. *J. Phys. Chem. Lett.* **2015**, 4204–4209.

(50) Lis, D.; Backus, E. H. G.; Hunger, J.; Parekh, S. H.; Bonn, M. Liquid Flow along a Solid Surface Reversibly Alters Interfacial Chemistry. *Science* **2014**, *344*, 1138–1142.

(51) Chaudhury, M. K.; Whitesides, G. M. How to Make Water Run Uphill. *Science* **1992**, 1539–1541.

(52) Arnolds, H. Vibrational Dynamics of Adsorbates – Quo Vadis? *Prog. Surf. Sci.* **2011**, *86*, 1–40.

(53) Heilweil, E. J.; Casassa, M. P.; Cavanagh, R. R.; Stephenson, J. C. Picosecond Vibrational Energy Transfer Studies of Surface Adsorbates. *Annu. Rev. Phys. Chem.* **1989**, 143–171.

(54) Gruebele, M.; Wolynes, P. G. Vibrational Energy Flow and Chemical Reactions. *Acc. Chem. Res.* **2004**, *37*, 261–267.

(55) Park, J. Y.; Baker, L. R.; Somorjai, G. a. Role of Hot Electrons and Metal–Oxide Interfaces in Surface Chemistry and Catalytic Reactions. *Chem. Rev.* **2015**, *115*, 2781–2817.

(56) Bendikov, M.; Wudl, F.; Perepichka, D. F. Tetrathiafulvalenes, Oligoacenenes, and Their Buckminsterfullerene Derivatives: The Brick and Mortar of Organic Electronics. *Chem. Rev.* **2004**, *104*, 4891–4945.

(57) Anthony, J. E. Functionalized Acenes and Heteroacenes for Organic Electronics. *Chem. Rev.* **2006**, *106*, 5028–5048.

(58) Zahn, D. R. T.; Gavrila, G. N.; Salvan, G. Electronic and Vibrational Spectroscopies Applied to Organic/inorganic Interfaces. *Chem. Rev.* **2007**, *107*, 1161–1232.

(59) Bakulin, A. A.; Lovrincic, R.; Yu, X.; Selig, O.; Bakker, H. J.; Rezus, Y. L. A.; Nayak, P. K.; Fonari, A.; Coropceanu, V.; Brédas, J.-L.; et al. Mode-Selective Vibrational Modulation of Charge Transport in Organic Electronic Devices. *Nat. Commun.* **2015**, *6*, 7880.

(60) Hagfeldt, A.; Boschloo, G.; Sun, L.; Kloo, L.; Pettersson, H. Dye-Sensitized Solar Cells. *Chem. Rev.* **2010**, *110*, 6595–6663.

(61) Yu, Z.; Li, F.; Sun, L. Recent Advances in Dye-Sensitized Photoelectrochemical Cells for Solar Hydrogen Production Based on Molecular Components. *Energy Environ. Sci.* **2014**, *8*, 760–775.

(62) Hagfeldt, A.; Grätzel, M. Molecular Photovoltaics. *Acc. Chem. Res.* **2000**, *33*, 269–277.

(63) Ashford, D. L.; Gish, M. K.; Vannucci, A. K.; Brennaman, M. K.; Templeton, J. L.; Papanikolas, J. M.; Meyer, T. J. Molecular Chromophore–Catalyst Assemblies for Solar Fuel Applications. *Chem. Rev.* **2015**, *115*, 13006–13049.

(64) Xia, W.; Mahmood, A.; Liang, Z.; Zou, R.; Guo, S. Earth-Abundant Nanomaterials for Oxygen Reduction. *Angew. Chemie - Int. Ed.* **2015**, 2650–2676.

(65) Meyers, J. P.; Mcgrath, J. E.; Borup, R.; Meyers, J.; Pivovar, B.; Kim, Y. S.; Mukundan, R.; Garland, N.; Myers, D.; Wilson, M.; et al. Scientific Aspects of Polymer Electrolyte Fuel Cell Durability and Degradation. *Chem. Rev* **2007**, *107*, 3904–3951.

(66) Park, S.; Wasileski, S. A.; Weaver, M. J. Some Interpretations of Surface Vibrational Spectroscopy Pertinent to Fuel-Cell Electrocatalysis. *Electrochim. Acta* **2002**, *47*, 3611–3620.

(67) Kordesch, K. V.; Simader, G. R. Environmental Impact of Fuel Cell Technology. *Chem. Rev.* **1995**, *95*, 191–207.

(68) Wang, K.-X.; Li, X.-H.; Chen, J.-S. Surface and Interface Engineering of Electrode Materials for Lithium-Ion Batteries. *Adv. Mater.* **2015**, *27*, 527–545.

(69) Armand, M.; Endres, F.; MacFarlane, D. R.; Ohno, H.; Scrosati, B. Ionic-Liquid Materials for the Electrochemical Challenges of the Future. *Nat. Mater.* **2009**, *8*, 621–629.

(70) Palacín, M. R. Recent Advances in Rechargeable Battery Materials: A Chemist's Perspective. *Chem. Soc. Rev.* **2009**, *38*, 2565–2575.

(71) Hamm, P.; Zanni, M. *Concepts and Methods of 2D Infrared Spectroscopy*; Cambridge University Press: New York, 2011.

(72) Tolstoij, V. P.; Chernyshova, I. V; Skryshevsky, V. A. *Handbook of Infrared Spectroscopy of Ultrathin Films*; John Wiley & Sons Inc.: Hoboken, New Jersey, 2003.

(73) Aroca, R. *Surface-Enhanced Vibrational Spectroscopy*; John Wiley & Sons, Ltd: Chichester, UK, 2006.

(74) Stuart, B. *Infrared Spectroscopy: Fundamentals and Applications*; Wiley-VCH Verlag: Chichester, UK, 2013.

(75) Fayer, M. D. *Ultrafast Infrared Vibrational Spectroscopy*; Fayer, M. D., Ed.; CRC Press: Boca Raton, London, New York, 2013.

(76) Cho, M. *Two-Dimensional Optical Spectroscopy*; 1st ed.; CRC press Taylor & Francis Group: Boca Raton, London, New York, 2009.

(77) Hamm, P.; Lim, M.; Hochstrasser, R. M. Structure of the Amide I Band of Peptides Measured by Femtosecond Nonlinear-Infrared Spectroscopy. *J. Phys. Chem. B* **1998**, *102*, 6123–6138.

(78) Kwak, K.; Rosenfeld, D. E.; Chung, J. K.; Fayer, M. D. Solute-Solvent Complex Switching Dynamics of Chloroform between Acetone and Dimethylsulfoxide-Two-Dimensional IR Chemical Exchange Spectroscopy. *J. Phys. Chem. B* **2008**, *112*, 13906–13915.

(79) De Marco, L.; Thämer, M.; Reppert, M.; Tokmakoff, A. Direct Observation of Intermolecular Interactions Mediated by Hydrogen Bonding. *J. Chem. Phys.* **2014**, *141*, 034502 1-10.

(80) Woutersen, S.; Mu, Y.; Stock, G.; Hamm, P. Hydrogen-Bond Lifetime Measured by Time-Resolved 2D-IR Spectroscopy : N -Methylacetamide in Methanol. *Chem. Phys.* **2001**, *266*, 137–147.

(81) Kim, Y. S.; Hochstrasser, R. M. Chemical Exchange 2D IR of Hydrogen-Bond Making and Breaking. *Proc. Natl. Acad. Sci. U. S. A.* **2005**, *102*, 11185–11190.

(82) Zheng, J.; Kwak, K.; Xie, J.; Fayer, M. D. Ultrafast Carbon-Carbon Single-Bond Rotational Isomerization in Room-Temperature Solution. *Science* **2006**, *313*, 1951–1955.

(83) Hamm, P.; Helbing, J.; Bredenbeck, J. Two-Dimensional Infrared Spectroscopy of Photoswitchable Peptides. *Annu. Rev. Phys. Chem.* **2008**, *59*, 291–317.

(84) Kim, Y. S.; Hochstrasser, R. M. Applications of 2D IR Spectroscopy to Peptides, Proteins, and Hydrogen-Bond Dynamics. *J. Phys. Chem. B* **2009**, *113*, 8231–8251.

(85) Zanni, M. T.; Hochstrasser, R. M. Two-Dimensional Infrared Spectroscopy: A Promising New Method for the Time Resolution of Structures. *Curr. Opin. Struct. Biol.* **2001**, *11*, 516–522.

(86) Fayer, M. D. Dynamics of Liquids, Molecules, and Proteins Measured with Ultrafast 2D IR Vibrational Echo Chemical Exchange Spectroscopy. *Annu. Rev. Phys. Chem.* **2009**, *60*, 21–38.

(87) Woys, A. M.; Almeida, A. M.; Wang, L.; Chiu, C. C.; McGovern, M.; De Pablo, J. J.; Skinner, J. L.; Gellman, S. H.; Zanni, M. T. Parallel β-Sheet Vibrational Couplings Revealed by 2D IR Spectroscopy of an Isotopically Labeled Macrocycle: Quantitative Benchmark for the Interpretation of Amyloid and Protein Infrared Spectra. *J. Am. Chem. Soc.* **2012**, *134*, 19118–19128.

(88) Kolano, C.; Helbing, J.; Kozinski, M.; Sander, W.; Hamm, P. Watching Hydrogen-Bond Dynamics in a Beta-Turn by Transient Two-Dimensional Infrared Spectroscopy. *Nature* **2006**, *444*, 469–472.

(89) Frischkorn, C.; Wolf, M. Femtochemistry at Metal Surfaces: Nonadiabatic Reaction Dynamics. *Chem. Rev.* **2006**, *106*, 4207–4233.

(90) Arnolds, H.; Bonn, M. Ultrafast Surface Vibrational Dynamics. *Surf. Sci. Rep.* **2010**, *65*, 45–66.

(91) Woutersen, S.; Bakker, H. J. Resonant Intermolecular Transfer of Vibrational Energy in Liquid Water. *Nature* **1999**, *402*, 507–509.

(92) Rosenfeld, D. E.; Fayer, M. D. Excitation Transfer Induced Spectral Diffusion and the Influence of Structural Spectral Diffusion. *J. Chem. Phys.* **2012**, *137*, 064109 1-18.

(93) Noda, I. Generalized Two-Dimensional Correlation Method Applicable to Infrared, Raman, and Other Types of Spectroscopy. *Appl. Spectrosc.* **1993**, *47*, 1329–1336.

(94) Noda, I. Progress in Two-Dimensional (2D) Correlation Spectroscopy. *J. Mol. Struct.* **2006**, *799*, 2–15.

(95) Mee Jung, Y.; Noda, I. New Approaches to Generalized Two-Dimensional Correlation Spectroscopy and Its Applications. *Appl. Spectrosc. Rev.* **2006**, *41*, 515–547.

(96) Noda, I. Two-Dimensional Infrared Spectroscopy. *J. Am. Chem. Soc.* **1989**, *111*, 8116–8118.

(97) Keller, E. L.; Brandt, N. C.; Cassabaum, A. A.; Frontiera, R. R. Ultrafast Surface-Enhanced Raman Spectroscopy. *Analyst* **2015**, *140*, 4922–4931.

(98) Frontiera, R. R.; Henry, A.-I.; Gruenke, N. L.; Van Duyne, R. P. Surface-Enhanced Femtosecond Stimulated Raman Spectroscopy. *J. Phys. Chem. Lett.* **2011**, *3*, 1199–1203.

(99) Ibach, H.; Mills, D. L. *Electron Energy Loss Spectroscopy and Surface Vibrations*; Academic press, 2013.

(100) Jonas, D. M. Two-Dimensional Femtosecond Spectroscopy. *Annu. Rev. Phys. Chem.* **2003**, *54*, 425–463.

(101) Cho, M. Coherent Two-Dimensional Optical Spectroscopy. *Chem. Rev.* **2008**, *108*, 1331–1418.

(102) Abramavicius, D.; Palmieri, B.; Voronine, D. V; Šanda, F.; Mukamel, S. Coherent Multidimensional Optical Spectroscopy of Excitons in Molecular Aggregates; Quasiparticle versus Supermolecule Perspectives. *Chem. Rev.* **2009**, *109*, 2350–2408.

(103) Mukamel, S. *Principles of Nonlinear Optical Spectroscopy*; Oxford University Press: New York, Oxford, 1995.

(104) Boyd, R. W. *Nonlinear Optics*; Third Edit.; Academic Press: San Diego, 2008.

(105) Bell, G. R.; Bain, C. D.; Ward, R. N. Sum-Frequency Vibrational Spectroscopy of Soluble Surfactants at the Air/water Interface. *J. Chem. Soc. Faraday Trans.* **1996**, *92*, 515–523.

(106) Nihonyanagi, S.; Kusaka, R.; Inoue, K.; Adhikari, A.; Yamaguchi, S. Accurate Determination of Complex χ(2) Spectrum of the Air/water Interface. *J. Chem. Phys.* **2015**, *143*, 124707 1-4.

(107) Nihonyanagi, S.; Mondal, J. A.; Yamaguchi, S.; Tahara, T. Structure and Dynamics of Interfacial Water Studied by Heterodyne-Detected Vibrational Sum-Frequency Generation. *Annu. Rev. Phys. Chem.* **2013**, *64*, 579–603.

(108) Ji, N.; Ostroverkhov, V.; Chen, C.; Shen, Y. Phase-Sensitive Sum-Frequency Vibrational Spectroscopy and Its Application to Studies of Interfacial Alkyl Chains. *J. Am. Chem. Soc.* **2007**, *129*, 10056–10057.

(109) Shen, Y. R.; Ostroverkhov, V. Sum-Frequency Vibrational Spectroscopy on Water Interfaces: Polar Orientation of Water Molecules at Interfaces. *Chem. Rev.* **2006**, *106*, 1140–1154.

(110) Ishiyama, T.; Imamura, T.; Morita, A. Theoretical Studies of Structures and Vibrational Sum Frequency Generation Spectra at Aqueous Interfaces. *Chem. Rev.* **2014**, *114*, 8447–8470.

(111) Laaser, J. E.; Zanni, M. T. Extracting Structural Information from the Polarization Dependence of One- and Two-Dimensional Sum Frequency Generation Spectra. *J. Phys. Chem. A* **2013**, *117*, 5875–5890.

(112) Moad, A. J.; Simpson, G. J. A Unified Treatment of Selection Rules and Symmetry Relations for Sum-Frequency and Second Harmonic Spectroscopies. *J. Phys. Chem. B* **2004**, *108*, 3548–3562.

(113) Zhu, X. D.; Suhr, H.; Shen, Y. R. Surface Vibrational Spectroscopy by Infrared-Visible Sum Frequency Generation. *Phys. Rev. B* **1987**, *35*, 3047–3050.

(114) Ahn, D.; Dhinojwala, A. *Advances in Silicon Science*; Owe, M. J.; Dvornic, P. R., Eds.; Springer Science+Business Media Dordrecht: Dordrecht, 2012; Vol. 4.

(115) Wang, H.; Velarde, L.; Gan, W.; Fu, L. Quantitative Sum-Frequency Generation Vibrational Spectroscopy of Molecular Surfaces and Interfaces: Lineshape, Polarization, and Orientation. *Annu. Rev. Phys. Chem.* **2015**, *66*, 189–216.

(116) Hirose, C.; Akamatsu, N.; Domen, K. Formulas for the Analysis of Surface Sum-Frequency Generation Spectrum by CH Stretching Modes of Methyl and Methylene Groups. *J. Chem. Phys.* **1992**, *96*, 997–1004.

(117) Bain, C. D. Sum-Frequency Vibrational Spectroscopy of the Solid/Liquid Interface. *J. Chem. Soc. Faraday Trans.* **1995**, *91*, 1281–1296.

(118) Zhuang, X.; Miranda, P.; Kim, D.; Shen, Y. Mapping Molecular Orientation and Conformation at Interfaces by Surface Nonlinear Optics. *Phys. Rev. B* **1999**, *59*, 12632–12640.

(119) Ghosh, A.; Ho, J.-J.; Serrano, A. L.; Skoff, D. R.; Zhang, T.; Zanni, M. T. Two-Dimensional Sum-Frequency Generation (2D SFG) Spectroscopy: Summary of Principles and Its Application to Amyloid Fiber Monolayers. *Faraday Discuss.* **2015**, *177*, 493–505.

(120) Superfine, R.; Huang, J. Y.; Shen, Y. R. Phase Measurement for Surface Infrared-Visible Sum-Frequency Generation. *Opt. Lett.* **1990**, *15*, 1276–1278.

(121) Laaser, J. E.; Skoff, D. R.; Ho, J.; Joo, Y.; Serrano, A. L.; Steinkruger, J. D.; Gopalan, P.; Gellman, S. H.; Zanni, M. T. Two-Dimensional Sum-Frequency Generation Reveals Structure and Dynamics of a Surface-Bound Peptide. *J. Am. Chem. Soc.* **2014**, *136*, 956–962.

(122) Lummerstorfer, T.; Kattner, J.; Hoffmann, H. Monolayers at Solid-Solid Interfaces Probed with Infrared Spectroscopy. *Anal. Bioanal. Chem.* **2007**, *388*, 55–64.

(123) Lummerstorfer, T.; Hoffmann, H. IR Reflection Spectra of Monolayer Films Sandwiched between Two High Refractive Index Materials. *Langmuir* **2004**, *20*, 6542–6545.

(124) Chabal, Y. Surface Infrared Spectroscopy. *Surf. Sci. Rep.* **1988**, *8*, 211–357.

(125) Sheppard, N.; Erkelens, J. Vibrational Spectra of Species Adsorbed on Surfaces: Forms of Vibrations and Selection Rules for Regular Arrays of Adsorbed Species. *Appl. Spectrosc.* **1984**, *38*, 471–485.

(126) Greenler, R. G. Infrared Study of Adsorbed Molecules on Metal Surfaces by Reflection Techniques. *J. Chem. Phys.* **1966**, *44*, 310–315.

(127) Greenler, R. G.; Snider, D. R.; Witt, D.; Sorbello, R. S. The Metal-Surface Selection Rule For Infrared Spectra of Molecules Adsorbed on Small Metal Particles. *Surf. Sci.* **1982**, *118*, 415–428.

(128) Iwasita, T.; Nart, F. C. In-Situ Infrared Spectroscopy at Electrochemical Interfaces. *Prog. Surf. Sci.* **1997**, *55*, 271–340.

(129) Merklin, G. T.; Griffiths, P. R. Effect of Microscopic Surface Roughness in Surface-Enhanced Infrared Absorption Spectrometry. *J. Phys. Chem. B* **1997**, *101*, 5810–5813.

(130) Osawa, M. Surface-Enhanced Infrared Absorption. In *Near-Field Optics and Surface Plasmon Polaritons*; S. Kawata, Ed.; Springer-Verlag Berlin Heidelberg, 2001; Vol. 81, pp. 163–187.

(131) Moskovits, M. Surface Selection Rules. *J. Chem. Phys.* **1982**, *77*, 4408–4416.

(132) Moskovits, M. Surface-Enhanced Spectroscopy. *Rev. Mod. Phys.* **1985**, *57*, 783–826.

(133) Eftekhari-Bafrooei, A.; Borguet, E. Effect of Surface Charge on the Vibrational Dynamics of Interfacial Water. *J. Am. Chem. Soc.* **2009**, *131*, 12034–12035.

(134) Eftekhari-Bafrooei, A.; Borguet, E. Effect of Hydrogen-Bond Strength on the Vibrational Relaxation of Interfacial Water. *J. Am. Chem. Soc.* **2010**, *132*, 3756–3761.

(135) Xiong, W.; Laaser, J. E.; Mehlenbacher, R. D.; Zanni, M. T. Adding a Dimension to the Infrared Spectra of Interfaces Using Heterodyne Detected 2D Sum-Frequency Generation (HD 2D SFG) Spectroscopy. *Proc. Natl. Acad. Sci. U. S. A.* **2011**, *108*, 20902–20907.

(136) Ulness, D. J.; Albrecht, A. C. Theory of Time-Resolved Coherent Raman Scattering with Spectrally Tailored Noisy Light. *J. Raman Spectrosc.* **1997**, *28*, 571–578.

(137) Kirkwood, J. C. J. C.; Ulness, D. J. D. J.; Albrecht, A. On the Classification of the Electric Field Spectroscopies: Application to Raman Scattering. *J. Phys. Chem. A* **2000**, *104*, 4167–4173.

(138) Khalil, M.; Demirdöven, N.; Tokmakoff, A. Coherent 2D IR Spectroscopy: Molecular Structure and Dynamics in Solution. *J. Phys. Chem. A* **2003**, *107*, 5258–5279.

(139) Khalil, M.; Demirdöven, N.; Tokmakoff, A. Vibrational Coherence Transfer Characterized with Fourier-Transform 2D IR Spectroscopy. *J. Chem. Phys.* **2004**, *121*, 362–373.

(140) Khalil, M.; Demirdöven, N.; Tokmakoff, A. Obtaining Absorptive Line Shapes in Two-Dimensional Infrared Vibrational Correlation Spectra. *Phys. Rev. Lett.* **2003**, *90*, 047401 1-4.

(141) Grimberg, B. I.; Lozovoy, V. V; Dantus, M.; Mukamel, S. Ultrafast Nonlinear Spectroscopic Techniques in the Gas Phase and Their Density Matrix Representation. *J. Phys. Chem. A* **2002**, *106*, 697–718.

(142) Brixner, T.; Mančal, T.; Stiopkin, I. V.; Fleming, G. R. Phase-Stabilized Two-Dimensional Electronic Spectroscopy. *J. Chem. Phys.* **2004**, *121*, 4221.

(143) Cho, M. Coherent Two-Dimensional Optical Spectroscopy. *Chem. Rev.* **2008**, *108*, 1331–1418.

(144) Richmond, G. L. Molecular Bonding and Interactions at Aqueous Surfaces as Probed by Vibrational Sum Frequency Spectroscopy. *Chem. Rev.* **2002**, *102*, 2693–2724.

(145) Vidal, F.; Tadjeddine, A. Sum-Frequency Generation Spectroscopy of Interfaces. *Reports Prog. Phys.* **2005**, *68*, 1095–1127.

(146) Bredenbeck, J.; Ghosh, A.; Nienhuys, H.-K.; Bonn, M. Interface-Specific Ultrafast Two-Dimensional Vibrational Spectroscopy. *Acc. Chem. Res.* **2009**, *42*, 1332–1342.

(147) Zhang, Z.; Piatkowski, L.; Bakker, H. J.; Bonn, M. Ultrafast Vibrational Energy Transfer at the Water/air Interface Revealed by Two-Dimensional Surface Vibrational Spectroscopy. *Nat. Chem.* **2011**, *3*, 888–893.

(148) Zhang, Z.; Piatkowski, L.; Bakker, H. J.; Bonn, M. Communication: Interfacial Water Structure Revealed by Ultrafast Two-Dimensional Surface Vibrational Spectroscopy. *J. Chem. Phys.* **2011**, *135*, 18–21.

(149) Bredenbeck, J.; Ghosh, A.; Smits, M.; Bonn, M. Ultrafast Two Dimensional-Infrared Spectroscopy of a Molecular Monolayer. *J. Am. Chem. Soc.* **2008**, *130*, 2152–2153.

(150) Voehringer, P.; Scherer, N. F. Transient Grating Optical Heterodyne Detected Impulsive Stimulated Raman Scattering in Simple Liquids. *J. Phys. Chem.* **1995**, *99*, 2684–2695.

(151) Goodno, G. D.; Dadusc, G.; Miller, R. J. D. Ultrafast Heterodyne-Detected Transient-Grating Spectroscopy Using Diffractive Optics. *J. Opt. Soc. Am. B* **1998**, *15*, 1791–1794.

(152) Maznev, A. A.; Nelson, K. A.; Rogers, J. A. Optical Heterodyne Detection of Laser-Induced Gratings. *Opt. Lett.* **1998**, *23*, 1319–1321.

(153) Goodno, G. D.; Astinov, V.; Miller, R. J. D. Diffractive Optics-Based Heterodyne-Detected Grating Spectroscopy: Application to Ultrafast Protein Dynamics. *J. Phys. Chem. B* **1999**, *103*, 603–607.

(154) Gallagher Faeder, S. M.; Jonas, D. M.; Faeder, S. M. G. Two-Dimensional Electronic Correlation and Relaxation Spectra: Theory and Model Calculations. *J. Phys. Chem. A* **1999**, *103*, 10489–10505.

(155) Backus, E. H. G.; Garrett-Roe, S.; Hamm, P. Phasing Problem of Heterodyne-Detected Two-Dimensional Infrared Spectroscopy. *Opt. Lett.* **2008**, *33*, 2665–2667.

(156) Bristow, A. D.; Karaiskaj, D.; Dai, X.; Cundiff, S. T. All-Optical Retrieval of the Global Phase for Two-Dimensional Fourier-Transform Spectroscopy. *Opt. Express* **2008**, *16*, 18017–18027.

(157) DeFlores, L. P.; Nicodemus, R. A.; Tokmakoff, A. Two-Dimensional Fourier Transform Spectroscopy in the Pump-Probe Geometry. *Opt. Lett.* **2007**, *32*, 2966–2968.

(158) Helbing, J.; Hamm, P. Compact Implementation of Fourier Transform Two-Dimensional IR Spectroscopy without Phase Ambiguity. *J. Opt. Soc. Am B* **2010**, *28*, 171–178.

(159) Shim, S.-H.; Strasfeld, D. B.; Ling, Y. L.; Zanni, M. T. Automated 2D IR Spectroscopy Using a Mid-IR Pulse Shaper and Application of This Technology to the Human Islet Amyloid Polypeptide. *Proc. Natl. Acad. Sci.* **2007**, *104*, 14197–14202.

(160) Shim, S.-H.; Zanni, M. T. How to Turn Your Pump-Probe Instrument into a Multidimensional Spectrometer: 2D IR and Vis Spectroscopies via Pulse Shaping. *Phys. Chem. Chem. Phys.* **2009**, *11*, 748–761.

(161) Vanselous, H.; Petersen, P. B. Extending the Capabilities of Heterodyne-Detected Sum-Frequency Generation Spectroscopy : Probing Any Interface in Any Polarization Combination. *J. Phys. Chem. C* **2016**, *120*, 8175–8184.

(162) Stiopkin, I. V; Jayathilake, H. D.; Bordenyuk, A. N.; Benderskii, A. V. Heterodyne-Detected Vibrational Sum Frequency Generation Spectroscopy. *J. Am. Chem. Soc.* **2008**, *130*, 2271–2275.

(163) Laaser, J. E.; Xiong, W.; Zanni, M. T. Time-Domain SFG Spectroscopy Using Mid-IR Pulse Shaping: Practical and Intrinsic Advantages. *J. Phys. Chem. B* **2011**, *115*, 2536–2546.

(164) Shen, Y. R. Phase-Sensitive Sum-Frequency Spectroscopy. *Annu. Rev. Phys. Chem.* **2013**, *64*, 129–150.

(165) Schleeger, M.; Grechko, M.; Bonn, M. Background-Free Fourth-Order Sum Frequency Generation Spectroscopy. *J. Phys. Chem. Lett.* **2015**, *6*, 2114–2120.

(166) Fuller, F. D.; Ogilvie, J. P. Experimental Implementations of Two-Dimensional Fourier Transform Electronic Spectroscopy. *Annu. Rev. Phys. Chem.* **2013**, *66*, 667–690.

(167) Jones, K. C.; Ganim, Z.; Tokmakoff, A. Heterodyne-Detected Dispersed Vibrational Echo Spectroscopy. *J. Phys. Chem. A* **2009**, *113*, 14060–14066.

(168) Golonzka, O.; Khalil, M.; Demirdöven, N.; Tokmakoff, A. Vibrational Anharmonicities Revealed by Coherent Two-Dimensional Infrared Spectroscopy. *Phys. Rev. Lett.* **2001**, *86*, 2154–2157.

(169) Park, S.; Kwak, K.; Fayer, M. D. Ultrafast 2D-IR Vibrational Echo Spectroscopy: A Probe of Molecular Dynamics. *Laser Phys. Lett.* **2007**, *4*, 704–718.

(170) Yan, C.; Yuan, R.; Pfalzgraff, W. C.; Nishida, J.; Wang, L.; Markland, T. E.; Fayer, M. D. Unraveling the Dynamics and Structure of Functionalized Self-Assembled Monolayers on Gold Using 2D IR Spectroscopy and MD Simulations. *Proc. Natl. Acad. Sci.* **2016**, *113*, 4929–4934.

(171) Rock, W.; Li, Y.; Pagano, P.; Cheatum, C. M. 2D IR Spectroscopy Using Four-Wave Mixing, Pulse Shaping, and IR Upconversion: A Quantitative Comparison. *J. Phys. Chem. A* **2013**, *117*, 6073–6083.

(172) Kraack, J. P.; Lotti, D.; Hamm, P. Ultrafast, Multidimensional Attenuated Total Reflectance Spectroscopy of Adsorbates at Metal Surfaces. *J. Phys. Chem. Lett.* **2014**, *5*, 2325–2329.

(173) Kraack, J. P.; Lotti, D.; Hamm, P. 2D Attenuated Total Reflectance Infrared Spectroscopy Reveals Ultrafast Vibrational Dynamics of Organic Monolayers at Metal-Liquid Interfaces. *J. Chem. Phys.* **2015**, *142*, 212413.

(174) Kraack, J. P.; Lotti, D.; Hamm, P. Surface-Enhanced, Multi-Dimensional Attenuated Total Reflectance Spectroscopy. In *Proc. of SPIE, Physical Chemistry of Interfaces and Nanomaterials XIV*; Sophia C. Hayes; Eric R. Bittner, Eds.; 2015; Vol. 9549, p. 95490S.

(175) Lotti, D.; Hamm, P.; Kraack, J. P. Surface-Sensitive Spectro-Electrochemistry Using Ultrafast 2D ATR IR Spectroscopy. *J. Phys. Chem. C* **2016**, *120*, 2883–2892.

(176) Kraack, J. P.; Kaech, A.; Hamm, P. Surface-Enhancement in Ultrafast 2D ATR IR Spectroscopy at the Metal-Liquid Interface. *J. Phys. Chem. C* **2016**, *120*, 3350–3359.

(177) Kraack, J. P.; Hamm, P. Vibrational Ladder-Climbing in Surface-Enhanced, Ultrafast Infrared Spectroscopy. *Phys. Chem. Chem. Phys.* **2016**, *18*, 16088–16093.

(178) Xu, Q.-H.; Ma, Y.-Z.; Fleming, G. R. Heterodyne Detected Transient Grating Spectroscopy in Resonant and Non-Resonant Systems Using a Simplified Diffractive Optics Method. *Chem. Phys. Lett.* **2001**, *338*, 254–262.

(179) Stenger, J.; Madsen, D.; Hamm, P.; Nibbering, E. T. J.; Elsaesser, T. A Photon Echo Peak Shift Study of Liquid Water. *J. Phys. Chem. A* **2002**, *106*, 2341–2350.

(180) Asbury, J. B.; Steinel, T.; Stromberg, C.; Gaffney, K. J.; Piletic, I. R.; Goun, A.; Fayer, M. D. Ultrafast Heterodyne Detected Infrared Multidimensional Vibrational Stimulated Echo Studies of Hydrogen Bond Dynamics. *Chem. Phys. Lett.* **2003**, *374*, 362–371.

(181) Rosenfeld, D. E.; Gengeliczki, Z.; Smith, B. J.; Stack, T. D. P.; Fayer, M. D. Structural Dynamics of a Catalytic Monolayer Probed by Ultrafast 2D IR Vibrational Echoes. *Science* **2011**, *334*, 634–639.

(182) Rosenfeld, D. E.; Nishida, J.; Yan, C.; Kumar, S. K. K.; Tamimi, A.; Fayer, M. D. Structural Dynamics at Monolayer–Liquid Interfaces Probed by 2D IR Spectroscopy. *J. Phys. Chem. C* **2013**, *117*, 1409–1420.

(183) Rosenfeld, D. E.; Nishida, J.; Yan, C.; Gengeliczki, Z.; Smith, B. J.; Fayer, M. D. Dynamics of Functionalized Surface Molecular Monolayers Studied with Ultrafast Infrared Vibrational Spectroscopy. *J. Phys. Chem. C* **2012**, *116*, 23428–23440.

(184) Zhang, Y.; Firestone, M. A.; Rauchfuss, T. B.; Bohn, P. W. Structural Characterization of Langmuir−Blodgett Films Derived from Multisulfur Heterocycles. *J. Phys. Chem.* **1996**, *100*, 13804–13810.

(185) Nishida, J.; Yan, C.; Fayer, M. D. Dynamics of Molecular Monolayers with Different Chain Lengths in Air and Solvents Probed by Ultrafast 2D IR Spectroscopy. *J. Phys. Chem. C* **2014**, *118*, 523–532.

(186) Nishida, J.; Fayer, M. D. Theory of Third-Order Spectroscopic Methods to Extract Detailed Molecular Orientational Dynamics for Planar Surfaces and Other Uniaxial Systems. *J. Chem. Phys.* **2014**, *140*, 144702 1-18.

(187) Tan, H.-S.; Piletic, I. R.; Fayer, M. D. Polarization Selective Spectroscopy Experiments: Methodology and Pitfalls. *J. Opt. Soc. Am. B* **2005**, *22*, 2009–2017.

(188) Zamadar, M.; Asaoka, S.; Grills, D. C.; Miller, J. R. Giant Infrared Absorption Bands of Electrons and Holes in Conjugated Molecules. *Nat. Commun.* **2013**, *4*, 2818.

(189) Abel, E. W.; Butler, I. S. Intensity of the Carbonyl Stretching Modes in Certain Halogenocarbonyl Derivatives of Chromium, Tungsten, Manganese, Rhenium and Iron. *Trans. Faraday Soc.* **1967**, *63*, 45–55.

(190) Porter, M. D. IR External Reflection Spectroscopy: A Probe for Chemically Modified Surfaces. *Anal. Chem.* **1988**, *60*, 1143–1155.

(191) Burghardt, T. P.; Thompson, N. L. Evanescent Intensity of a Focused Gaussian Light Beam Undergoing Total Internal Reflection in a Prism. *Opt. Eng.* **1984**, *23*, O62–O67.

(192) Zaera, F. New Advances in the Use of Infrared Absorption Spectroscopy for the Characterization of Heterogeneous Catalytic Reactions. *Chem. Soc. Rev.* **2014**, *43*, 7624–7663.

(193) Andanson, J.-M.; Baiker, A. Exploring Catalytic Solid/liquid Interfaces by in Situ Attenuated Total Reflection Infrared Spectroscopy. *Chem. Soc. Rev.* **2010**, *39*, 4571–4584.

(194) Bürgi, T.; Baiker, A. Attenuated Total Reflection Infrared Spectroscopy of Solid Catalysts Functioning in the Presence of. *Adv. Catal.* **2006**, *50*, 227–283.

(195) Ferri, D.; Bürgi, T.; Baiker, A. Pt and Pt / Al2O3 Thin Films for Investigation of Catalytic Solid - Liquid Interfaces by ATR-IR Spectroscopy : CO Adsorption , H2 -Induced Reconstruction and Surface-Enhanced Absorption. *J. Phys. Chem. B* **2001**, *105*, 3187–3195.

(196) Mojet, B. L.; Ebbesen, S. D.; Lefferts, L. Light at the Interface: The Potential of Attenuated Total Reflection Infrared Spectroscopy for Understanding Heterogeneous Catalysis in Water. *Chem. Soc. Rev.* **2010**, *39*, 4643–4655.

(197) Ebbesen, S. D.; Mojet, B. L.; Lefferts, L. CO Adsorption and Oxidation at the Catalyst-Water Interface: An Investigation by Attenuated Total Reflection Infrared Spectroscopy. *Langmuir* **2006**, *22*, 1079–1085.

(198) Mojet, B. L.; Ebbesen, S. D.; Lefferts, L. Light at the Interface: The Potential of Attenuated Total Reflection Infrared Spectroscopy for Understanding Heterogeneous Catalysis in Water. *Chem. Soc. Rev.* **2010**, *39*, 4643–4655.

(199) Ramer, G.; Lendl, B. Fourier Transform Infrared Spectroscopy. In *Encyclopedia of Analytical Chemistry*; John Wiley & Sons, Ltd: New York, 2006; pp. 1–24.

(200) Novotny, L.; Hecht, B. *Principles of Nano-Optics*; 1st ed.; Cambridge University Press: New York, 2006.

(201) Azzam, R. M. A. Circular and near-Circular Polarization States of Evanescent Monochromatic Light Fields in Total Internal Reflection. *Appl. Opt.* **2011**, *50*, 6272–6276.

(202) Kaneko, F.; Miyamoto, H.; Kobayashi, M. Polarized Infrared Attenuated Total Reflection Spectroscopy for Three-Dimensional Structural Analysis on Long-Chain Compounds. *J. Chem. Phys.* **1996**, *105*, 4812–4822.

(203) Harrick, N. J. Electric Field Strengths at Totally Reflecting Interfaces. *J. Opt. Soc. Am.* **1965**, *55*, 851–857.

(204) Mirabella, F. M. Surface Orientation of Polypropylene . I . Theoretical Considerations for the Application of Internal Reflection Spectroscopy. *J. Polym. Sci.* **1984**, *22*, 1283–1291.

(205) Goormaghtigh, E.; Raussens, V.; Ruysschaert, J. M. Attenuated Total Reflection Infrared Spectroscopy of Proteins and Lipids in Biological Membranes. *Biochim. Biophys. Acta* **1999**, *1422*, 105–185.

(206) Burghardt, T. P.; Thompson, N. L. Total Internal Reflection Fluorescence. *Ann. Rev. Biophys. Bioeng.* **1984**, *13*, 247–268.

(207) Woods, D. A.; Bain, C. D. Total Internal Reflection Spectroscopy for Studying Soft Matter. *Soft Matter* **2014**, *10*, 1071–1096.

(208) Urakawa, A.; Wirz, R.; Bu, T.; Baiker, A. ATR-IR Flow-Through Cell for Concentration Modulation Excitation Spectroscopy : Diffusion Experiments and Simulations. *J. Phys. Chem. B* **2003**, *107*, 13061–13068.

(209) Demirdöven, N.; Khalil, M.; Golonzka, O.; Tokmakoff, A. Dispersion Compensation with Optical Materials for Compression of Intense Sub-100-Fs Mid-Infrared Pulses. *Opt. Lett.* **2002**, *27*, 433–435.

(210) Rowell, N. L.; Tay, L.; Lockwood, D. J.; Baribeau, J.-M.; Bardwell, J. A.; Boukherroub, R. Organic Monolayers Detected by Single Reflection Attenuated Total Reflection Infrared Spectroscopy. *J. Vac. Sci. Technol. A Vacuum, Surfaces, Film.* **2006**, *24*, 668–672.

(211) Collman, J. P.; Devaraj, N. K.; Chidsey, C. E. D. "Clicking" functionality onto Electrode Surfaces. *Langmuir* **2004**, *20*, 1051–1053.

(212) Collman, J. P.; Devaraj, N. K.; Eberspacher, T. P. A.; Chidsey, C. E. D. Mixed Azide-Terminated Monolayers: A Platform for Modifying Electrode Surfaces. *Langmuir* **2006**, *22*, 2457–2464.

(213) Griffiths, M. B. E.; Pallister, P. J.; Mandia, D. J.; Barry, S. T. Atomic Layer Deposition of Gold Metal. *Chem. Mater.* **2016**, *28*, 44–46.

(214) Jadhav, S. a. Self-Assembled Monolayers (SAMs) of Carboxylic Acids: An Overview. *Cent. Eur. J. Chem.* **2011**, *9*, 369–378.

(215) Paniagua, S. A.; Giordano, A. J.; Smith, O. L.; Barlow, S.; Li, H.; Armstrong, N. R.; Pemberton, J. E.; Brédas, J.-L.; Ginger, D.; Marder, S. R. Phosphonic Acids for Interfacial Engineering of Transparent Conductive Oxides. *Chem. Rev.* **2016**, *116*, 7117–7158.

(216) Kiefer, L. M.; King, J. T.; Kubarych, K. J. Equilibrium Excited State Dynamics of a Photoactivated Catalyst Measured with Ultrafast Transient 2DIR. *J. Phys. Chem. A* **2014**, *118*, 9853–9860.

(217) Kiefer, L. M.; King, J. T.; Kubarych, K. J. Dynamics of Rhenium Photocatalysts Revealed through Ultrafast Multidimensional Spectroscopy. *Acc. Chem. Res.* **2015**, *48*, 1123–1130.

(218) Belali, R.; Vigoureux, J. Dispersion Effects on Infrared Spectra in Attenuated Total Reflection. *J. Opt. Soc. Am* **1995**, *12*, 2377–2381.

(219) Max, J. J.; Chapados, C. Influence of Anomalous Dispersion on the ATR Spectra of Aqueous Solutions. *Appl. Spectrosc.* **1999**, *53*, 1045–1053.

(220) Miljković, M.; Bird, B.; Diem, M. Line Shape Distortion Effects in Infrared Spectroscopy. *Analyst* **2012**, *137*, 3954–3964.

(221) Ramasesha, K.; De Marco, L.; Mandal, A.; Tokmakoff, A. Water Vibrations Have Strongly Mixed Intra- and Intermolecular Character. *Nat. Chem.* **2013**, *5*, 935–940.

(222) Perakis, F.; Hamm, P. Two-Dimensional Infrared Spectroscopy of Neat Ice Ih. *Phys. Chem. Chem. Phys.* **2012**, *14*, 6250–6256.

(223) Liang Shi; J. L. Skinner; Jansen, T. L. C. Two-Dimensional Infrared Spectroscopy of Neat Ice Ih. *Phys. Chem. Chem. Phys.* **2016**, *18*, 3772--3779.

(224) Heaps, D. A.; Griffiths, P. R. Band Shapes in the Infrared Spectra of Thin Organic Films on Metal Nanoparticles. *Vib. Spectrosc.* **2006**, *42*, 45–50.

(225) Bürgi, T. ATR-IR Spectroscopy at the Metal–liquid Interface: Influence of Film Properties on Anomalous Band-Shape. *Physical Chemistry Chemical Physics*, 2001, *3*, 2124–2130.

(226) Enders, D.; Nagao, T.; Pucci, A.; Nakayama, T.; Aono, M. Surface-Enhanced ATR-IR Spectroscopy with Interface-Grown Plasmonic Gold-Island Films near the Percolation Threshold. *Phys. Chem. Chem. Phys.* **2011**, *13*, 4935–4941.

(227) Priebe, A.; Sinther, M.; Fahsold, G.; Pucci, A. The Correlation between Film Thickness and Adsorbate Line Shape in Surface Enhanced Infrared Absorption. *J. Chem. Phys.* **2003**, *119*, 4887–4890.

(228) Krauth, O.; Fahsold, G.; Magg, N.; Pucci, A. Anomalous Infrared Transmission of Adsorbates on Ultrathin Metal Films: Fano Effect near the Percolation Threshold. *J. Chem. Phys.* **2000**, *113*,

6330–6333.

(229) Luk'yanchuk, B.; Zheludev, N. I.; Maier, S. a; Halas, N. J.; Nordlander, P.; Giessen, H.; Chong, C. T. The Fano Resonance in Plasmonic Nanostructures and Metamaterials. *Nat. Mater.* **2010**, *9*, 707–715.

(230) Adato, R.; Aksu, S.; Altug, H. Engineering Mid-Infrared Nanoantennas for Surface Enhanced Infrared Absorption Spectroscopy. *Mater. Today* **2015**, *18*, 436–446.

(231) Alonso-González, P.; Albella, P.; Schnell, M.; Chen, J.; Huth, F.; García-Etxarri, A.; Casanova, F.; Golmar, F.; Arzubiaga, L.; Hueso, L. E.; et al. Resolving the Electromagnetic Mechanism of Surface-Enhanced Light Scattering at Single Hot Spots. *Nat. Commun.* **2012**, *3*, 684.

(232) Neuman, T.; Huck, C.; Vogt, J.; Neubrech, F.; Hillenbrand, R.; Aizpurua, J.; Pucci, A. Importance of Plasmonic Scattering for an Optimal Enhancement of Vibrational Absorption in SEIRA with Linear Metallic Antennas. *J. Phys. Chem. C* **2015**, *119*, 26652–26662.

(233) Neubrech, F.; Pucci, A. Plasmonic Enhancement of Vibrational Excitations in the Infrared. *IEEE J. Sel. Top. Quantum Electron.* **2013**, *19*, 4600809–4600809.

(234) Neubrech, F.; Pucci, A.; Cornelius, T. W.; Karim, S.; García-Etxarri, A.; Aizpurua, J. Resonant Plasmonic and Vibrational Coupling in a Tailored Nanoantenna for Infrared Detection. *Phys. Rev. Lett.* **2008**, *101*, 157403 1-4.

(235) Wu, C.; Khanikaev, A. B.; Adato, R.; Arju, N.; Yanik, A. A.; Altug, H.; Shvets, G. Fano-Resonant Asymmetric Metamaterials for Ultrasensitive Spectroscopy and Identification of Molecular Monolayers. *Nat. Mater.* **2012**, *11*, 69–75.

(236) Ueba, H. Vibrational Lineshapes of Adsorbates on Solid Surfaces. *Prog. Surf. Sci.* **1986**, *22*, 181–321.

(237) Lee, J. D.; Nishino, M. Nonlinear Time-Resolved Study of Dynamics of a CO Adsorbate on a Metal: Time-Evolving Fano Resonance with Electron-Hole Continuum. *Phys. Rev. B - Condens. Matter Mater. Phys.* **2005**, *72*, 1–5.

(238) Morkel, M.; Unterhalt, H.; Klüner, T.; Rupprechter, G.; Freund, H. J. Interpreting Intensities in Vibrational Sum Frequency Generation (SFG) Spectroscopy: CO Adsorption on Pd Surfaces. *Surf. Sci.* **2005**, *586*, 146–156.

(239) Lis, D.; Cecchet, F. Localized Surface Plasmon Resonances in Nanostructures to Enhance Nonlinear Vibrational Spectroscopies: Towards an Astonishing Molecular Sensitivity. *Beilstein J. Nanotechnol.* **2014**, *5*, 2275–2292.

(240) Corva, M.; Feng, Z.; Dri, C.; Salvador, F.; Bertoch, P.; Comelli, G.; Vesselli, E. Carbon Dioxide Reduction on Ir(111): Stable Hydrocarbon Surface Species at near-Ambient Pressure. *Phys. Chem. Chem. Phys.* **2016**, *18*, 6763–6772.

(241) Dreesen, L.; Volcke, C.; Sartenaer, Y.; Peremans, A.; Thiry, P. A.; Humbert, C.; Grugier, J.; Marchand-Brynaert, J. Comparative Study of Decyl Thiocyanate and Decanethiol Self-Assembled Monolayers on Gold Substrates. *Surf. Sci.* **2006**, *600*, 4052–4057.

(242) Frontiera, R. R.; Gruenke, N. L.; Van Duyne, R. P. Fano-like Resonances Arising from Long-Lived Molecule-Plasmon Interactions in Colloidal Nanoantennas. *Nano Lett.* **2012**, *12*, 5989–5994.

(243) Dey, S.; Banik, M.; Hulkko, E.; Rodriguez, K.; Apkarian, V. A.; Galperin, M.; Nitzan, A. Observation and Analysis of Fano-like Lineshapes in the Raman Spectra of Molecules Adsorbed at Metal Interfaces. *Phys. Rev. B* **2016**, *93*, 035411 1-6.

(244) Ye, J.; Wen, F.; Sobhani, H.; Lassiter, J. B.; Van Dorpe, P.; Nordlander, P.; Halas, N. J. Plasmonic

Nanoclusters : Near Field Properties of the Fano Resonance Interrogated with Surface Enhanced Raman Scattering. *Nano Lett.* **2012**, *12*, 1660–1667.

(245) Lombardi, J. R.; Birke, R. L. Excitation Profiles and the Continuum in SERS: Identification of Fano Line Shapes. *J. Phys. Chem. C* **2010**, *114*, 7812–7815.

(246) Temirov, R.; Soubatch, S.; Lassise, A.; Tautz, F. S. Bonding and Vibrational Dynamics of a Large π-Conjugated Molecule on a Metal Surface. *J. Phys. Condens. Matter* **2008**, *20*, 224010 1-10.

(247) Tautz, F. S. Structure and Bonding of Large Aromatic Molecules on Noble Metal Surfaces: The Example of PTCDA. *Prog. Surf. Sci.* **2007**, *82*, 479–520.

(248) Ghosh, A.; Smits, M.; Sovago, M.; Bredenbeck, J.; Müller, M.; Bonn, M. Ultrafast Vibrational Dynamics of Interfacial Water. *Chem. Phys.* **2008**, *350*, 23–30.

(249) Ho, J.-J.; Skoff, D. R.; Ghosh, A.; Zanni, M. T. Structural Characterization of Single-Stranded DNA Monolayers Using Two-Dimensional Sum Frequency Generation Spectroscopy. *J. Phys. Chem. B* **2015**, *119*, 10586–10596.

(250) Ghosh, A.; Ho, J.; Serrano, A. L.; Sko, D. R.; Zhang, T.; Zanni, M. T. Two-Dimensional Sum-Frequency Generation (2D SFG) Spectroscopy : Summary of Principles and Its Application to Amyloid Fi Ber Monolayers. *Faraday Discuss.* **2015**, *177*, 493–505.

(251) Li, Y.; Wang, J.; Clark, M. L.; Kubiak, C. P.; Xiong, W. Characterizing Interstate Vibrational Coherent Dynamics of Surface Adsorbed Catalysts by Fourth-Order 3D SFG Spectroscopy. *Chem. Phys. Lett.* **2016**, *650*, 1–6.

(252) Li, Z.; Wang, J.; Li, Y.; Xiong, W. Solving the “Magic Angle” Challenge in Determining Molecular Orientation at Interfaces. *J. Phys. Chem. C* **2016**, *120*, 20239–20246.

(253) Stiopkin, I. V.; Jayathilake, H. D.; Weeraman, C.; Benderskii, A. V. Temporal Effects on Spectroscopic Line Shapes, Resolution, and Sensitivity of the Broad-Band Sum Frequency Generation. *J. Chem. Phys.* **2010**, *132*, 234503 1-9.

(254) Weeraman, C.; Mitchell, S. A.; Lausten, R.; Johnston, L. J.; Stolow, A. Vibrational Sum Frequency Generation Spectroscopy Using Inverted Visible Pulses. *Opt. Express* **2010**, *18*, 11483–11494.

(255) Lagutchev, A.; Lozano, A.; Mukherjee, P.; Hambir, S. A.; Dlott, D. D. Compact Broadband Vibrational Sum-Frequency Generation Spectrometer with Nonresonant Suppression. *Spectrochim. Acta - Part A Mol. Biomol. Spectrosc.* **2010**, *75*, 1289–1296.

(256) Lagutchev, A.; Hambir, S. A.; Dlott, D. D. Nonresonant Background Suppression in Broadband Vibrational Sum-Frequency Generation Spectroscopy. *J. Phys. Chem. C* **2007**, *111*, 13645–13647.

(257) Schleeger, M.; Grechko, M.; Bonn, M. Background-Free Fourth-Order Sum Frequency Generation Spectroscopy. *J. Phys. Chem. Lett.* **2015**, *6*, 2114–2120.

(258) Bracco, G.; Holst, B. *Surface Science Techniques*; Springer Science & Business Media: Berlin Heidelberg, 2013.

(259) Liu, W.-T.; Shen, Y. R. In Situ Sum-Frequency Vibrational Spectroscopy of Electrochemical Interfaces with Surface Plasmon Resonance. *Proc. Natl. Acad. Sci.* **2014**, *111*, 1293–1297.

(260) Williams, C. T.; Yang, Y.; Bain, C. D. Total Internal Reflection Sum-Frequency Spectroscopy: A Strategy for Studying Molecular Adsorption on Metal Surfaces. *Langmuir* **2000**, *16*, 2343–2350.

(261) Tourillon, G.; Dreesen, L.; Volcke, C.; Sartenaer, Y.; Thiry, P. A.; Peremans, A. Total Internal Reflection Sum-Frequency Generation Spectroscopy and Dense Gold Nanoparticles Monolayer: A Route for Probing Adsorbed Molecules. *Nanotechnology* **2007**, *18*, 415301 1-7.

(262) Bratlie, K. M.; Komvopoulos, K.; Somorjai, G. A. Sum Frequency Generation Vibrational Spectroscopy of Pyridine Hydrogenation on Platinum Nanoparticles. *J. Phys. Chem. C* **2008**, *112*, 11865–11868.

(263) Hsieh, C.-S.; Okuno, M.; Hunger, J.; Backus, E. H. G.; Nagata, Y.; Bonn, M. Aqueous Heterogeneity at the Air/Water Interface Revealed by 2D-HD-SFG Spectroscopy. *Angew. Chem. Int. Ed. Engl.* **2014**, *53*, 8146–8149.

(264) Nagata, Y.; Mukamel, S. Spectral Diffusion at the Water/lipid Interface Revealed by Two-Dimensional Fourth-Order Optical Spectroscopy: A Classical Simulation Study. *J. Am. Chem. Soc.* **2011**, *133*, 3276–3279.

(265) Singh, P. C.; Inoue, K. I.; Nihonyanagi, S.; Yamaguchi, S.; Tahara, T. Femtosecond Hydrogen Bond Dynamics of Bulk-like and Bound Water at Positively and Negatively Charged Lipid Interfaces Revealed by 2D HD-VSFG Spectroscopy. *Angew. Chemie - Int. Ed.* **2016**, *55*, 10621–10625.

(266) Livingstone, R. A.; Nagata, Y.; Bonn, M.; Backus, E. H. G. Two Types of Water at the Water-Surfactant Interface Revealed by Time-Resolved Vibrational Spectroscopy. *J. Am. Chem. Soc.* **2015**, *137*, 14912–14919.

(267) Singh, P. C.; Nihonyanagi, S.; Yamaguchi, S.; Tahara, T. Ultrafast Vibrational Dynamics of Water at a Charged Interface Revealed by Two-Dimensional Heterodyne-Detected Vibrational Sum Frequency Generation. *J. Chem. Phys.* **2012**, *137*, 094706 1-6.

(268) Inoue, K. I.; Nihonyanagi, S.; Singh, P. C.; Yamaguchi, S.; Tahara, T. 2D Heterodyne-Detected Sum Frequency Generation Study on the Ultrafast Vibrational Dynamics of H2O and HOD Water at Charged Interfaces. *J. Chem. Phys.* **2015**, *142*, 212431 1-12.

(269) Piatkowski, L.; Zhang, Z.; Backus, E. H. G.; Bakker, H. J.; Bonn, M. Extreme Surface Propensity of Halide Ions in Water. *Nat. Commun.* **2014**, *5*, 4083.

(270) Anfuso, C. L.; Ricks, A. M.; Rodr, W.; Lian, T. Ultrafast Vibrational Relaxation Dynamics of a Rhenium Bipyridyl. *J. Phys. Chem. C* **2012**, *116*, 26377–26384.

(271) Lu, G. Q.; Lagutchev, A.; Dlott, D. D.; Wieckowski, A. Quantitative Vibrational Sum-Frequency Generation Spectroscopy of Thin Layer Electrochemistry: CO on a Pt Electrode. *Surf. Sci.* **2005**, *585*, 3–16.

(272) Lagutchev, A.; Lu, G. Q.; Takeshita, T.; Dlott, D. D.; Wieckowski, A. Vibrational Sum Frequency Generation Studies of the (2×2)→(√19×√19) Phase Transition of CO on Pt(111) Electrodes. *J. Chem. Phys.* **2006**, *125*, 154705 1-10.

(273) Bordenyuk, A. N.; Benderskii, A. V. Spectrally- and Time-Resolved Vibrational Surface Spectroscopy: Ultrafast Hydrogen-Bonding Dynamics at D2O/CaF2 Interface. *J. Chem. Phys.* **2005**, *122*, 134713 1-11.

(274) Nihonyanagi, S.; Eftekhari-Bafrooei, A.; Borguet, E. Ultrafast Vibrational Dynamics and Spectroscopy of a Siloxane Self-Assembled Monolayer. *J. Chem. Phys.* **2011**, *134*, 084701 1-7.

(275) Zheng, J.; Kwak, K.; Fayer, M. D. Ultrafast 2D IR Vibrational Echo Spectroscopy. *Acc. Chem. Res.* **2007**, *40*, 75–83.

(276) Van Wilderen, L. J. G. W.; Bredenbeck, J. From Ultrafast Structure Determination to Steering

Reactions: Mixed IR/Non-IR Multidimensional Vibrational Spectroscopies. *Angew. Chemie - Int. Ed.* **2015**, *54*, 11624–11640.

(277) Hunt, N. T. Transient 2D-IR Spectroscopy of Inorganic Excited States. *Dalt. Trans.* **2014**, *43*, 17578–17589.

(278) Hunt, N. T. 2D-IR Spectroscopy: Ultrafast Insights into Biomolecule Structure and Function. *Chem. Soc. Rev.* **2009**, *38*, 1837–1848.

(279) Strasfeld, D. B.; Shim, S.-H.; Zanni, M. T. New Advances in Mid-IR Pulse Shaping and Its Application to 2D IR Spectroscopy and Ground-State Coherent Control. *Adv. Chem. Phys.* **2009**, *141*, 1–28.

(280) Remorino, A.; Hochstrasser, R. M. Three-Dimensional Structures by Two- Dimensional Vibrational Spectroscopy. *Acc. Chem. Res.* **2012**, *45*, 1896–1905.

(281) Nishida, J.; Tamimi, A.; Fei, H.; Pullen, S.; Ott, S.; Cohen, S. M.; Fayer, M. D. Structural Dynamics inside a Functionalized Metal-Organic Framework Probed by Ultrafast 2D IR Spectroscopy. *Proc. Nat. Acad. Sci. USA* **2014**, *111*, 18442–18447.

(282) Nihonyanagi, S.; Yamaguchi, S.; Tahara, T. Direct Evidence for Orientational Flip-Flop of Water Molecules at Charged Interfaces: A Heterodyne-Detected Vibrational Sum Frequency Generation Study. *J. Chem. Phys.* **2009**, *130*, 204704 1-5.

(283) Woutersen, S.; Pfister, R.; Hamm, P.; Mu, Y.; Kosov, D. S.; Stock, G. Peptide Conformational Heterogeneity Revealed from Nonlinear Vibrational Spectroscopy and Molecular-Dynamics Simulations. *J. Chem. Phys.* **2002**, *117*, 6833–6840.

(284) Roberts, S. T.; Loparo, J. J.; Tokmakoff, A. Characterization of Spectral Diffusion from Two-Dimensional Line Shapes. *J. Chem. Phys.* **2006**, *125*, 084502 1-8.

(285) Piatkowski, L.; Eisenthal, K. B.; Bakker, H. J. Ultrafast Intermolecular Energy Transfer in Heavy Water. *Phys. Chem. Chem. Phys.* **2009**, *11*, 9033–9038.

(286) Laaser, J. E.; Christianson, R.; Oudenhoven, T. A.; Joo, Y.; Gopalan, P.; Schmidt, J. R.; Zanni, M. T. Dye Self-Association Identified by Intermolecular Couplings between Vibrational Modes As Revealed by Infrared Spectroscopy, and Implications for Electron Injection. *J. Phys. Chem. C* **2014**, *118*, 5854–5861.

(287) Oudenhoven, T. A.; Joo, Y.; Laaser, J. E.; Gopalan, P.; Zanni, M. T. Dye Aggregation Identified by Vibrational Coupling Using 2D IR Spectroscopy. *J. Chem. Phys.* **2015**, *142*, 212449 1-12.

(288) Rubtsova, N. I.; Rubtsov, I. V. Vibrational Energy Transport in Molecules Studied by Relaxation-Assisted Two-Dimensional Infrared Spectroscopy. *Annu. Rev. Phys. Chem.* **2015**, *66*, 717–738.

(289) Lin, Z.; Rubtsova, N. I.; Kireev, V. V; Rubtsov, I. V. Ballistic Energy Transport in PEG Oligomers . *Acc. Chem. Res.* **2015**, *48*, 2547–2555.

(290) Müller-Werkmeister, H. M.; Li, Y.-L.; Lerch, E.-B. W.; Bigourd, D.; Bredenbeck, J. Ultrafast Hopping from Band to Band: Assigning Infrared Spectra Based on Vibrational Energy Transfer. *Angew. Chem. Int. Ed. Engl.* **2013**, *52*, 6214–6217.

(291) Selig, O.; Siffels, R.; Rezus, Y. L. A. Ultrasensitive Ultrafast Vibrational Spectroscopy Employing the Near Field of Gold Nanoantennas. *Phys. Rev. Lett.* **2015**, *114*, 233004 1-5.

(292) Xiong, W.; Laaser, J. E.; Paoprasert, P.; Franking, R. A.; Hamers, R. J.; Gopalan, P.; Zanni, M. T. Transient 2D IR Spectroscopy of Charge Injection in Dye-Sensitized Nanocrystalline Thin Films. *J. Am. Chem. Soc.* **2009**, *131*, 18040–18041.

(293) Machan, C. W.; Sampson, M. D.; Chabolla, S. A.; Kubiak, C. P. Developing a Mechanistic Understanding of Molecular Electrocatalysts for CO2 Reduction Using Infrared Spectroelectrochemistry. *Organometallics* **2014**, *33*, 4550–4559.

(294) Lomont, J. P.; Harris, C. B. Primary Photochemical Dynamics of Metal Carbonyl Dimers and Clusters in Solution : Insights into the Results of Metal – Metal Bond Cleavage from Ultrafast Spectroscopic Studies. *Inorganica Chim. Acta* **2014**, *424*, 38–50.

(295) Kwak, K.; Rosenfeld, D. E.; Fayer, M. D. Taking Apart the Two-Dimensional Infrared Vibrational Echo Spectra: More Information and Elimination of Distortions. *J. Chem. Phys.* **2008**, *128*, 204505 1-10.

(296) Sokolowsky, K. P.; Bailey, H. E.; Fayer, M. D. New Divergent Dynamics in the Isotropic to Nematic Phase Transition of Liquid Crystals Measured with 2D IR Vibrational Echo Spectroscopy. *J. Chem. Phys.* **2014**, *194502*, 1–38.

(297) Sokolowsky, K. P.; Fayer, M. D. Dynamics in the Isotropic Phase of Nematogens Using 2D IR Vibrational Echo Measurements on Natural-Abundance 13CN and Extended Lifetime Probes. *J. Phys. Chem. B* **2013**, *117*, 15060–15071.

(298) Andrews, S. S.; Boxer, S. G. Vibrational Stark Effects of Nitriles. I. Methods and Experimental Results. *J. Phys. Chem. A* **2000**, *104*, 11853–11863.

(299) Hush, N. S.; Reimers, J. R. Vibrational Stark Spectroscopy. 1. Basic Theory and Application to the CO Stretch. *J. Phys. Chem.* **1995**, *99*, 15798–15805.

(300) Kim, H.; Cho, M. Infrared Probes for Studying the Structure and Dynamics of Biomolecules. *Chem. Rev.* **2013**, *113*, 5817–5847.

(301) Suydam, I. T.; Boxer, S. G. Vibrational Stark Effects Calibrate the Sensitivity of Vibrational Probes for Electric Fields in Proteins. *Biochemistry* **2003**, *42*, 12050–12055.

(302) Waegele, M. M.; Culik, R. M.; Gai, F. Site-Specific Spectroscopic Reporters of the Local Electric Field, Hydration, Structure, and Dynamics of Biomolecules. *J. Phys. Chem. Lett.* **2011**, *2*, 2598–2609.

(303) Bloem, R.; Koziol, K.; Waldauer, S. A.; Buchli, B.; Walser, R.; Samatanga, B.; Jelesarov, I.; Hamm, P. Ligand Binding Studied by 2D IR Spectroscopy Using the Azidohomoalanine Label. *J. Phys. Chem. B* **2012**, *116*, 13705–13712.

(304) Rodriguez, P.; Kwon, Y.; Koper, M. T. M. The Promoting Effect of Adsorbed Carbon Monoxide on the Oxidation of Alcohols on a Gold Catalyst. *Nat. Chem.* **2012**, *4*, 177–182.

(305) Wodtke, A. M.; Matsiev, D.; Auerbach, D. Energy Transfer and Chemical Dynamics at Solid Surfaces: The Special Role of Charge Transfer. *Prog. Surf. Sci.* **2008**, *83*, 167–214.

(306) Saalfrank, P. Quantum Dynamical Approach to Ultrafast Molecular Desorption from Surfaces. *Chem. Rev.* **2006**, *106*, 4116–4159.

(307) Peremans, A.; Tadjeddine, A. Vibrational Spectroscopy of Electrochemically Deposited Hydrogen on Platinum. *Phys. Rev. Lett.* **1994**, *73*, 3010–3013.

(308) Russell, A. E. Electrocatalysis: Theory and Experiment at the Interface. *Phys. Chem. Chem. Phys.* **2008**, *10*, 3607–3608.

(309) Matranga, C.; Guyot-Sionnest, P. Vibrational Relaxation of Cyanide at the Metal/electrolyte Interface. *J. Chem. Phys.* **2000**, *112*, 7615.

(310) Tian, L.; Li, J.-T.; Ye, J.-Y.; Zhen, C.-H.; Sun, S.-G. In Situ FTIR Studies of Coadsorption of CN−

and CO on Pt(110) Electrode Surface. *J. Electroanal. Chem.* **2011**, *662*, 137–142.

(311) Bovensiepen, U. Ultrafast Electron Transfer, Localization and Solvation at Ice–metal Interfaces: Correlation of Structure and Dynamics. *Prog. Surf. Sci.* **2005**, *78*, 87–100.

(312) Hodgson, A.; Haq, S. Water Adsorption and the Wetting of Metal Surfaces. *Surf. Sci. Rep.* **2009**, *64*, 381–451.

(313) Carrasco, J.; Hodgson, A.; Michaelides, A. A Molecular Perspective of Water at Metal Interfaces. *Nat. Mater.* **2012**, *11*, 667–674.

(314) Onda, K.; Li, B.; Zhao, J.; Jordan, K. D.; Yang, J.; Petek, H. Wet Electrons at the H2O/TiO2(110) Surface. *Science* **2005**, *308*, 1154–1158.

(315) Sun, S.-G.; Cai, W.-B.; Wan, L.-J.; Osawa, M. Infrared Absorption Enhancement for CO Adsorbed on Au Films in Perchloric Acid Solutions and Effects of Surface Structure Studied by Cyclic Voltammetry, Scanning Tunneling Microscopy, and Surface-Enhanced IR Spectroscopy. *J. Phys. Chem. B* **1999**, *103*, 2460–2466.

(316) Woutersen, S.; Hamm, P. Nonlinear Two-Dimensional Vibrational Spectroscopy of Peptides. *J. Phys. Condens. Matter* **2002**, *1035*, R1035–R1062.

(317) Cowan, M. L.; Bruner, B. D.; Huse, N.; Dwyer, J. R.; Chugh, B.; Nibbering, E. T. J.; Elsaesser, T.; Miller, R. J. D. Ultrafast Memory Loss and Energy Redistribution in the Hydrogen Bond Network of Liquid H2O. *Nature* **2005**, *434*, 199–202.

(318) Livingstone, R. A.; Zhang, Z.; Piatkowski, L.; Bakker, H. J.; Hunger, J.; Bonn, M.; Backus, E. H. G. Water in Contact with a Cationic Lipid Exhibits Bulk-Like Vibrational Dynamics. *J. Phys. Chem. B* **2016**, *120*, 10069–10078.

(319) Zhang, X.; Yadavalli, V. K. Functional Self-Assembled DNA Nanostructures for Molecular Recognition. *Nanoscale* **2012**, *4*, 2439–2446.

(320) Zheng, J.; Birktoft, J. J.; Chen, Y.; Wang, T.; Sha, R.; Constantinou, P. E.; Ginell, S. L.; Mao, C.; Seeman, N. C. From Molecular to Macroscopic via the Rational Design of a Self-Assembled 3D DNA Crystal. *Nature* **2009**, *461*, 74–77.

(321) Yan, H.; Park, S. H.; Finkelstein, G.; Reif, J. H.; Labean, T. H. DNA-Templated Self-Assembly of Conductive Nanowires. *Science* **2003**, *301*, 1882–1884.

(322) Zanni, M. T.; Ge, N. H.; Kim, Y. S.; Hochstrasser, R. M. Two-Dimensional IR Spectroscopy Can Be Designed to Eliminate the Diagonal Peaks and Expose Only the Crosspeaks Needed for Structure Determination. *Proc. Natl. Acad. Sci. U. S. A.* **2001**, *98*, 11265–11270.

(323) Anderson, N. A.; Lian, T. Ultrafast Electron Transfer At the Molecule-Semiconductornanoparticle Interface. *Annu. Rev. Phys. Chem.* **2005**, *56*, 491–519.

(324) Persson, B. N. J. Damping of Excited Molecules Located above a Metal Surface. *Solid State Commun.* **1978**, *27*, 417–421.

(325) Bandarenka, A. S.; Koper, M. T. M. Structural and Electronic Effects in Heterogeneous Electrocatalysis: Toward a Rational Design of Electrocatalysts. *J. Catal.* **2013**, *308*, 11–24.

(326) Jiang, X.; Zaitseva, E.; Schmidt, M.; Siebert, F.; Engelhard, M.; Schlesinger, R.; Ataka, K.; Vogel, R.; Heberle, J. Resolving Voltage-Dependent Structural Changes of a Membrane Photoreceptor by Surface-Enhanced IR Difference Spectroscopy. *Proc. Natl. Acad. Sci. U. S. A.* **2008**, *105*, 12113–12117.

(327) Ataka, K.; Stripp, S. T.; Heberle, J. Surface-Enhanced Infrared Absorption Spectroscopy

(SEIRAS) to Probe Monolayers of Membrane Proteins. *Biochim. Biophys. Acta - Biomembr.* **2013**, *1828*, 2283–2293.

(328) Ataka, K.; Richter, B.; Heberle, J. Orientational Control of the Physiological Reaction of Cytochrome c Oxidase Tethered to a Gold Electrode. *J. Phys. Chem. B* **2006**, *110*, 9339–9347.

(329) Grätzel, M. Photoelectrochemical Cells. *Nature* **2001**, *414*, 338–344.

(330) Hagfeldt, A.; Graetzel, M. Light-Induced Redox Reactions in Nanocrystalline Systems. *Chem. Rev.* **1995**, *95*, 49–68.

(331) Schkolnik, G.; Salewski, J.; Millo, D.; Zebger, I.; Franzen, S.; Hildebrandt, P. Vibrational Stark Effect of the Electric-Field Reporter 4-Mercaptobenzonitrile as a Tool for Investigating Electrostatics at Electrode/SAM/Solution Interfaces. *Int. J. Mol. Sci.* **2012**, *13*, 7466–7482.

(332) Ashley, K.; Pons, S. Infrared Spectroelectrochemistry. *Chem. Rev.* **1988**, *88*, 673–695.

(333) El Khoury, Y.; van Wilderen, L. J. G. W.; Vogt, T.; Winter, E.; Bredenbeck, J. A Spectroelectrochemical Cell for Ultrafast Two-Dimensional Infrared Spectroscopy. *Rev. Sci. Instrum.* **2015**, *86*, 083102 1-5.

(334) Samjeské, G.; Komatsu, K.; Osawa, M. Dynamics of CO Oxidation on a Polycrystalline Platinum Electrode: A Time-Resolved Infrared Study. *J. Phys. Chem. C* **2009**, *113*, 10222–10228.

(335) Lambert, D. K. Vibrational Stark Effect of Adsorbates at Electrochemical Interfaces. *Electrochim. Acta* **1996**, *41*, 623–630.

(336) Ray, N. K.; Anderson, A. B. Variations in C-O and Pt-C Frequencies for CO on a Platinum Electrode. *J. Phys. Chem.* **1982**, *86*, 4851–4852.

(337) Fried, S. D.; Boxer, S. G. Measuring Electric Fields and Noncovalent Interactions Using the Vibrational Stark Effect. *Acc. Chem. Res.* **2015**, *48*, 998–1006.

(338) Chattopadhyay, A.; Boxer, S. G. Vibrational Stark Effect Spectroscopy. *J. Am. Chem. Soc.* **1995**, *117*, 1449–1450.

(339) Rudnev, A. V.; Zhumaev, U.; Utsunomiya, T.; Fan, C.; Yokota, Y.; Fukui, K.; Wandlowski, T. Ferrocene-Terminated Alkanethiol Self-Assembled Monolayers: An Electrochemical and in Situ Surface-Enhanced Infra-Red Absorption Spectroscopy Study. *Electrochim. Acta* **2013**, *107*, 33–44.

(340) Ataka, K.; Yotsuyanagi, T.; Osawa, M. Potential-Dependent Reorientation of Water Molecules at an Electrode / Electrolyte Interface Studied by Surface-Enhanced Infrared Absorption Spectroscopy. **1996**, *3654*, 10664–10672.

(341) Nellist, M. R.; Laskowski, F. A. L.; Lin, F.; Mills, T. J.; Boettcher, S. W. Semiconductor - Electrocatalyst Interfaces: Theory, Experiment, and Applications in Photoelectrochemical Water Splitting. *Acc. Chem. Res.* **2015**, *49*, 733–740.

(342) Eckermann, A. L.; Feld, D. J.; Shaw, J. a; Meade, T. J. Electrochemistry of Redox-Active Self-Assembled Monolayers. *Coord. Chem. Rev. Rev.* **2010**, *254*, 1769–1802.

(343) Bourrez, M.; Molton, F.; Chardon-Noblat, S.; Deronzier, A. [Mn(bipyridyl)(CO)3Br]: An Abundant Metal Carbonyl Complex as Efficient Electrocatalyst for CO2 Reduction. *Angew. Chemie - Int. Ed.* **2011**, *50*, 9903–9906.

(344) Kornyshev, A. A. Double-Layer in Ionic Liquids: Paradigm Change? *J. Phys. Chem. B* **2007**, *111*, 5545–5557.

(345) Chmiola, J.; Largeot, C.; Taberna, P. L.; Simon, P.; Gogotsi, Y. Desolvation of Ions in

Subnanometer Pores and Its Effect on Capacitance and Double-Layer Theory. *Angew. Chemie - Int. Ed.* **2008**, *47*, 3392–3395.

(346) Costentin, C.; Drouet, S.; Robert, M.; Savéant, J. M. Turnover Numbers, Turnover Frequencies, and Overpotential in Molecular Catalysis of Electrochemical Reactions. Cyclic Voltammetry and Preparative-Scale Electrolysis. *J. Am. Chem. Soc.* **2012**, *134*, 11235–11242.

(347) Wada, T.; Tsuge, K.; Tanaka, K. Electrochemical Oxidation of Water to Dioxygen Catalyzed by the Oxidized Form of the Bis(ruthenium - Hydroxo) Complex in H2O. *Angew. Chemie - Int. Ed.* **2000**, *39*, 1479–1482.

(348) Yagi, M.; Kaneko, M. Molecular Catalysts for Water Oxidation. *Chem. Rev.* **2001**, *101*, 21–35.

(349) Chen, Z.; Concepcion, J. J.; Jurss, J. W.; Meyer, T. J. Single-Site, Catalytic Water Oxidation on Oxide Surfaces. *J. Am. Chem. Soc.* **2009**, *131*, 15580–15581.

(350) Fujita, E. Photochemical Carbon Dioxide Reduction with Metal Complexes. *Coord. Chem. Rev.* **1999**, *185–186*, 373–384.

(351) Costamagna, J.; Ferraudi, G.; Canales, J.; Vargas, J. Carbon Dioxide Activation by Aza-Macrocyclic Complexes. *Coord. Chem. Rev.* **1996**, *148*, 221–248.

(352) Osawa, M.; Ataka, K. Electromagnetic Mechanism of Enhanced Infrared Absorption of Molecules Adsorbed on Metal Island Films. *Surf. Sci. Lett.* **1992**, *262*, L118–L122.

(353) Johnson, E.; Aroca, R. Surface-Enhanced Infrared Spectroscopy of Monolayers. *J. Phys. Chem.* **1995**, *99*, 9325–9330.

(354) Hatta, A.; Suzuki, Y.; Suëtaka, W. Infrared Absorption Enhancement of Monolayer Species on Thin Evaporated Ag Films by Use of a Kretschmann Configuration: Evidence for Two Types of Enhanced Surface Electric Fields. *Appl. Phys. A Solids Surfaces* **1984**, *35*, 135–140.

(355) Suzuki, Y.; Osawa, M.; Hatta, A.; Suëtaka, W. Mechanism of Absorption Enhancement in Infrared ATR Spectra Observed in the Kretschmann Configuration. *Appl. Surf. Sci.* **1988**, *34*, 875–881.

(356) Hatta, A.; Chiba, Y.; Suëtaka, W. Infrared Absorption Study of Adsorbed Species at Metal/water Interface by Use of the Kretschmann Configuration. *Surf. Sci. Lett.* **1985**, *158*, 616–623.

(357) Hartstein, A.; Kirtley, J. R.; Tsang, J. C. Enhancement of the Infrared Absorption from Molecular Monolayers with Thin Metal Overlayers. *Phys. Rev. Lett.* **1980**, *45*, 201–204.

(358) Aizpurua, J.; Taubner, T.; García de Abajo, F. J.; Brehm, M.; Hillenbrand, R. Substrate-Enhanced Infrared near-Field Spectroscopy. *Opt. Express* **2008**, *16*, 1529–1545.

(359) Osawa, M. Dynamic Processes in Electrochemical Reactions Studied by Surface-Enhanced Infrared Absorption Spectroscopy (SEIRAS). *Bull. Chem. Soc. Jpn.* **1997**, *70*, 2861–2880.

(360) Aroca, R. F.; Ross, D. J. Surface-Enhanced Infrared Spectroscopy. *Appl. Spectrosc.* **2004**, *58*, 324A–338A.

(361) Hatta, A.; Chiba, Y.; Suetaka, W. In-Situ Infrared Measurement of Thiocyanate at a Silver/electrolyte Interface by the Excitation of Surface Plasmon Polaritons. *Appl. Surf. Sci.* **1986**, *25*, 327–332.

(362) Bharadwaj, P.; Beams, R.; Novotny, L. Nanoscale Spectroscopy with Optical Antennas. *Chem. Sci.* **2011**, *2*, 136–140.

(363) Novotny, L.; van Hulst, N. Antennas for Light. *Nat. Photonics* **2011**, *5*, 83–90.

(364) Neuman, T.; Alonso-González, P.; Garcia-Etxarri, A.; Schnell, M.; Hillenbrand, R.; Aizpurua, J. Mapping the near Fields of Plasmonic Nanoantennas by Scattering-Type Scanning near-Field Optical Microscopy. *Laser Photon. Rev.* **2015**, *9*, 637–649.

(365) Schlücker, S. Surface-Enhanced Raman Spectroscopy: Concepts and Chemical Applications. *Angew. Chem. Int. Ed. Engl.* **2014**, *53*, 4756–4795.

(366) E. J. Zeman, G. C. S. An Accurate Electromagnetic Theory Study of Surface Enhancement Factors for Ag, Au, Cu, Li, Na, Al, Ga, In, Zn, and Cd. *J. Phys. Chem.* **1987**, *91*, 634–643.

(367) Schatz, G. C.; van Duyne, R. P. Electromagnetic Mechanism of Surface-Enhanced Spectroscopy. In *Handbook of Vibrational Spectroscopy*; John Wiley & Sons, Ltd.: Chichester, UK, 2002; pp. 1–16.

(368) Hao, E.; Schatz, G. C. Electromagnetic Fields around Silver Nanoparticles and Dimers. *J. Chem. Phys.* **2004**, *120*, 357–366.

(369) Barnes, W. L.; Dereux, A.; Ebbesen, T. W. Surface Plasmon Subwavelength Optics. *Nature* **2003**, *424*, 824–830.

(370) Pendry, J. B.; Martín-Moreno, L.; Garcia-Vidal, F. J. Mimicking Surface Plasmons with Structured Surfaces. *Science* **2008**, *305*, 847–848.

(371) Zayats, A. V.; Smolyaninov, I. I.; Maradudin, A. A. Nano-Optics of Surface Plasmon Polaritons. *Phys. Rep.* **2005**, *408*, 131–314.

(372) Zayats, A.; Smolyaninov, I. Near-Field Photonics: Surface Plasmon Polaritons and Localized Surface Plasmons. *J. Opt. A Pure Appl. Opt.* **2003**, *16*, S16-50.

(373) Sambles, J.; Bradbery, G.; Yang, F. Optical Excitation of Surface Plasmons: An Introduction. *Contemporary physics*, 1991, *32*, 173–183.

(374) Golibrzuch, K.; Bartels, N.; Auerbach, D. J.; Wodtke, A. M. The Dynamics of Molecular Interactions and Chemical Reactions at Metal Surfaces: Testing the Foundations of Theory. *Annu. Rev. Phys. Chem.* **2015**, *66*, 399–425.

(375) Silva, M.; Jongma, R.; Field, R. W.; Wodtke, A. M. The Dynamics Of “stretched Molecules”: Experimental Studies of Highly Vibrationally Excited Molecules with Stimulated Emission Pumping. *Annu. Rev. Phys. Chem.* **2001**, *52*, 811–852.

(376) Krüger, B. C.; Meyer, S.; Kandratsenka, A.; Wodtke, A. M.; Schäfer, T. Vibrational Inelasticity of Highly Vibrationally Excited NO on Ag(111). *J. Phys. Chem. Lett.* **2016**, *7*, 441–446.

(377) Kneba, M.; Wolfrum, J. Bimolecular Reactions of Vibrationally Excited Molecules. *Annu. Rev. Phys. Chem.* **1980**, *31*, 47–79.

(378) Maas, D. J.; Duncan, D. I.; Vrijen, R. B.; van der Zande, W. J.; Noordam, L. D. Vibrational Ladder Climbing in NO by (Sub)picosecond Frequency-Chirped Infrared Laser Pulses. *Chem. Phys. Lett.* **1998**, *290*, 75–80.

(379) Nuernberger, P.; Vieille, T.; Ventalon, C.; Joffre, M. Impact of Pulse Polarization on Coherent Vibrational Ladder Climbing Signals. *J. Phys. Chem. B* **2011**, *115*, 5554–5563.

(380) Ventalon, C.; Fraser, J. M.; Vos, M. H.; Alexandrou, A.; Martin, J.-L.; Joffre, M. Coherent Vibrational Climbing in Carboxyhemoglobin. *Proc. Natl. Acad. Sci. U. S. A.* **2004**, *101*, 13216–13220.

(381) Falvo, C.; Daniault, L.; Vieille, T.; Kemlin, V.; Lambry, J.-C.; Meier, C.; Vos, M. H.; Bonvalet, A.; Joffre, M. Ultrafast Dynamics of Carboxy-Hemoglobin: Two-Dimensional Infrared

Spectroscopy Experiments and Simulations. *J. Phys. Chem. Lett.* **2015**, 2216–2222.

(382) Witte, T.; Hornung, T.; Windhorn, L.; Proch, D.; De Vivie-Riedle, R.; Motzkus, M.; Kompa, K. L. Controlling Molecular Ground-State Dissociation by Optimizing Vibrational Ladder Climbing. *J. Chem. Phys.* **2003**, *118*, 2021–2024.

(383) Windhorn, L.; Yeston, J. S.; Witte, T.; Fuß, W.; Motzkus, M.; Proch, D.; Kompa, K. L.; Moore, C. B. Getting ahead of IVR: A Demonstration of Mid-Infrared Induced Molecular Dissociation on a Sub-Statistical Time Scale. *J. Chem. Phys.* **2003**, *119*, 641–645.

(384) Windhorn, L.; Witte, T.; Yeston, J. S.; Proch, D.; Motzkus, M.; Kompa, K. L.; Fuß, W. Molecular Dissociation by Mid-IR Femtosecond Pulses. *Chem. Phys. Lett.* **2002**, *357*, 85–90.

(385) Tegeder, P. Optically and Thermally Induced Molecular Switching Processes at Metal Surfaces. *J. Phys. Condens. Matter* **2012**, *24*, 394001 1-34.

(386) Ai-Ekabi, H.; Mayo, P. De. Surface Photochemistry: CdS Photoinduced Cis-Trans Isomerization of Olefins. *J. Phys. Chem.* **1985**, *386*, 5815–5821.

(387) Lee, I.; Delbecq, F.; Morales, R.; Albiter, M. A.; Zaera, F. Tuning Selectivity in Catalysis by Controlling Particle Shape. *Nat. Mater.* **2009**, *8*, 132–138.

(388) Denzler, D.; Frischkorn, C.; Hess, C.; Wolf, M.; Ertl, G. Electronic Excitation and Dynamic Promotion of a Surface Reaction. *Phys. Rev. Lett.* **2003**, *91*, 226102 1-4.

(389) Denzler, D. N.; Frischkorn, C.; Wolf, M.; Ertl, G. Surface Femtochemistry : Associative Desorption of Hydrogen from Ru (001) Induced by. *J. Phys. Chem. B* **2004**, 14503–14510.

(390) Denzler, D. N.; Hess, C.; Dudek, R.; Wagner, S.; Frischkorn, C.; Wolf, M.; Ertl, G. Interfacial Structure of Water on Ru(001) Investigated by Vibrational Spectroscopy. *Chem. Phys. Lett.* **2003**, *376*, 618–624.

(391) Cai, L.; Xiao, X.; Loy, M. M. T. Femtosecond Desorption of CO from Metal Surfaces : The Role of the 2pi*-Derived States. *Surf. Sci. Lett.* **2001**, *492*, L688–L692.

(392) Funk, S.; Bonn, M.; Denzler, D. N.; Hess, C.; Wolf, M.; Ertl, G. Desorption of CO from Ru(001) Induced by near-Infrared Femtosecond Laser Pulses. *J. Chem. Phys.* **2000**, *112*, 9888–9897.

(393) Bejan, D. Photodesorption of Molecular Adsorbates From Metallic Surfaces. *J. Optoelectron. Adv. Mater.* **2004**, *6*, 359–384.

(394) Rosker, M. J.; Rose, T. S.; Zewail, A. H. Femtosecond Real-Time Dynamics of Photofragment-Trapping Resonances on Dissociative Potential-Energy Surfaces. *Chem. Phys. Lett.* **1988**, *146*, 175–179.

(395) Darling, G. R.; Holloway, S. The Dissociation of Diatomic Molecules at Surfaces. *Reports Prog. Phys.* **1995**, *58*, 1595–1672.

(396) Liu, Z. P.; Hu, P. General Rules for Predicting Where a Catalytic Reaction Should Occur on Metal Surfaces: A Density Functional Theory Study of C-H and C-O Bond Breaking/making on Flat, Stepped, and Kinked Metal Surfaces. *J. Am. Chem. Soc.* **2003**, *125*, 1958–1967.

(397) Zewail, A. H. Laser Femtochemistry. *Science (80-.).* **1988**, *242*, 1645–1653.

(398) Adato, R.; Altug, H. In-Situ Ultra-Sensitive Infrared Absorption Spectroscopy of Biomolecule Interactions in Real Time with Plasmonic Nanoantennas. *Nat. Commun.* **2013**, *4*, 2154.

(399) Dregely, D.; Neubrech, F.; Duan, H.; Vogelgesang, R.; Giessen, H. Vibrational near-Field Mapping of Planar and Buried Three-Dimensional Plasmonic Nanostructures. *Nat. Commun.* **2013**, *4*, 2237.

(400) Lal, S.; Grady, N. K.; Kundu, J.; Levin, C. S.; Lassiter, J. B.; Halas, N. J. Tailoring Plasmonic Substrates for Surface Enhanced Spectroscopies. *Chem. Soc. Rev.* **2008**, *37*, 898–911.

(401) Rezus, Y. L. A.; Selig, O. Impact of Local-Field Effects on the Plasmonic Enhancement of Vibrational Signals by Infrared Nanoantennas. *Opt. Express* **2016**, *24*, 12202–12227.

(402) Miroshnichenko, A. E.; Flach, S.; Kivshar, Y. S. Fano Resonances in Nanoscale Structures. *Rev. Mod. Phys.* **2010**, *82*, 2257–2298.

(403) Giannini, V.; Francescato, Y.; Amrania, H.; Phillips, C. C.; Maier, S. A. Fano Resonances in Nanoscale Plasmonic Systems : A Parameter-Free Modeling Approach. *Nano Lett.* **2011**, *11*, 2835–2840.

(404) Francescato, Y.; Giannini, V.; Maier, S. A. Plasmonic Systems Unveiled by Fano Resonances. *ACS Nano* **2012**, *6*, 1830–1838.

(405) Ataka, K.; Heberle, J. Biochemical Applications of Surface-Enhanced Infrared Absorption Spectroscopy. *Anal. Bioanal. Chem.* **2007**, *388*, 47–54.

(406) Li, M.; Cushing, S. K.; Wu, N. Plasmon-Enhanced Optical Sensors: A Review. *Analyst* **2015**, *140*, 386–406.

(407) Furukawa, Y.; Seto, K.; Nakajima, K.; Itoh, Y.; Eguchi, J.; Sugiyama, T.; Fujimura, H. Infrared and Raman Spectroscopy of Organic Thin Films Used for Electronic Devices. *Vib. Spectrosc.* **2012**, *60*, 5–9.

(408) Gregoriou, V. G.; Rodman, S. E. Vibrational Spectroscopy of Thin Organic Films. In *Handbook of Vibrational Spectroscopy*; 2006; pp. 2670–2693.

(409) Hoang, C. V; Oyama, M.; Saito, O.; Aono, M.; Nagao, T. Monitoring the Presence of Ionic Mercury in Environmental Water by Plasmon-Enhanced Infrared Spectroscopy. *Sci. Rep.* **2013**, *3*, 1175 1-6.

(410) Aroca, R. F. Plasmon Enhanced Spectroscopy. *Phys. Chem. Chem. Phys.* **2013**, *15*, 5355–5363.

(411) Daniel, M. C.; Astruc, D. Gold Nanoparticles: Assembly, Supramolecular Chemistry, Quantum-Size-Related Properties, and Applications Toward Biology, Catalysis, and Nanotechnology. *Chem. Rev.* **2004**, *104*, 293–346.

(412) Leblanc, R. M. Molecular Recognition at Langmuir Monolayers. *Curr. Opin. Chem. Biol.* **2006**, *10*, 529–536.

(413) Persch, E.; Dumele, O.; Diederich, F. Molekulare Erkennung in Chemischen Und Biologischen Systemen. *Angew. Chemie* **2015**, *127*, 3341–3382.

(414) Ni, M.; Leung, M. K. H.; Leung, D. Y. C.; Sumathy, K. A Review and Recent Developments in Photocatalytic Water-Splitting Using TiO2 for Hydrogen Production. *Renew. Sustain. Energy Rev.* **2007**, *11*, 401–425.

(415) Zhang, X.; Chen, Y. L.; Liu, R.-S.; Tsai, D. P. Plasmonic Photocatalysis. *Rep. Prog. Phys.* **2013**, *76*, 046401 1-41.

(416) Nakata, K.; Fujishima, A. TiO 2 Photocatalysis: Design and Applications. *J. Photochem. Photobiol. C Photochem. Rev.* **2012**, *13*, 169–189.

(417) Ibhadon, A.; Fitzpatrick, P. Heterogeneous Photocatalysis: Recent Advances and Applications. *Catalysts* **2013**, *3*, 189–218.

(418) Gaya, U. I.; Abdullah, A. H. Heterogeneous Photocatalytic Degradation of Organic Contaminants over Titanium Dioxide: A Review of Fundamentals, Progress and Problems. *J.*

Photochem. Photobiol. C Photochem. Rev. **2008**, *9*, 1–12.

(419) Herrmann, J. Heterogeneous Photocatalysis: Fundamentals and Applications to the Removal of Various Types of Aqueous Pollutants. *Catal. Today* **1999**, *53*, 115–129.

(420) Litter, M. I. Heterogeneous Photocatalysis: Transition Metal Ions in Photocatalytic Systems. *Appl. Catal. B Environ.* **1999**, *23*, 89–114.

(421) Linsebigler, A. L.; Linsebigler, A. L.; Yates Jr, J. T.; Lu, G.; Lu, G.; Yates, J. T. Photocatalysis on TiO2 Surfaces: Principles, Mechanisms, and Selected Results. *Chem. Rev.* **1995**, *95*, 735–758.

(422) Bredenbeck, J.; Helbing, J.; Behrendt, R.; Renner, C.; Moroder, L.; Wachtveitl, J.; Hamm, P.; Klopferspitz, A.; Martinsried, D.-. Transient 2D-IR Spectroscopy : Snapshots of the Nonequilibrium Ensemble during the Picosecond Conformational Transition of a Small Peptide. *J. Phys. Chem. B* **2003**, *107*, 8654–8660.

(423) Bredenbeck, J.; Helbing, J.; Kolano, C.; Hamm, P. Ultrafast 2D–IR Spectroscopy of Transient Species. *ChemPhysChem* **2007**, *8*, 1747–1756.

(424) Bredenbeck, J.; Helbing, J.; Hamm, P. Labeling Vibrations by Light: Ultrafast Transient 2D-IR Spectroscopy Tracks Vibrational Modes during Photoinduced Charge Transfer. *J. Am. Chem. Soc.* **2004**, *126*, 990–991.

(425) Kalosakas, G.; Bezel, I. Electron Dynamics in Two-Dimensions: A Hunt for the Ground-State Polarons. *Chem. Phys. Lett.* **2005**, *403*, 89–94.

(426) Baiz, C. R.; Nee, M. J.; McCanne, R.; Kubarych, K. J. Ultrafast Nonequilibrium Fourier-Transform Two-Dimensional Infrared Spectroscopy. *Opt. Lett.* **2008**, *33*, 2533–2535.

(427) Asbury, J. B.; Hao, E.; Wang, Y.; Lian, T. Bridge Length-Dependent Ultrafast Electron Transfer from Re Polypyridyl Complexes to Nanocrystalline TiO2 Thin Films Studied by Femtosecond Infrared Spectroscopy. *J. Phys. Chem. B* **2000**, *104*, 11957–11964.

(428) Anderson, N. A.; Lian, T. Ultrafast Electron Transfer At the Molecule-Semiconductor Nanoparticle Interface. *Annu. Rev. Phys. Chem-* **2005**, *56*, 491–519.

(429) Asbury, J. B.; Ellingson, R. J.; Ghosh, H. N.; Ferrere, S.; Nozik, A. J.; Lian, T. Femtosecond IR Study of Excited-State Relaxation and Electron-Injection Dynamics of Ru(dcbpy)2(NCS) 2 in Solution and on Nanocrystalline TiO 2 and Al 2 O 3 Thin Films. *J. Phys. Chem. B* **1999**, *103*, 3110–3119.

(430) Asbury, J. B.; Hao, E.; Wang, Y.; Ghosh, H. N.; Lian, T. Ultrafast Electron Transfer Dynamics from Molecular Adsorbates to Semiconductor Nanocrystalline Thin Films. *J. Phys. Chem. B* **2001**, *105*, 4545–4557.

(431) Heimer, T. A.; Heilweil, E. J. Direct Time-Resolved Infrared Measurement of Electron Injection in Dye-Sensitized Titanium Dioxide Films. *J. Phys. Chem. B* **1997**, *101*, 10990–10993.

(432) Heimer, T. A.; Heilweil, E. J.; Bignozzi, C. A.; Meyer, G. J. Electron Injection, Recombination, and Halide Oxidation Dynamics at Dye-Sensitized Metal Oxide Interfaces. *J. Phys. Chem. A* **2000**, *104*, 4256–4262.

(433) Asbury, J. B.; Anderson, N. a; Hao, E.; Ai, X.; Lian, T. Parameters Affecting Electron Injection Dynamics from Ruthenium Dyes to Titanium Dioxide Nanocrystalline Thin Film. *J. Phys. Chem. B* **2003**, *107*, 7376–7386.

(434) Butler, J. M.; George, M. W.; Schoonover, J. R.; Dattelbaum, D. M.; Meyer, T. J. Application of Transient Infrared and near Infrared Spectroscopy to Transition Metal Complex Excited States and Intermediates. *Coord. Chem. Rev.* **2007**, *251*, 492–514.

(435) Polo, A. S.; Itokazu, M. K.; Murakami Iha, N. Y. Metal Complex Sensitizers in Dye-Sensitized Solar Cells. *Coord. Chem. Rev.* **2004**, *248*, 1343–1361.

(436) She, C.; Guo, J.; Lian, T. Comparison of Electron Injection Dynamics from Re-Bipyridyl Complexes to TiO2 Nanocrystalline Thin Films in Different Solvent Environments. *J. Phys. Chem. B* **2007**, *111*, 6903–6912.

(437) Echenique, P. M.; Berndt, R.; Chulkov, E. V.; Fauster, T.; Goldmann, A.; Höfer, U. Decay of Electronic Excitations at Metal Surfaces. *Surf. Sci. Rep.* **2004**, *52*, 219–317.

(438) Chulkov, E. V; Borisov, G.; Gauyacq, J. P.; Sanchez-Portal, D.; Silkin, V. M.; Zhukov, V. P.; Echenique, P. M. Electronic Excitations in Metals and at Metal Surfaces. *Chem. Rev.* **2006**, *106*, 4160–4206.

(439) Güdde, J.; Berthold, W.; Höfer, U. Dynamics of Electronic Transfer Processes at Metal/insulator Interfaces. *Chem. Rev.* **2006**, *106*, 4261–4280.

(440) Muller, E. A.; Strader, M. L.; Johns, J. E.; Yang, A.; Caplins, B. W.; Shearer, A. J.; Suich, D. E.; Harris, C. B. Femtosecond Electron Solvation at the Ionic Liquid/metal Electrode Interface. *J. Am. Chem. Soc.* **2013**, *135*, 10646–10653.

(441) Caplins, B. W.; Suich, D. E.; Shearer, A. J.; Harris, C. B. Metal/phthalocyanine Hybrid Interface States on Ag(111). *J. Phys. Chem. Lett.* **2014**, *5*, 1679–1684.

(442) Lindstrom, C. D.; Zhu, X.-Y. Photoinduced Electron Transfer at Molecule-Metal Interfaces. *Chem. Rev.* **2006**, *106*, 4281–4300.

(443) Barlow, S. M.; Raval, R. Complex Organic Molecules at Metal Surfaces: Bonding, Organisation and Chirality. *Surf. Sci. Rep.* **2003**, *50*, 201–341.

(444) Kuroda, D. G.; Bauman, J. D.; Challa, J. R.; Patel, D.; Troxler, T.; Das, K.; Arnold, E.; Hochstrasser, R. M. Snapshot of the Equilibrium Dynamics of a Drug Bound to HIV-1 Reverse Transcriptase. *Nat. Chem.* **2013**, *5*, 174–181.

(445) Kratochvil, H. T.; Carr, J. K.; Matulef, K.; Annen, A. W.; Li, H.; Maj, M.; Ostmeyer, J.; Serrano, A. L.; Raghuraman, H.; Moran, S. D.; et al. Instantaneous Ion Configurations in the K+ Ion Channel Selectivity Filter Revealed by 2D IR Spectroscopy. *Science* **2016**, *353*, 1040–1044.

(446) Loparo, J. J.; Roberts, S. T.; Nicodemus, R. A.; Tokmakoff, A. Variation of the Transition Dipole Moment across the OH Stretching Band of Water. *Chem. Phys.* **2007**, *341*, 218–229.

(447) Perakis, F.; Hamm, P. Two-Dimensional Infrared Spectroscopy of Supercooled Water. *J. Phys. Chem. B* **2011**, *115*, 5289–5293.

(448) Eaves, J. D.; Loparo, J. J.; Fecko, C. J.; Roberts, S. T.; Tokmakoff, A.; Geissler, P. L. Hydrogen Bonds in Liquid Water Are Broken Only Fleetingly. *Proc. Natl. Acad. Sci. U. S. A.* **2005**, *102*, 13019–13022.

(449) Nicodemus, R. A.; Ramasesha, K.; Roberts, S. T.; Tokmakoff, A. Hydrogen Bond Rearrangements in Water Probed with Temperature-Dependent 2D IR. *J. Phys. Chem. Lett.* **2010**, *1*, 1068–1072.

(450) Medders, G. R.; Paesani, F. Water Dynamics in Metal − Organic Frameworks: Effects of Heterogeneous Confinement Predicted by Computational Spectroscopy. *J. Phys. Chem. Lett.* **2014**, *5*, 2897−2902.

(451) Moilanen, D. E.; Levinger, N. E.; Spry, D. B.; Fayer, M. D. Confinement or the Nature of the Interface? Dynamics of Nanoscopic Water. *J. Am. Chem. Soc.* **2007**, *129*, 14311–14318.

(452) Volkov, V. V.; Palmer, D. J.; Righini, R. Distinct Water Species Confined at the Interface of a Phospholipid Membrane. *Phys. Rev. Lett.* **2007**, *99*, 1–4.

(453) Bakulin, A. A.; Cringus, D.; Pieniazek, P. A.; Skinner, J. L.; Jansen, T. L. C.; Pshenichnikov, M. S. Dynamics of Water Confined in Reversed Micelles: Multidimensional Vibrational Spectroscopy Study. *J. Phys. Chem. B* **2013**, *117*, 15545–15558.

(454) Zhang, M.; de Respinis, M.; Frei, H. Time-Resolved Observations of Water Oxidation Intermediates on a Cobalt Oxide Nanoparticle Catalyst. *Nat. Chem.* **2014**, *6*, 362–367.

(455) Herlihy, D. M.; Waegele, M. M.; Chen, X.; Pemmaraju, C. D.; Prendergast, D.; Cuk, T. Detecting the Oxyl Radical of Photocatalytic Water Oxidation at an N-SrTiO3/aqueous Interface through Its Subsurface Vibration. *Nat. Chem.* **2016**, *8*, 1–7.

(456) Dong, Y.; Hu, G.; Hu, X.; Xie, G.; Lu, J.; Luo, M. Hydrogen Adsorption and Oxidation on Pt Film : An in Situ Real-Time Attenuated Total Re Fl Ection Infrared (ATR-IR) Spectroscopic Study. *J. Phys. Chem. C* **2013**, *117*, 12537−12543.

(457) Futamata, M.; Luo, L.; Nishihara, C. ATR-SEIR Study of Anions and Water Adsorbed on Platinum Electrode. *Surf. Sci.* **2005**, *590*, 196–211.

(458) Dolamic, I.; Bürgi, T. Photoassisted Decomposition of Malonic Acid on TiO2 Studied by in Situ Attenuated Total Reflection Infrared Spectroscopy. *J. Phys. Chem. B* **2006**, *110*, 14898–14904.

(459) Dolamic, I.; Bürgi, T. Photocatalysis of Dicarboxylic Acids over TiO2: An in Situ ATR-IR Study. *J. Catal.* **2007**, *248*, 268–276.

(460) Savolainen, J.; Ahmed, S.; Hamm, P. Two-Dimensional Raman-THz Spectroscopy of Water. *Proc. Natl. Acad. Sci.* **2013**, *110*, 20402–20407.

(461) Elsaesser, T.; Reimann, K.; Woerner, M. Focus: Phase-Resolved Nonlinear Terahertz Spectroscopy - From Charge Dynamics in Solids to Molecular Excitations in Liquids. *J. Chem. Phys.* **2015**, *142*, 212301 1-9.

(462) Kuehn, W.; Reimann, K.; Woerner, M.; Elsaesser, T.; Hey, R. Two-Dimensional Terahertz Correlation Spectra of Electronic Excitations in Semiconductor Quantum Wells. *J. Phys. Chem. B* **2011**, *115*, 5448–5455.

(463) Teo, S. M.; Ofori-Okai, B. K.; Werley, C. A.; Nelson, K. A. Invited Article: Single-Shot THz Detection Techniques Optimized for Multidimensional THz Spectroscopy. *Rev. Sci. Instrum.* **2015**, *86*, 051301 1-17.

(464) Schultz, D. M.; Yoon, T. P. Solar Synthesis: Prospects in Visible Light Photocatalysis. *Science (80-.).* **2014**, *343*, 1239176 1-8.

(465) Osterloh, F. E.; Parkinson, B. a. Recent Developments in Solar Water-Splitting Photocatalysis. *MRS Bull.* **2011**, *36*, 17–22.

(466) Alibabaei, L.; Brennaman, M. K.; Norris, M. R.; Kalanyan, B.; Song, W.; Losego, M. D.; Concepcion, J. J.; Binstead, R. A.; Parsons, G. N.; Meyer, T. J. Solar Water Splitting in a Molecular Photoelectrochemical Cell. *Proc. Nat. Acad. Sci. USA* **2013**, *110*, 20008–20013.

(467) Kudo, A.; Miseki, Y. Heterogeneous Photocatalyst Materials for Water Splitting. *Chem. Soc. Rev.* **2009**, *38*, 253–278.

(468) Warren, S. C.; Thimsen, E. Plasmonic Solar Water Splitting. *Energy Environ. Sci.* **2012**, *5*, 5133–5146.

(469) Wang, C. C.; Li, J. R.; Lv, X. L.; Zhang, Y. Q.; Guo, G. S. Photocatalytic Organic Pollutants

Degradation in Metal-Organic Frameworks. *Energy Environ. Sci.* **2014**, *7*, 2831–2867.

(470) Kubota, J.; Yoda, E.; Ishizawa, N.; Wada, A.; Domen, K.; Kano, S. S. Site-Hopping of Adsorbed CO in c(4×2)-CO/Ni(111) by Laser-Induced Temperature Jump: Time-Resolved Sum-Frequency Generation Observation. *J. Phys. Chem. B* **2003**, *107*, 10329–10332.

(471) Yamakata, A.; Osawa, M. Dynamics of Double-Layer Restructuring on a Platinum Electrode Covered by CO: Laser-Induced Potential Transient Measurement. *J. Phys. Chem. C* **2008**, *112*, 11427–11432.

(472) Yamakata, A.; Uchida, T.; Kubota, J.; Osawa, M. Laser-Induced Potential Jump at the Electrochemical Interface Probed by Picosecond Time-Resolved Surface-Enhanced Infrared Absorption Spectroscopy. *J. Phys. Chem. B* **2006**, *110*, 6423–6427.

(473) Smith, K. K.; Kaufmann, K. J.; Huppert, D.; Gutman, M. Picosecond Proton Ejection: An Ultrafast pH Jump. *Chem. Phys. Lett.* **1979**, *64*, 522–527.

(474) Cavanagh, R.; King, D. Dynamics of Nonthermal Reactions: Femtosecond Surface Chemistry. *J. Phys. Chem.* **1993**, *97*, 786–798.

(475) Li, J.; Cushing, S. K.; Meng, F.; Senty, T. R.; Bristow, A. D.; Wu, N. Plasmon-Induced Resonance Energy Transfer for Solar Energy Conversion. *Nat. Photonics* **2015**, *9*, 601–607.

(476) Li, J.; Cushing, S. K.; Zheng, P.; Meng, F.; Chu, D.; Wu, N. Plasmon-Induced Photonic and Energy-Transfer Enhancement of Solar Water Splitting by a Hematite Nanorod Array. *Nat. Commun.* **2013**, *4*, 1–8.

(477) Muller, E. A.; Pollard, B.; Raschke, M. B. Infrared Chemical Nano-Imaging: Accessing Structure, Coupling, and Dynamics on Molecular Length Scales. *J. Phys. Chem. Lett.* **2015**, *6*, 1275–1284.

(478) Aeschlimann, M.; Brixner, T.; Fischer, A.; Kramer, C.; Melchior, P.; Pfeiffer, W.; Schneider, C.; Struber, C.; Tuchscherer, P.; Voronine, D. V. Coherent Two-Dimensional Nanoscopy. *Science (80-.).* **2011**, *333*, 1723–1726.

(479) Luther, B. M.; Tracy, K. M.; Gerrity, M.; Brown, S.; Krummel, A. T. 2D IR Spectroscopy at 100 kHz Utilizing a Mid-IR OPCPA Laser Source. *Opt. Express* **2016**, *24*, 4117–4127.

(480) Chalus, O.; Bates, P. K.; Smolarski, M.; Biegert, J. Mid-IR Short-Pulse OPCPA with Micro-Joule Energy at 100kHz. *Opt. Express* **2009**, *17*, 3587–3594.

(481) Thai, A.; Hemmer, M.; Bates, P. K.; Chalus, O.; Biegert, J. Sub-250-Mrad, Passively Carrier–envelope-Phase-Stable Mid-Infrared OPCPA Source at High Repetition Rate. *Opt. Lett.* **2011**, *36*, 3918–3920.

(482) Baiz, C. R.; Schach, D.; Tokmakoff, A. Ultrafast 2D IR Microscopy. *Opt. Express* **2014**, *22*, 18724–18735.

(483) Xu, X. G.; Raschke, M. B. Near-Field Infrared Vibrational Dynamics and Tip-Enhanced Decoherence. *Nano Lett.* **2013**, *13*, 1588–1595.

(484) Muller, E. A.; Pollard, B.; Raschke, M. B. Infrared Chemical Nano-Imaging: Accessing Structure, Coupling, and Dynamics on Molecular Length Scales. *J. Phys. Chem. Lett.* **2015**, *6*, 1275–1284.

(485) Wang, L.; Long, R.; Prezhdo, O. V. Time-Domain Ab Initio Modeling of Photoinduced Dynamics at Nanoscale Interfaces. *Annu. Rev. Phys. Chem.* **2015**, *66*, 549–579.

(486) Srinivas, G.; Nielsen, S. O.; Moore, P. B.; Klein, M. L. Molecular Dynamics Simulations of Surfactant Self-Organization at a Solid-Liquid Interface. *J. Am. Chem. Soc.* **2006**, *128*, 848–853.

(487) Schiffmann, F.; Hutter, J.; Vandevondele, J. Atomistic Simulations of a Solid/liquid Interface: A

Combined Force Field and First Principles Approach to the Structure and Dynamics of Acetonitrile near an Anatase Surface. *J. Phys. Condens. Matter* **2008**, *20*, 64206.

(488) Nørskov, J. K.; Bligaard, T.; Rossmeisl, J.; Christensen, C. H. Towards the Computational Design of Solid Catalysts. *Nat. Chem.* **2009**, *1*, 37–46.

(489) Hutter, J.; Iannuzzi, M.; Schiffmann, F.; Vandevondele, J. Cp2k: Atomistic Simulations of Condensed Matter Systems. *Wiley Interdiscip. Rev. Comput. Mol. Sci.* **2014**, *4*, 15–25.